Universitetet i Stavanger

FACULTY OF SCIENCE AND TECHNOLOGY

MASTER'S THESIS

Study program/specialization: Petroleum Engineering/Drilling Engineering	Spring 2017 Open access
Author: Malik Alsenwar	(signature of author)
Supervisor: Mesfin Belayneh	
Title of master's thesis: **NCS Drilling Data Based ROP Modelling and its Application**	
Credits: 30	
Keywords: ROP Modelling Analysis Drilling optimization Multiple regression Warren model Method of least squares MSE D-exponent	Number of pages: 96 + enclosure: 5 Stavanger, June 15, 2017

Abstract

Predicting the ROP (rate of penetration) before drilling is essential to improve the overall drilling efficiency and thereby reduce the non-productive time and costs. For this, good ROP model is required. Several ROP models are available in the industry which is derived based on both mechanistic and empirical methods. However, each model has its strengths and shortcomings.

In this thesis, five ROP modelling workflows are used to model field data. These are the methods of multiple regression, least squares, MSE, D-exponent and the Warren model. The applicability and the limitations of the models are tested on nearby, distant and very distant field data in the North Sea. Six wells are used for the analysis located in the Alvheim, Kvitebjørn and Valhall fields.

During modelling, two hypotheses were tested. One common observation from the result is that the model application is limited within the same block, where the lateral geology expected to be similar. Based on the assessment of the results, applicability and limitations of the five modelling techniques are summarized. In addition to the overall study, an optimization procedure is also developed.

Acknowledgments

I would like to thank my supervisor Dr Mesfin Belayneh for supervision and guidance, who has been continuously available for support and feedback. I would also like to thank the Norwegian Petroleum Directorate for the valuable provided well data. I would also thank the University of Stavanger for giving me this golden opportunity to do this thesis and fulfil my master's degree. Last but not least, I would like to thank my family and friends who supported me and led me to complete my thesis within a limited time frame.

Stavanger, June 2017

Malik Alsenwar

Table of Contents

List of Figures

List of Tables

Nomenclature

ρ – Density
ρ_c – Mud weight
γ_f – Fluid specific gravity
μ – Bit specific coefficient of sliding friction / Apparent viscosity
$\emptyset$ – Porosity
Δt – Sonic travel time
A – Area
A_M – Rock matrix strength constant
A_v – Ratio of jet velocity to return velocity
C_b – cost of bit
C_f – Drilling cost per foot drilled
C_m – Downhole motor cost
C_f – Rig cost
D – Depth
dD/dt – Penetration rate
d_b – Bit diameter
d_c – Corrected D-exponent
d_{exp} – D-exponent
d_n – Bit nozzle diameter
e – Specific energy
E – Rotary speed exponent
F – Thrust
F_j – Jet impact force
F_{jm} – Modified jet impact force
ft – feet
g_p – Pore pressure gradient
gal – Gallon
h – Fractional tooth height worn
hr – Hour
I_s – Point load index
in – Inch
lb – Pound
lbf – Pound-force
kpsi/ksi – Kilo-pound per square inch
log – Logarithm
N – Rotational speed (RPM)
$Norm$ – Normalized
psi – Pounds per square inch
q – Flowrate
Q – Least squares sum
S – Rock Strength
T – Torque
t_c – Non-rotating time

t_r – Bit rotating time
t_t – Trip time
v_f – Return fluid velocity
v_n – Nozzle velocity

List of Abbreviations

Bit D – Bit diameter
CCS – Confined compressive strength
D-Exp – D-exponent
DG – Dull bit grade
DOC – Depth of cut
ECD – Equivalent circulating density
Eq. – Equation
Fig. – Figure
FM – Formation
FP – Formation pressure
GP – Group
HYP – Hypothesis
IADC – International Association of Drilling Contractors
EFFM – Mechanical efficiency factor
MD – Measured depth
MSE – Mechanical specific energy
MSE_{adj} – Adjusted mechanical specific energy
MSL – Mean sea level
NCS – Norwegian continental shelf
NPD – Norwegian Petroleum Directorate
NPP – Normal pore pressure
PDC – Polycrystalline diamond compact
RKB – Rotary Kelly bushing
ROP – Rate of penetration
RPM – Revolutions per minute
TVD – True vertical depth
UCS – Unconfined compressive strength
USD – U.S. dollar
WOB – Weight on bit

Chapter 1

Introduction

This thesis presents NCS (Norwegian Continental Shelf) field data based ROP model development and testing with near and far field wells. Five different modelling approaches have been implemented, and their application and limitations have been tested. ROP optimisation procedure is also developed with the objective of increasing ROP, reduced drilling time and hence reduces drilling cost.

1.1 Background and Motivation

In rotary drilling methods, the rotational and axial load applied on the bit shatter, crush and scrap the fragments out of the rock surface to drill deeper through the rock layers. Drilling is the operation of making a hole to connect the surface with the reservoir. The drilling performance is evaluated by the rate of process, which is measured by the distance penetrated by the drill bit in a unit length of time (e.g. feet drilled per hour) [1].

According to Teale [2], rotary drilling can be regarded as a combination of two different mechanisms under rotational, axial loading as illustrated in Fig. 1: 'indentation', by which the teeth of the bit are continuously pushed into the rock forcing them into the formation by the applied WOB (weight on bit); and 'cutting', by which the bit is given lateral movements to scrape the surface and break out fragments of the formation. However, these two loadings are in practice acting simultaneously. The energy required to drill a unit volume of rock was introduced by Teale as the MSE (mechanical specific energy) concept [2].

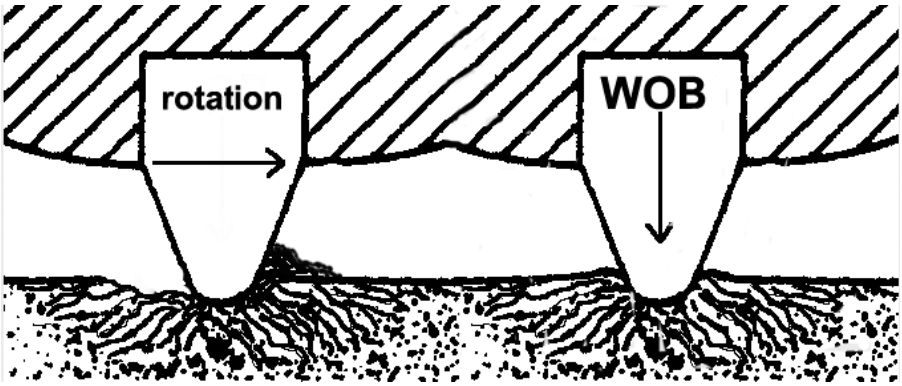

Fig. 1. Rotary drilling is described as a combination of two actions: indentation and cutting [3].

Drilling is a costly factor for the petroleum industry. During the planning phase, drilling optimization simulation study is common practice in the industry. This can be characterized by the higher rate of penetration, which indirectly reduces drilling time and also lower bit wear, which indirectly reduces undesired tripping operations. The overall effect is reflected in reducing costs. For this, it is important to have good ROP predictive model.

Scientist started looking for optimized ways for efficient and reduced costs of drilling since the late 1960s. The basic idea of optimization in drilling industry relies on using old data of existing wells. Data of similar wells, in similar geological characteristics, are collected to operate a process of well drilling at minimum costs, minimum operational risks and maximum efficient results. ROP is one of the parameters that can be analyzed to achieve this goal [4].

In literature, there are several ROP models available. These models are a function of different drilling mechanical and operational parameters. Depending on their simplicity and complexity nature of the models, their prediction also varies. In other words, every model has its own shortcomings and its own strong sides. For instance, Galle and Woods [5] have developed a model for drilling of soft-formations. However, Estes and Randall [6] explains that the model breaks an assumption that was used to derive the model when applied in real conditions. There is also Maurer's [7] "perfect cleaning" model that was found not applicable for drilling most soft-formations. Cunningham's [8] model also fails to match the experimental data [9].

The motivation of this thesis is the ROP modelling work presented by Morten Adamsen Husvæg (2015) [10]. He developed field data based modelling and tested them on the same block data. The author's modelling approach was based on the whole well data and was applied on nearby well data. The results look promising. However, in some cases, the modelling approach doesn't capture the true ROP well, and limitations of the application are not documented.

1.2 Problem Formulation

Well-to-well correlation is widely used despite its inaccuracy. This method is based on the use of collected survey data is exploration wells or adjacent drilled wells in the planning of other nearby wells. It can be used because in most cases the formation properties and pressures vary only with depth within an area, not horizontally [10-12]. This method may be beneficial in saving time and effort when drilling a new well based on data from a close-by well that most likely went through the same formation deposits and pressure regimes in roughly the same depth. Moreover, this method helps in avoiding many risks and reduce possible incidents and mistakes [13].

Even though the Husvæg's method is promising, the limitations of the application are not documented. Unlike Husvæg's (2015) modelling approach, this thesis work's attempts to develop and describe the modelling results based on the geological features and spatial distribution.

During drilling phase, drilling operational data, well logs and cuttings of the drilled formations are available. For efficient drilling operation, as mentioned earlier, a good ROP model is needed to predict the drilling performance when planning in a nearby well.

In this thesis, the ROP modelling, and optimization procedure developments are the main focus.

The research issues to be addressed are:

- A model derived based on a part of the well (e.g. reservoir section), what is the limit of application of the model on its well, nearby and far wells? Is it applicable to the whole wellbore section?
- A model derived based on the whole section of the well, what is the spatial limit of application (i.e. near and away from the originating well)?
- Whether there is a relationship between the model predictions and the geological well-to-well correlations.
- Developing an ROP optimization method based on a parametric sensitivity study.

1.3 Objective

The main objective of this thesis is to develop ROP model and test it on the NCS. Based on the modelling results, this thesis aims to answer and interpret the research questions addressed in the previous section.

The activities are:

- Review literature models.
- Sort out field drilling data obtained from the considered block wells and develop an empirical model.
- Test the application of the models on nearby, far and very far field wells.
- Perform sensitivity study, analyze time and analyse ROP.
- Finally, generate ROP optimization procedure.

1.4 Hypotheses and Research Methodology

The research is based on modelling and testing as illustrated in Fig. 2. For this, five techniques are examined on six wells; three of them (24/6-B-1, 24/6-B-4 and 24/6-B-5) are located next to each other in the Alvheim field. Two of them (34/11-A-4 and 34/11-A-5) are located in the far field Kvitebjørn, which is about 173 km away from the Alvheim field. And one well called 2/11-S-10 is located at the very far distant field, in Valhall, which is about 376 km away from the Alvheim filed. A map showing the location of the three fields is provided later in Chapter 3.

Well 24/6-B-4 is chosen to be as the reference well in this research methodology. By using modelling method, an ROP model is developed from the reference well data based on two hypotheses:

- For hypothesis I, the ROP model is developed based on reservoir section of the reference well, which is well 24/6-B-4 AY2H.
- For hypothesis II, the ROP model is developed based on data of the whole wellbore section of the reference well.

For verification, the models are tested on very nearby, far and very far wells. They are first tested locally on two nearby wells in the same block (i.e. wells 24/6-B-1 and 24/6-B-5) and on two remote wells in another block (i.e. wells 34/11-A-4 and 34/11-A-5). The models are then examined on a far distant well (i.e. well 2/11-S-10).

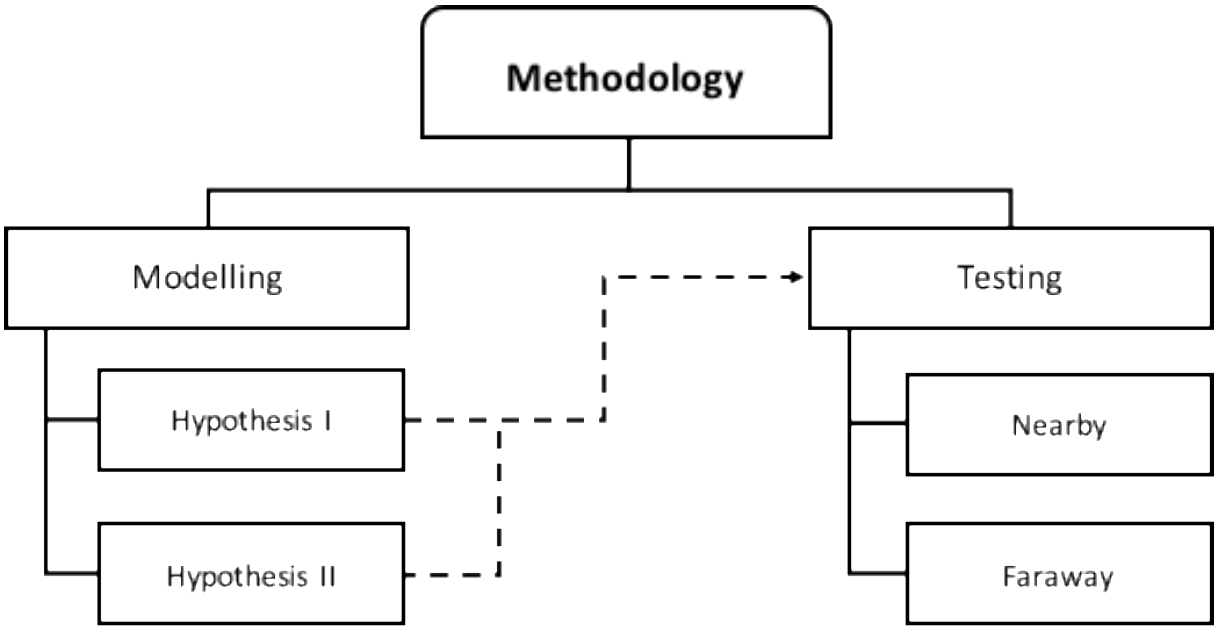

Fig. 2. Structure and methodology of the thesis.

Chapter 2

Literature Study

This chapter presents literature documented ROP models, which some of them to be implemented in this thesis work. The main elements and factors of the drilling process (such as drilling bits and formation strength) and the factors that may affect the ROP are presented. In addition to some of the models which were not used in this thesis work, these are briefly mentioned in this chapter. The details of the unused models are provided in Appendix I.

2.1 Drill Bits

A drill bit is a boring tool which is located at the end of the drill string. Its main function is to cut rocks at the bottom of the hole. It consists of a cutting component (cutters) and a fluid circulation component (nozzles). The combination of the indentation action (i.e. WOB) and the cutting action (i.e. rotation) of the drill bit results in crushing and penetration of rocks (see Fig. 1). The broken rock fragments are removed from the wellbore by circulating drilling fluid down the drill string passes through the bit pin bore and bit nozzles. Drilling fluid applies a hydraulic force known as the jet impact force, which improves the rate of penetration [14].

Drilling bits varies, there are many different types and designs of drilling bits that suit different purposes. All incidents of early bit failures, gauge wear and tooth dulling should be noted to determine the proper bit type [15]. Rotary drilling bits are usually categorized according to their design as either rolling cutter bits or fixed cutter bits [16].

2.1.1 Roller Cone Bits

Roller cones bits are usually made up of three equal-sized cones attached to three identical legs with a pin connection. The three cones rotate about the axis of the cone as the bit is rotated at the bottom of the hole. The three cones are mounted on each of their bearing pins which extend from the bit body. The pin connection is welded to the legs providing means of attachment to drill string. Each leg is provided with a nozzle to obtain high jetting velocities necessary to efficiently clean the hole and the bit [14, 15].

Roller cone bits is the most common used bit worldwide. It is designed to break the rock in compression and can be classified into two types depending on the structure of the cutting surface of the cones: ‘milled tooth bits’, having the cutting structure of teeth milled out of the cone; ‘insert bits’, having the cutting structure as a series of inserts pressed into the cones [15]. Fig. 3 [17] represents a typical tricone

roller cone insert bit. Insert bits are used in medium to hard formations, while milled-tooth bits are used in both soft and hard formations where longer teeth suit harder formations [14].

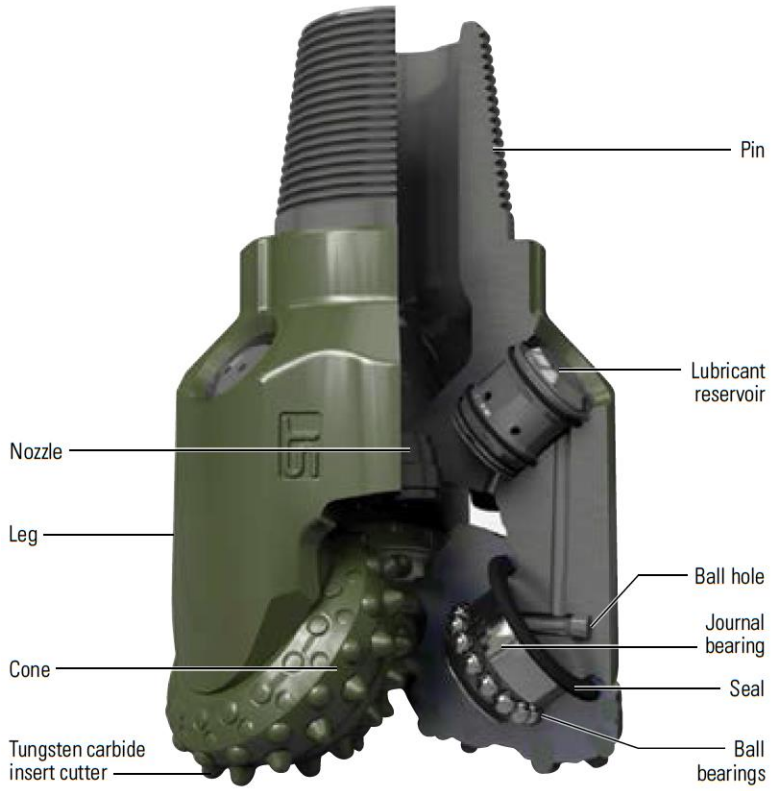

Fig. 3. Roller cone (insert) bit with the major components of the bit including the cutters/teeth, cones, legs, nozzles and pin [17].

The steel design of the roller cones makes these tools require specific working conditions, e.g. an appropriate degree of hardness and strength, heat toleration and impact resistance. Again, the best design is always influenced by the type of rock to be drilled and the desired size of the hole. ROP also plays a pivotal role when evaluating the performance of a roller cone bit [18]. Therefore, designers focus on several points when designing bits. They focus on the hydraulic requirements, materials used, operation mechanical requirements, planned hole deviation, desired rotary speed and not least the geometry part and the required cutting shape [15].

2.1.2 Fixed Cutter Bits

A fixed cutter bit is also called a drag bit, this type of bits employs no moving part (i.e. there are no bearings). The cutters are permanently mounted onto blades, which are integral to the body of the bit. Unlike the roller cone bit, this bit is designed to break the rock in shear, which requires significantly less energy than compression, hence less WOB is required resulting in less wear and tear on the drill string and rig. The shearing action of fixed cutter bits makes the cutting more dynamic than the crushing of the inserts or teeth on the cones of the roller-cone bit [14, 17, 19, 20].

Polycrystalline diamond compact (PDC) bit dominates this category. Its body is made either from steel or a matrix composed of an alloy and a tungsten carbide substrate. There are different types of PDC drill bits depending on the type of formation to be drilled. These bits are flexible when it comes to shape since it has no moving parts. However, the use of diamond bits has its limitations. The performance of a diamond bit in a soft formation is way better than it is in hard formation. Diamond bits are provided with synthetic diamond cutters on the surface. They are also provided with junk slots and fluid courses to keep the flow path away from the bit face to help in cuttings removal. PDC bits are particularly suitable for drilling in shales and other soft formations [17, 20-22].

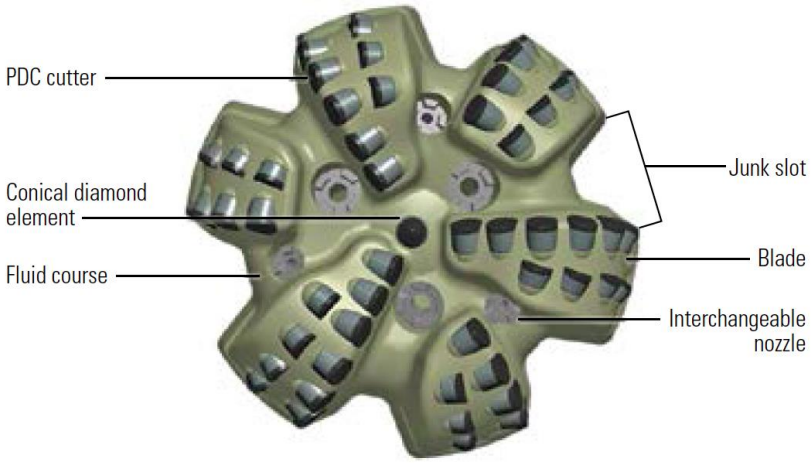

Fig. 4. Polycrystalline diamond compact (PDC) bit face. Major components of the bit face include the fluid courses, junk slots, blades, cutters and nozzles [17].

2.1.3 Bit Optimization

Over the years and inventions in the drilling industry, the drill bits have been continuously developed and improved. This master piece is founded and improved throughout the time to obtain best results in drilling with lowest costs and with most efficient and safe operations with long last bits.

The overall drilling cost is represented in the cost Eq. (2.1), it is included in the drill bit configuration [23, 24].

$$C_f = \frac{(t_r + t_t + t_c)C_r + t_r C_m + C_b}{\Delta D} \tag{2.1}$$

Where C_f, C_r, $C_m$and C_b are the drilling cost, the rig cost, the downhole motor cost and the cost of the bit in [USD/ft]. ΔD is the depth drilled in [ft] and t_r, t_t and t_c are the drilling time, the trip time and the connection time in [hrs].

The selection of the drilling bit plays a very important role in the drilling process and the resulted drilling rate [25]. Choosing the right bit depends on the formation being drilled, its characteristics, rule of thumb and some mathematical models [26, 27]. Choosing the right bit depends on several elements like its diameter, weight, wear and its hydraulics [28].

Also, many operating factors affecting the performance of the drill bit, like the WOB, RPM, formation properties, hydraulic efficiency and mud properties [27].

As mentioned before, the two main types of drilling bits are roller cone bits and diamond bits. Geometrically, the design of roller-cone bits is more complicated than diamond bits. Moreover, the diamond bits have a wider selection and wider designs [29]. Therefore, and as a result of experiences, diamond bits have shown better performance in many different conditions [30].

2.2 Rock Strength

Determination of rock strength is considered to have a significant role in the analysis of drilling and when selecting the optimal completion solution [31-33]. Rock strength usually refers to rock's uniaxial compressive strength (UCS). Rock's tensile strength is about 10% of its compressive strength where it is more likely to fail under tension [34]. The strength of rock is commonly determined by laboratory core experiments. Several strength experiments exist, but the most common experiment and the simplest is the unconfined compressive strength (UCS) [35].

UCS is the maximum axial compressive stress that a cylindrical specimen of rock can withstand before failure under unconfined pressure (i.e. atmospheric pressure) [32]. It can determine indirectly using empirical mathematical relationships or directly measured experimentally [36].

Another used parameter to characterize the strength of rocks is the confined compressive strength (CCS). It represents the rock's maximum resistance value on a specified confined load condition [32].

Using stress-loading tests, UCS is determined in the laboratory by analyzing the compressive behaviour of rock samples. The strength value obtained from UCS is usually lower than CCS. Testing the strength of the rock in laboratory is costlier but more accurate than the indirect methods. Indirect methods are more favourable because they are simpler and more cost and time efficient. This is because no sample preparation is required [32, 36].

Regression techniques are used in indirect methods of relating some physical properties of the rock material and simple index parameters to UCS. P-wave velocity, ultrasonic velocity, Schmidt hammer rebound number and point load index (I_s) are examples of such parameters [36].

Kahraman [37] proposed an equation using least-squares regression by correlating I_S values to the corresponding UCS. The resultant equation is given by:

$$UCS = 10.91 I_s + 27.41 \tag{2.2}$$

Where UCS and I_S are in Mpa.

Amani [36] proposed an equation using multiple regression that correlates porosity (Ø) and sonic travel time (Δt) to UCS. This relies on the idea that rock strength is a result of contribution of several rock properties, such as porosity, degree of compaction, fluid content and grains texture.

$$UCS = 194.4 - 0.6072\Delta t - 646.1Ø - 0.01644\Delta t^2 + 8.792(Ø * \Delta t) \quad (2.3)$$

2.3 Factors Affecting ROP

Drilling conditions and factors that influence drilling are many, some of them are controllable, and some of them are not [38]. Some of these factors should be controlled in order to obtain the required speed during drilling that is sufficient to break the rock formation, in addition to avoiding problems that may arise during the drilling process [39]. Some of the controllable operational factors that may affect the rate of penetration are the weight on bit (WOB), rotations per minute (RPM), the type of bit used, jet impact force and bit hydraulics. A parametric sensitivity analysis is performed later in this thesis to investigate which controllable operational parameter(s) that affect the developed ROP model most.

The Permeability and the strength of the formation affect the rate of penetration. In addition to the drilling fluid properties like fluid density, rheology, viscosity, chemical composition, solid content and filtration characteristics [39]. ROP tends to decrease by increasing fluid viscosity, fluid density, solids and lubricants content and increase by increasing filtration rate [40, 41]. Other factors such as torque, cuttings transport and the equivalent circulating density (ECD) influence also the rate of penetration. ROP tends to increase as ECD decreases [42].

In order to maximize rates of penetration and minimize the drilling costs, a quantitative and qualitative measurements is needed for the drilling process efficiency [43]. The classic drilling curve (from Dupriest [44]) is used for this purpose. The curve is divided into three regions as shown in Fig. 5.

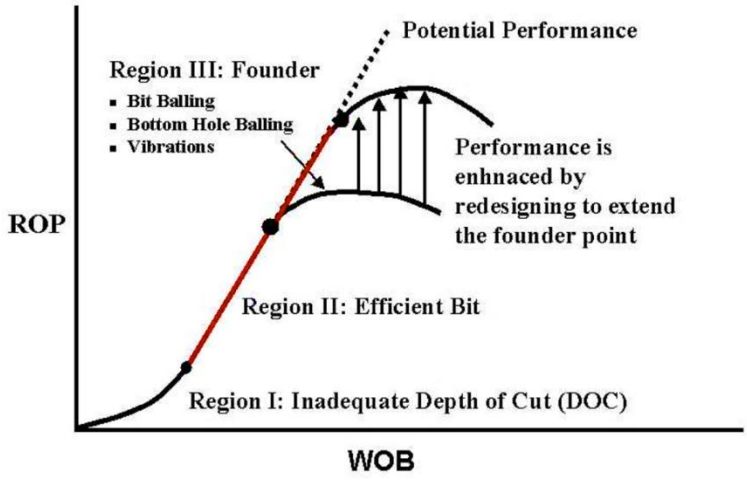

Fig. 5. A plot of ROP versus WOB. A bit is in its efficient range if linear relation between ROP and WOB is achieved. The performance of the bit is enhanced by extending the founder point [44].

In region I, the relationship between ROP and WOB is non-linear, and the performance is constrained by the loss of energy due to inadequate depth of cut (DOC) due to low WOB. Region II starts when the DOC becomes adequate for the bit's performance to stabilize. A Linear relationship between ROP and WOB is obtained in this region, and bit is efficient and tends to transfer the maximum amount of energy. As shown in Fig. 6 [44], the maximum amount of energy is only in the order of 30-40%. In region III the transfer of energy from bit to rock is inefficient, and ROP decreases by increasing WOB; this occurs when reaching the founder point. The founder point could occur due to bit balling, poor hole cleaning and vibrations [44].

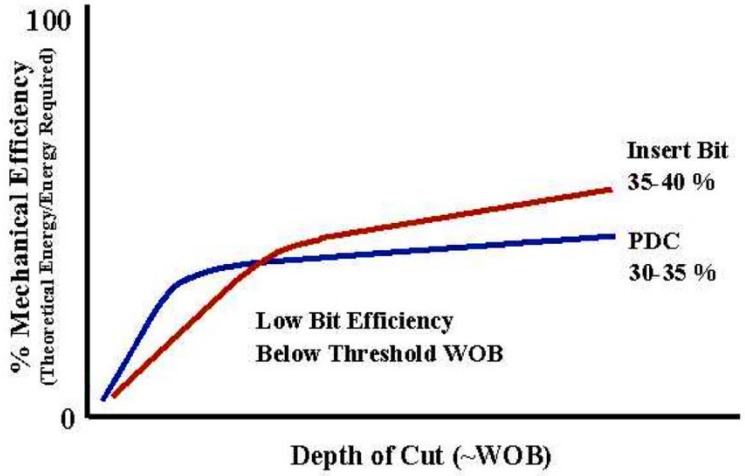

Fig. 6. Plot of % Mechanical efficiency versus depth of cut. Bits are usually 30-40% efficient at peak performance [44].

2.4 ROP Models

The process of optimization is not as simple as we think. Many factors and parameters may stand as obstacles to increase the ROP and reduce the non-productive time and costs of the drilling operations. Parameters are just like the weight on bit (WOB), rotary speed of drill string (RPM), bit type and vibrations. In addition to other properties, like mud and the mechanical conditions of each formation. However, these parameters may be controllable, which may make the common challenges vanish. Pump flow rate and its pressure, weight on bit, mud weight and rotary speed of drill string are examples of such controllable parameters. Many mathematical models have been proposed in an effort to describe the relationship of several drilling variables to the penetration rate. According to previous studies, many mathematical models are suggested in order to analyze the parameters, describe their relationship to the rate of penetration and find solutions to have control over them. In order to clarify it, various known models are described in this thesis [45].

2.4.1 MSE - Mechanical Specific Energy

In 1965, Teale [2] has proposed the concept of mechanical specific energy (MSE). By definition, it's defined as input energy to the output ROP [46].

$$MSE \approx \frac{Input\ Energy}{Output\ ROP} \tag{2.4}$$

MSE is a quantitative measurement that predicts the power (i.e. torque and RPM) required to drill a given formation type for a certain bit type [1, 47]. In non-percussive rotary drilling, work is done by the thrust (F) and the torque (T). The total work performed within one minute is ($Fu + 2\pi NT$), where (N), (A) and (u) are the rotation speed, the area of excavation and the penetration rate respectively. Dividing the work done in one minute by the volume excavated in one minute (Au) gives the specific energy (e). The resultant equation for (e) is given by [2]:

$$e = \left(\frac{F}{A}\right) + \left(\frac{2\pi}{A}\right)\left(\frac{NT}{u}\right) \tag{2.5}$$

Eq. (2.5) can also be written as:

$$MSE = \frac{480 * T * N}{{d_b}^2 * ROP} + \frac{4WOB}{\pi {d_b}^2} \tag{2.6}$$

In order to achieve the highest possible ROP, the MSE should be monitored and kept as low as possible. Maintaining the MSE value as close as possible to the formation's compressive strength ensures a more technical and economical efficient drilling process [1].

Teale's formula for computing MSE value assumes that its value would equal the rock compressive strength at perfect efficiency. However, as shown in Fig. 6 [44], the efficiency of drill bits at peak performance (before reaching founder point) is usually only in the order of 30-40%. Dupriest proposed an adjusted MSE, (MSE_{adj}) value that includes a mechanical efficiency factor, EFF_M, in order to make it more useful for drilling operations [1, 2, 44].

$$MSE_{adj} = EFF_M * MSE \tag{2.7}$$

$$MSE_{adj} = EFF_M \left(\frac{480 * T * N}{{d_b}^2 * ROP} + \frac{4WOB}{\pi {d_b}^2}\right) \tag{2.8}$$

Teale's formula requires torque (T) as an important parameter. However, the common field data is in the form of WOB, RPM and ROP. A bit-specific coefficient of sliding friction (μ) was therefore introduced by Pessier and Fear [48] to express torque (T) and as a function of WOB [47]. The resulting equation for torque (T) is as follows:

$$T = \mu \frac{d_b WOB}{36} \tag{2.9}$$

Substituting (T) in the adjusted MSE, and solving Eq. (2.8) for ROP gives:

$$ROP = \frac{13.33 \mu N}{d_b \left(\frac{MSE_{adj}}{EFF_M WOB} - \frac{4}{\pi d_b^2} \right)} \tag{2.10}$$

2.4.2 Bourgoyne and Young Model

Bourgoyne and young [28] developed a model in 1974 that simplifies the rotary drilling process into one single model. This model depends on statistical past drilling data and is done by multiple regression analysis for the past drilling data. It is considered as the most suitable model for real-time drilling optimization [28, 42]. Bourgoyne and Young introduced the penetration rate as a function of various drilling variables that are considered to have an effect on the ROP which are: formation strength, formation depth, formation compaction, the pressure differential across the hole bottom, bit diameter, bit weight, rotary speed, bit wear and bit hydraulics. The selected penetration rate model to predict the effect of the above-mentioned drilling parameters is available in Appendix I.

This model relies on eight different parameters, which makes it difficult when it comes to modelling because all of the parameters should be in place. Unfortunately, this thesis doesn't analyze the application of this model due to lack of some data required for analysis.

2.4.3 Warren Model

Many drilling models were presented in the literature that relates the different drilling mechanical factors to ROP. Many of these models are inadequate. Galle and Woods [5] had at that time the most popular and most commonly used model for drilling of soft-formations. However, Estes and Randall [6] explains that the model breaks an assumption that was used to derive the model when applied in real conditions. There is also Maurer's [7] "perfect cleaning" model that was found not applicable to the drilling of most soft-formations. Cunningham's [8] model also fails to match the experimental data.

In 1981, Warren [9] has therefore presented an adequate model for tricone bits that predicts ROP for soft-formation bits. The model was derived with experimental data that were obtained from laboratory test. The test was performed using large-scale rig under conditions similar to that experienced in the field. The model accounts for various drilling parameters, something that makes it very useful for understanding the effect of these parameters on ROP.

The model relates the ROP to various drilling parameters, something that makes it very useful for understanding the effect of these parameters on ROP. The model relates ROP to the rock strength, WOB, rotary speed, bit type and bit size [9, 24, 40].

Perfect-Cleaning Model

Warren's initial model assumes perfect cleaning conditions and is reviewed as a starting point for the development of an imperfect-cleaning model [49, 50]. The two-term perfect-cleaning basic model was developed in 1981 [9] using generalized response curves and dimensional analysis. This dimensionless model is a result of modified model presented earlier by Wardlaw [51]. It was modified to give a better fit with the laboratory obtained experimental data. The model that complied best and found to be the best fit of the experimental data is given as:

$$ROP = \left(\frac{aS^2{d_b}^3}{N^b WOB^2} + \frac{c}{Nd_b}\right)^{-1} \tag{2.11}$$

Here the constants (a and c) are the bit constants in penetration model. The first term of the model ($aS^2{d_b}^3/N^b WOB^2$) expresses the maximum rate at which the rock is crushed into cuttings by the bit. The second term (c/Nd_b) of the model adjusts the model to consider the distribution of the applied WOB to more teeth as the WOB is increased and the teeth penetrates deeper into the rock [24, 40]. At low WOB values for a given rock, ROP increases at an increasing rate as WOB is increased. ROP passes an inflection point and begins to increase at a decreasing rate [40]. This happens due to the fact that the first term of the model ($aS^2{d_b}^3/N^b WOB^2$) is predominant at low ROP values and the second term (c/Nd_b) is predominant at higher ROP values.

Imperfect-Cleaning Model

Warren developed the initial perfect-cleaning model to simplify the complex modelling that is required to develop a good predictable ROP model. The initial "perfect-cleaning" model has then been modified in 1987 by Warren [40] to account for more realistic, imperfect-cleaning drilling conditions.

The idea is that under steady-state drilling conditions, the rate of cutting removal from the bit is equal to the rate at which new cuttings are formed. This infers that the rate of penetration is affected by the cutting generation process, the cutting removal process, or a combination of both [40]. Warren used dimensional analysis to isolate variables consisting of the modified impact force (F_{jm}) and mud properties. These were incorporated into the perfect-cleaning model in Eq. (2.11) to account for cutting removal [24]. This results in the following imperfect-cleaning model:

$$ROP = \left(\frac{aS^2{d_b}^3}{NWOB^2} + \frac{b}{Nd_b} + \frac{cd_b\gamma_f\mu}{F_{jm}}\right)^{-1} \tag{2.12}$$

Here the constants (a, b and c) are the bit constants in penetration model. The modified impact force (F_{jm}) is given as:

$$F_{jm} = \left(1 - {A_v}^{-0.122}\right)F_j \tag{2.13}$$

Where the ratio of jet velocity to return velocity (A_v) and (F_j) are given in field units as:

$$F_j = 0.000516\rho q v_n \tag{2.14}$$

$$A_v = \frac{v_n}{v_f} = \frac{0.15{d_b}^2}{3{d_n}^2} \tag{2.15}$$

2.4.4 Modified Warren Model

There are many processes and actions that occur during the drilling operation with a significant impact on the penetration rate. It's difficult to completely model the ROP with all the factors and conditions affecting the penetration process. However, an attempt was made to improve the model presented by Warren by addressing more quantifiable conditions and effects in the model.

Addressing chip hold down effect

"Chip hold down effect" was not addressed in the ROP model presented by Warren (1987) in spite of its importance and impact on the ROP [52, 53]. In 1993, Hareland and Hoberock [52] modified Warren's model by addressing chip hold down effects. This was done using data from laboratory full-scale drilling tests. The tests were performed by varying the bottom-hole pressure while other conditions remained constant. The resultant "chip hold down function" ($f_c(P_e)$) is given by:

$$f_c(P_e) = c_c + a_c(P_e - 120)^{b_c} \tag{2.16}$$

Where (a_c, b_c and c_c) are lithology dependent constants and (P_e) is the differential pressure. Units on (a_c, b_c and c_c) where chosen such that ($f_c(P_e)$) is dimensionless [24]. The resultant modified equation including "chip hold down effect" is given by:

$$ROP = \left[f_c(P_e)\left(\frac{aS^2{d_b}^3}{NWOB^2} + \frac{b}{Nd_b}\right) + \frac{cd_b\gamma_f\mu}{F_{jm}}\right]^{-1} \tag{2.17}$$

Addressing bit wear effect

Hareland and Hoberock [52] also included bit wear effect to strengthen Warren's model. Bit wear has a negative impact on drilling process by reducing the rate of penetration. Hareland and Hoberock modified Warren's ROP model to account for bit wear effect by introducing a wear function (W_f) into the model [24]:

$$ROP = W_f\left[f_c(P_e)\left(\frac{aS^2{d_b}^3}{NWOB^2} + \frac{b}{Nd_b}\right) + \frac{cd_b\gamma_f\mu}{F_{jm}}\right]^{-1} \tag{2.18}$$

The wear function (W_f) is given by:

$$W_f = 1 - \frac{\Delta BG}{8} \tag{2.19}$$

Where (ΔBG) represents the change in bit tooth wear and is given as: ($\Delta BG = W_c \sum_{i=1}^{A} WOB_i * RPM_i * Ar_{abr_i} * S_i$). Here ($S$) is the rock compressive strength which is a function of rock lithology and confining pressure, given by: ($S = S_o\left(1 + a_s {P_e}^{bs}\right)$) [54].

2.4.5 Real-Time Bit Wear Model

In 2008, Rashidi, Hareland and Nygaard [46] developed a new real-time bit wear model based on two approaches for drilling optimization, which are: Bourgoyne and Young [28] ROP model and Teale's [2] Mechanical specific energy concept. The eight functions in Bourgoyne and Young model (from Appendix I) can be inverted to obtain the formation drillability function (f_1). Details of the model are available in Appendix I.

2.4.6 Hareland and Rampersad Model

The Hareland and Rampersad developed a model that predicts the ROP for drag bits for full efficient bit cleaning. This model takes into account the bit geometry, blade geometry and bit wear which in turn takes into account the applied WOB, RPM and rock strength at a depth of drilling [30, 55]. More details are presented in Appendix I.

2.4.7 Maurer Model

In 1962, Maurer [7] has developed a theoretical model for roller-cone bits that relates ROP to WOB, rotational speed (RPM) rock strength and bit size. This model was derived assuming a perfect bottomhole cleaning condition with an incomplete bit tooth. The model was developed based on observations made in single-insert impact experiments, which are [45, 56]:

- The crater volume produced (V_c) in rock is proportional to the square of the depth of penetration (X) (i.e. $V_c \propto X^2$).
- With constant force on the tooth, the depth of penetration (X) is inversely proportional to the rock strength (S) (i.e. $X \propto 1/S$).

More details are available in Appendix I.

2.4.8 Bingham Model

The Bingham model is a simple modified version of Maurer model which is applicable for low WOB and rotational speed (N) [45, 57]. More details of the model are available in Appendix I.

2.5 Drillability D-Exponent

Detection of over-pressured zones using the ROP is difficult to apply in practice. This is due to the influence of several other factors on ROP apart from formation pressure, such as WOB, bit properties, rotary speed, mud properties, pump rate and many others. In order to improve interpretation of drilling rate and improve its detection of formation pressure and over-pressured zones, a direct relationship between ROP and formation pressure should be established. This was achieved by normalizing ROP for the variations in drilling parameters. The D-exponent is an example of such normalized ROP [58, 59].

In 1964, Bingham developed a model for D-exponent to improve drilling rate's detection of over-pressured zones. This model is formulated in the following generalized equation [60]:

$$ROP = A_M N^E \left(\frac{WOB}{d_b}\right)^{d_{exp}} \tag{2.20}$$

Here (A_M) is the rock matrix strength constant and (E) is the rotary speed exponent.
Jorden and Shirley [61] simplified Bingham's model in 1966 by assuming that the rock matrix strength constant remained unchanged to be equal to one (i.e. A_M = 1) and the rotary speed exponent was equal to one (i.e. E = 1). Based on these assumptions, Eq. (2.20) is reorganized for the D-exponent resulting in the following modified equation [58]:

$$d_{exp} = \frac{\log\left(\frac{ROP}{60\,N}\right)}{\log\left(\frac{12\,WOB}{10^6 d_b}\right)} \tag{2.21}$$

The D-exponent is proportional to rock strength and increases linearly with depth for normally pressured formations. However, it decreases with depth for abnormally pressurized formations (shales), while ROP tends to increase in this interval if all other drilling parameters remain unchanged. Fig. 7 [62] shows a plot of ROP and the D-exponent as a function of depth and the effect of overpressure on them. This is because as the bit drills through the over-pressured zone, the rock becomes less dense and more porous, resulting in increased Drillability of the formation. ROP also increases due to reduced pressure differential between the drilling fluid and formation pressure [59, 62, 63].

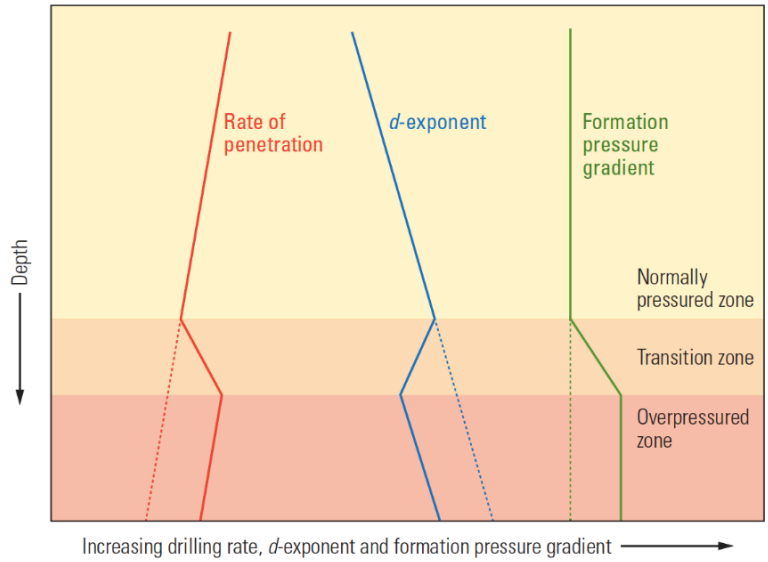

Fig. 7. Overpressure effect on D-exponent and ROP [62].

The D-exponent in Eq. (2.21) corrects the ROP to changes in WOB, RPM and hole-size. In 1971, Rehm et al. [63] developed an equation that corrects the D-exponent for the changes in mud weight given by:

$$d_c = d_{exp}\left(\frac{NPP}{ECD}\right) \tag{2.22}$$

Where (d_c) is the corrected D-exponent, NPP is the normal pore pressure gradient and ECD is the equivalent circulating density. The corrected D-exponent is more sensitive to changes in both pore pressure and mud weight. The correction equation has no theoretical derivation. Nevertheless, it is globally used due to the conservative calculations it provides for mud weight changes (overbalance drilling process) [59].

Every method has its advantages and limitations. The same thing applies for the D-exponent. It is an efficient way to calculate the pressure in clean shells pore or clean argillaceous. Limitations of using the method of D-exponent is that it only can be used for this purpose. In addition, in a situation of an increase in mud weight, the value of (d_c) can be reduced because of large increase in mud weigh that may take a place during calculations. This method is also affected by other factors that can narrow its functions, just like the lithology, poor hydraulics, bit type, bit wear, motor or turbine runs and unconformities in the formation [59].

Chapter 3

Modelling Implementation and Workflow

Having an existing drilled well information, helps a lot when planning to drill a new well next to it. In this thesis, predicting the rate of penetration is the main tool in order to accomplish a successful drilling operation. Using the well data of pre-drilled wells helps in obtaining the drilling optimization by reducing costs and time of the drilling operation. The process of analyzing the drilling parameters and factors from previous experiences makes the drilling process faster and efficient when drilling in the same geology.

ROP modelling is the main focus of this thesis work. The methods to be implemented by estimating model fitting parameters from old well and apply these parameters for other wells to predict their ROP. These predicted ROP profiles will then be compared with the actual collected profiles. The ROP model is based on applying the techniques of multiple regression and other methods on the collected drilling data. It is worth mentioning that some of the methods applied in this thesis have been applied before by Morten Adamsen Husvæg on other fields on the NCS [10].

3.1 Wells Used for Modelling

By e-mail communication with the Norwegian Petroleum Directorate, particularly Svein Finnestad [64], the required data was collected from the North Sea. These data are in the form of well reports and mud log reports. Three different fields were used for modelling and testing; Alvheim, Kvitebjørn and Valhall. A basemap of the three fields is provided in Fig. 8. The data used are logged for every 5-meter depth and have been converted to Microsoft Excel format.

The more data we model, compare and test, the more reliable models we can provide. Six wells are therefore modelled and tested in this thesis to verify the applicability of the models both locally and on a distant; three of them (24/6-B-1, 24/6-B-4 and 24/6-B-5) are located next to each other in Alvheim field, two of them (34/11-A-4 and 34/11-A-5) are located in the nearby field Kvitebjørn and one well is called 2/11-S-10 and located in the remote field Valhall. The last mentioned well is used to verify the model on a distant well. Further information about wells is provided in Table 1.

Several methods are tested and discussed in this chapter in order to obtain best predicted rate of penetration. These methods are progressed by the Warren model and the methods of multiple regression, least squares, MSE and D-exponent.

Table 1. Well data [65].

Well name		Total depth (MD) [ft RKB]	Total depth (TVD) [ft RKB]	Classification	Operator	Well path	Field	Kelly bushing elevation [ft]	Water depth [ft]
Reference well 24/6-B-4 ⚑	Pilot 24/6-B-4 H	10 270	7 014	Pilot	Marathon	Deviated	Alvheim	82	404
	Mainbore AY1H	18 442	7 076	Producer					
	Lateral AY2H	19 240	7 075						
24/6-B-1	Mainbore AY1H	9 826	7 443	Observation	Marathon	Deviated	Alvheim	75	407
	Lateral AY2H	10 072	7 476						
	BH	10 660	7 440						
	CH	15 633	6 962	Producer					
24/6-B-5	Pilot 24/6-B-5 H	10 970	7 211	Pilot	Marathon	Deviated	Alvheim	85	407
	Mainbore AY1H	16 394	7 080	Producer					
	Lateral AY2H	17 280	7 080						
	Lateral AY3H	18 550	7 077						
34/11-A-4		14 865	13 950	Producer	Statoil	Deviated	Kvitebjørn	198	623
34/11-A-5		14 232	13 790	Producer	Statoil	Deviated	Kvitebjørn	198	623
2/11-S-10		17 126	8 410	Producer	BP	Deviated	Valhall	194	219

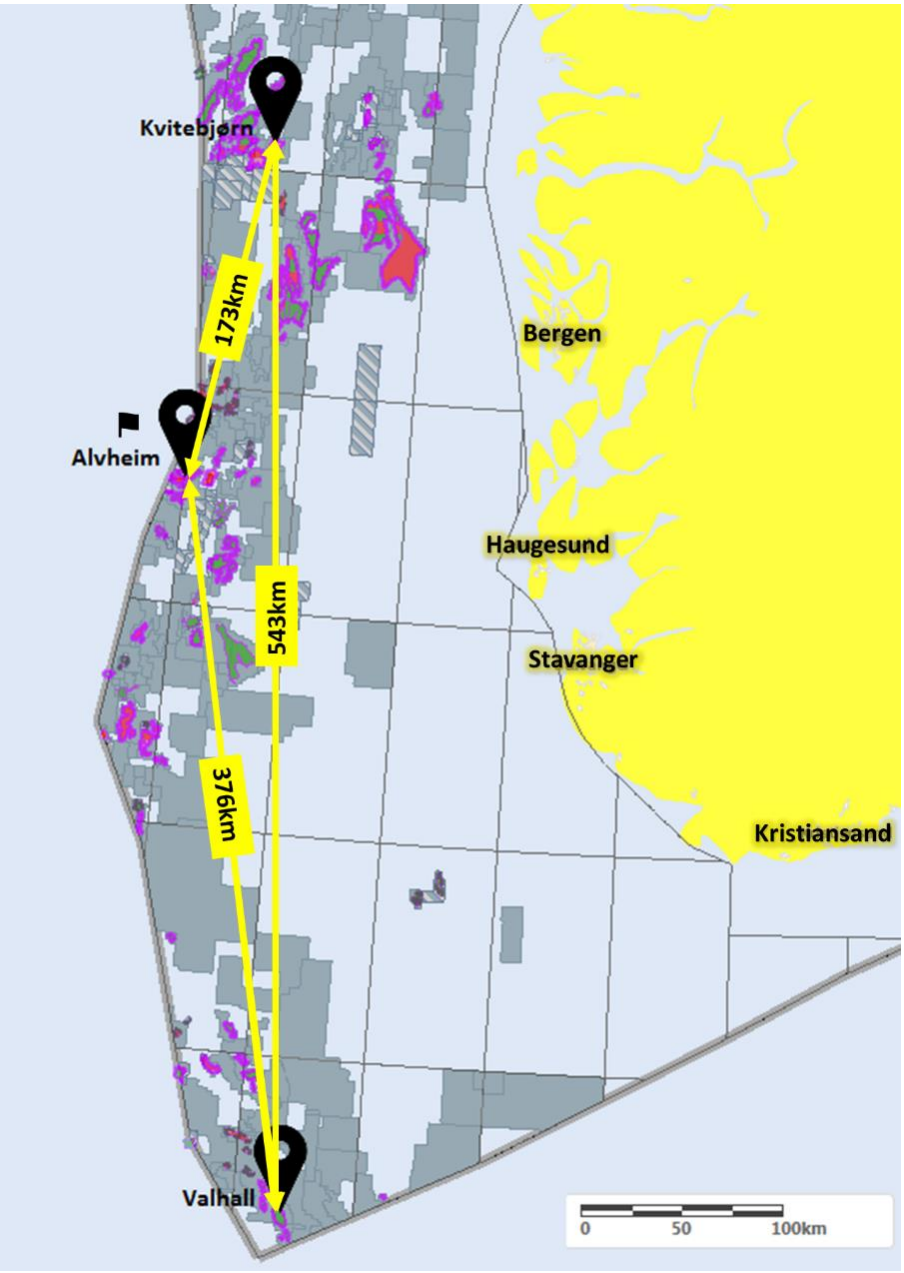

Fig. 8. Basemap of the three fields [66].

3.2 Multiple Regression Workflow

Regression analysis is used to estimate the relationships among one dependent and two or more independent variables [17]. This method of data analysis is useful when examining a quantitative variable in relation to other factors. The Multivariate analysis describes an observation factor by having several variables, taking into consideration all changes of properties that may happen simultaneously. I.e. the multiple regression equation of (Y) factor on variables ($X_1, X_2, \ldots, X_n$) is given by [67-69]:

$$Y = \beta_0 + \beta_1 X_1 + \beta_2 X_2 + \beta_3 X_3 + \cdots + \beta_n X_n \tag{3.1}$$

Where Y is the dependet variable, β_0 is the intercept term and the regression coefficients (β_1, β_2, …, β_n) are the analogues to the slope in linear regression equation.

The rate of penetration is based on several different variables. Based on Eq. (3.1), the ROP would be referred to it as the factor of observation (Y) in this thesis. The (Y) value is based in its turn on several properties simultaneously, in addition to the drilling operational factors. Relevant drilling parameters make up the regression variables (X_{1-5}). By having these values in a Microsoft Excel sheet and by processing the regression data analysis, we will end up with the values of the coefficients (b_{0-5}). Now, by having the values of the coefficients, we will be able to estimate the (Y) value.

This analysis is done for the reservoir section (e.g. the 8.5" hole section) of well 24/6-B-4. The data used in multiple regression analysis are in the form of WOB, torque, RPM, modified jet impact force (F_{jm}) and formation pressure, together with the observation factor ROP.

A parametric sensitivity analysis is preformed later in this thesis to find out which parameters have a greater impact on the ROP model. The modified jet impact force (F_{jm}) given in Eq. (2.13) was therefore chosen to replace the Flowrate and the stand pipe pressure (SPP) in the model. This is due to the ability to control this parameter if it is proven to affect the ROP.

The implementation of this method in Microsoft Excel software is presented in Appendix II to give a better explanation. The regression data analysis is first performed. As described above, the (Y) range represents the ROP, while (X) range is the remaining data. The depth on the other hand, is only included as a reference and is not included in the analysis. The coefficients, which is the area of interest, are then provided by the analysis. The intercept value is represented by the initial value of coefficients (b_0). The other coefficients (b_{1-5}) are then multiplied according to their order with the regression variables (X_{1-5}). Eq. (3.2) is used to model the ROP and is given by:

$$Y = b_0 + b_1X_1 + b_2X_2 + b_3X_3 + b_4X_4 + b_5X_5 \tag{3.2}$$

This equation can also be written in terms of ROP and the other drilling parameters as:

$$Modelled\ ROP = b_0 + b_1WOB + b_2Torque + b_3RPM + b_4F_{jm} + b_5FP \tag{3.3}$$

The multiple regression procedure shown in Fig. 9 is applied on both the first and second hypothesis. In the first hypothesis, the multiple regression procedure is applied on the reservoir section of the reference well 24/6-B-4, providing the six coefficients (b_{0-5}). By using Eq. (3.3), the coefficients are then implemented to the overburden section of well 24/6-B-4 in order to predict the ROP. The coefficients are then implemented to both overburden and reservoir sections of the other nearby wells. In the second hypothesis, the multiple regression procedure is applied on the whole wellbore section of the reference well 24/6-B-4, providing six other coefficients (b_{0-5}). By using Eq. (3.3), the coefficients are then implemented to the other nearby wells.

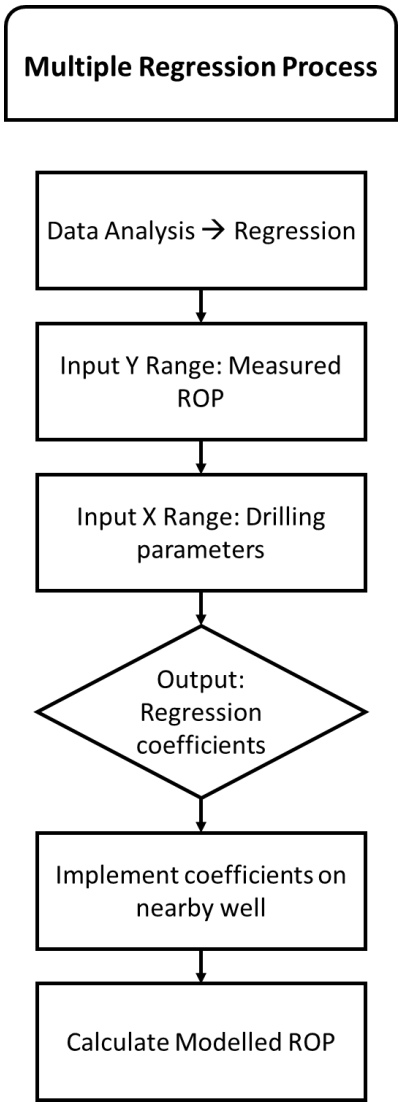

Fig. 9. Multiple Regression process flowchart [10].

3.3 The Method of Least Squares Workflow

The method of least squares is the relevant used approach in regression analysis, which reduces the residual sum between predicted and observed values [70]. This method can be mathematically expressed by the following equation:

$$R^2 = \sum [Y_i - f(X_i, \beta_1, \beta_2, \dots, \beta_{\mathrm{n}})]^2 \tag{3.4}$$

Where (R^2) is the sum of the error squared of a set of n data points from a function f [71]. (Y_i) is the observed output, (X_i) are the coefficients values, and the function $f(X_i, \beta_1, \beta_2, \dots, \beta_{\mathrm{n}})$ is the predicted output [70].

This method is applied to model ROP. The coefficients predicted from the analysis will be applied to the nearby/remote wells. The observed factor (Y_i) and the factor to be predicted are the penetration rate in this case. Eq. (3.4) can be expressed as:

$$\text{Sum of error squared} = \sum_{i=1}^{n} \left[ROP_{predicted} - ROP_{observed}\right]^2 \tag{3.5}$$

Where ($ROP_{predicted}$) is the modelled ROP shown in Eq. (3.3).

The same collected well data is used again. The error squared is first calculated by squaring the difference between the predicted ROP and the actual ROP. This is done for each depth point. These are then summed up using Eq. (3.5) to give the sum of error squared. The Microsoft Excel's solver add-in is then used to minimize the sum of error squared resulting in newly computed coefficients (b_{0-5}).

The newly computed coefficients can now be used in Eq. (3.3) to model the ROP with minimized error. The workflow of this method is presented in Fig. 10 [10].

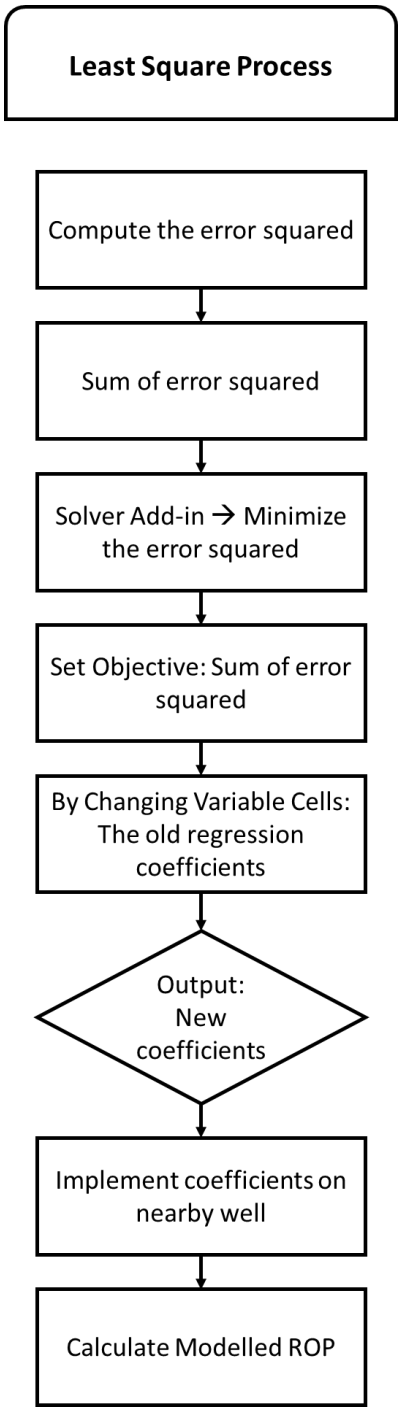

Fig. 10. Least squares process flowchart [10].

3.4 MSE - Mechanical Specific Energy Workflow

The MSE model is one of the methods used in this thesis. It quantifies the amount of energy required to drill a given volume of rock.

As mentioned before, the MSE of existing nearby wells can be used to calculate the ROP. The technique developed in this thesis assumes that the amount of energy necessary to drill a certain volume of rock is correlative within nearby wells.

The MSE values are first calculated for a well using Eq. (2.6). These values are then implemented to the nearby wells. Eq. (3.6) is derived from Eq. (2.6) below to calculate the ROP values in the neighbouring wells. The MSE based workflow modelling process is presented in Fig. 11 [10].

Eq. (2.6) $\rightarrow$ $1000\ MSE\ {d_b}^2 = \frac{480*T*N}{ROP} + \frac{4\ WOB}{\pi}$

$\rightarrow$ $\frac{480*T*N}{ROP} = 1000\ MSE\ {d_b}^2 - \frac{4\ WOB}{\pi}$ $\rightarrow$ $\frac{1}{ROP} = \frac{1000\ MSE\ {d_b}^2 - 4\ WOB/\pi}{480*T*N}$

$$\rightarrow \quad ROP = \left[\frac{1000\ MSE\ {d_b}^2 - 4\ WOB/\pi}{480 * T * N}\right]^{-1} \tag{3.6}$$

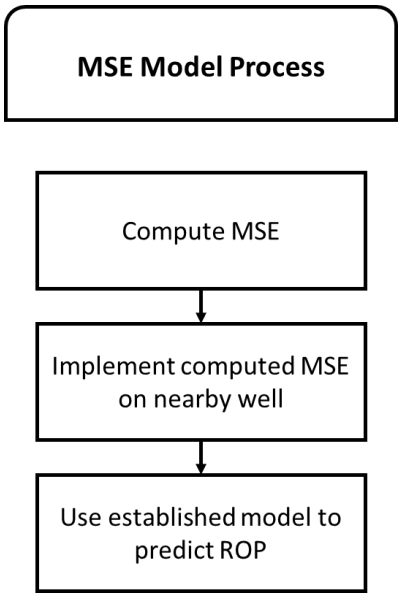

Fig. 11. MSE model process flowchart [10].

3.5 Drillability D-Exponent Workflow

The drillability D-exponent is one of the methods used to calculate the ROP. It normalizes the ROP for the variations in drilling parameters. The drillability D-exponent is given in Eq. (2.21). A corrected equation that corrects the D-exponent for the changes in mud weight was later developed by Rehm et al. [63]. This corrected D-exponent requires ECD values as shown in Eq. (2.22).

However, The ECD values are not available in the data, Eq. (2.21) is used therefore in this thesis. The D-exponent modelling technique assumes that the drillability of a well is correlative within nearby wells.

The D-exponent values are first calculated for a well using Eq. (2.21). These values are then implemented to the nearby wells. Eq. (3.7) is used to predict the ROP profiled in the adjacent wells. The D-exponent modelling workflow process is illustrated in Fig. 12 [10].

Eq. (2.21) → $\log\left(\frac{ROP}{60\,N}\right) = d_{exp} * \log\left(\frac{12\,WOB}{10^6 d_b}\right)$

→ $\log ROP = d_{exp} * \ log\left(\frac{12\,WOB}{10^6 d_b}\right) + \log 60\,N$

→ $ROP = 10^{d_{exp} * log\left(\frac{12\,WOB}{10^6 d_b}\right) + \log 60\,N}$ (3.7)

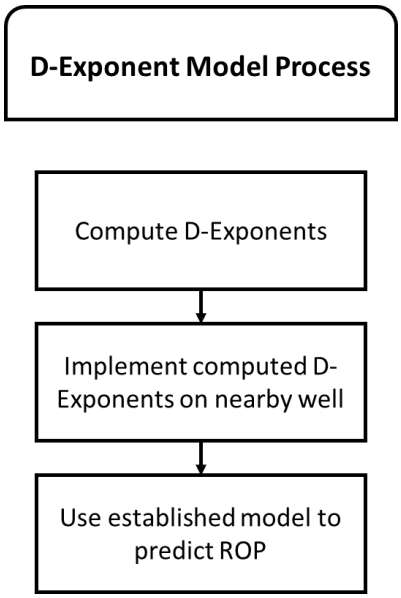

Fig. 12. D-exponent process flowchart [10].

3.6 Warren Model Workflow

Warren's model introduced in chapter 2.4.2 relates ROP to:

- Rock strength
- WOB
- Rotary speed (N)
- Bit type
- Bit size (d_b)
- Modified jet impact force (F_{jm})

Rock strength has first to be calculated. In order to do this, the following assumption is made. Based on Teale's formula introduced in chapter 2.4.1, it was mentioned that the formula assumes that MSE equals the rock compressive strength at perfect efficiency. However, as shown in Fig. 6 [44], the efficiency of drill bits at peak performance usually occurs in order of 30-40%. The rock compressive strength (UCS) is therefore assumed to equal 35% of the MSE value.

Warren model introduced in Eq. (2.12) can be expressed as:

$$\left(\frac{S^2{d_b}^3}{NWOB^2}ROP\right)a+\left(\frac{1}{Nd_b}ROP\right)b+\left(\frac{d_b\gamma_f\mu}{F_{jm}}ROP\right)c=1 \tag{3.8}$$

The first term $\left(\frac{S^2{d_b}^3}{NWOB^2}ROP\right)$, the second term $\left(\frac{1}{Nd_b}ROP\right)$ and the third term $\left(\frac{d_b\gamma_f\mu}{F_{jm}}ROP\right)$ of Eq. (3.8) are calculated in Microsoft Excel software. The implementation of this method in Microsoft Excel software is available in Appendix II, which gives a better explanation. Eq. (3.8) can be expressed in matrix form as:

$$\mathrm{AX}=\mathrm{B} \tag{3.9}$$

or

$$\begin{bmatrix}x_1 & y_1 & z_1\\ x_2 & y_2 & z_2\\ \vdots & \vdots & \vdots\\ x_n & y_n & z_n\end{bmatrix}\begin{bmatrix}a\\ b\\ c\end{bmatrix}=\begin{bmatrix}1\\ 1\\ \vdots\\ 1\end{bmatrix} \tag{3.10}$$

Where x, y and z are the first, the second and the third terms respectively.

Eq. (3.10) is then solved for vector X in MATLAB software to compute Warren constants a, b and c. Warren ROP can then be calculated using the following equation:

$$\text{Warren } ROP = \frac{ROP}{\left(\frac{S^2 {d_b}^3}{NWOB^2} ROP\right) a + \left(\frac{1}{N d_b} ROP\right) b + \left(\frac{d_b \gamma_f \mu}{F_{jm}} ROP\right) c} \tag{3.11}$$

Warren model process flowchart is presented in Fig. 13.

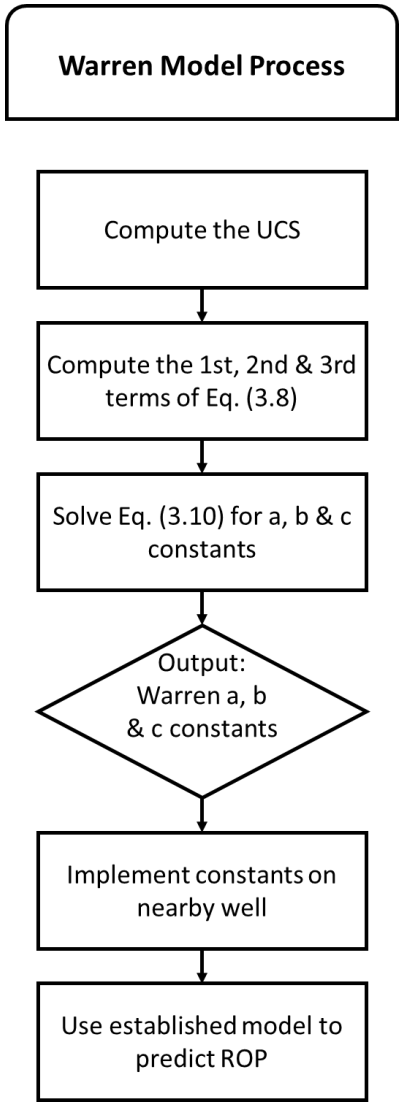

Fig. 13. Warren model process flowchart (this thesis work).

Chapter 4

ROP Modelling and Testing Results

The details of ROP modelling and analysis results are presented in this chapter. The stratigraphic correlation of the wells is first constructed to clarify the geological similarities of the sedimentary facies. The implementation results of the five methods discussed in chapter 3 are then presented. Moreover, the predicted ROP profiles of the drilling section are compared with their corresponding ROP field data. The actual ROP is always plotted in grey in this chapter.

The Alvheim well 24/6-B-4 is chosen to be the reference well. By using the multiple regression analysis, a single-well based model is developed from the reference well data based on two hypotheses. In the first hypothesis, the ROP model is developed based on the data of the reservoir section of the reference well. While the ROP model is developed based on the data of the whole wellbore section of the reference well in the second hypothesis. In order to obtain the ROP and implement the developed model, well-to-well correlation procedure and the drilling data of the new well to-be-drilled will facilitate the mission.

The model will then be tested on three different fields to verify it. It will first be tested locally on the remaining Alvheim wells (i.e. wells 24/6-B-1 and 24/6-B-5) and the Kvitebjørn wells (i.e. wells 34/11-A-4 and 34/11-A-5). The model will then be tested on a remote well located in the Valhall field (i.e. well 2/11-S-10).

Having variety of data of three different fields with several wells will support the results of testing out the ROP models. This variety of data leads to greater accuracy in results-based conclusions.

4.1 Stratigraphic Correlation

To study the lateral geological features among the considered wells in this thesis work, a stratigraphic correlation is performed to compare rock sequences which cross through the wells used in this thesis. This process attempts to establish a stratigraphic correlation between different wells from different areas based on either the type of deposited material or the depositional time of material [72, 73].

Petrel software is used to establish the stratigraphic relationships between the Alvheim, Kvitebjørn and Valhall fields. This will help in general understanding how the geology varies locally and regionally. In return, this can be used to analyze the performance of the ROP whether or not it is well modelled as well as to investigate the limitations of the model application.

The three fields are located in the Deep Cretaceous basin, but part of the Valhall field is located in the Cretaceous High stratigraphy. Unfortunately, only five of the wells are included in this analysis due to lack of lithology data of well 34/11-A-5. The generated stratigraphic correlation is displayed in Fig. 14. The main observations obtained from Fig. 14 are summarized as:

- List of stratigraphic sequences that cross through all five wells:
  - **Hordaland group:** the depth of this group varies significantly across the five wells between 2150 and 5600 ft.
  - **Balder formation:** this formation is located at approximately the same depth for the four wells from Alvheim and Kvitebjørn fields at about 6300 ft, while located at 2200 ft deeper in the Valhall well 2/11-S-10.
  - **Sele formation:** this formation is located at approximately the same depth for the four wells from Alvheim field and Kvitebjørn field at about 6500 ft, while located at 2000 ft deeper in the Valhall well 2/11-S-10.
  - **Lista formation:** this formation is located at approximately the same depth for the four wells from Alvheim field and Kvitebjørn field at about 6700 ft of depth, while located at 1800 ft deeper in the Valhall well 2/11-S-10.

- The Grid, Balder, Balder Tuff, Sele, Lista and Heimdal formations cross through all three Alvheim wells (i.e. 24/6-B-4, 24/6-B-1 and 24/6-B-5) at approximately the same depth. While the depth of the Hordaland formation varies significantly across these three wells between 2150 and 4070 ft.

- The Utsira formation, Lower Hordaland group, Base Grid formation, Shetland group, Tor and Hod formations show discontinuity and appear to cross through only one or two wells.

- The Nordland formation crosses through all wells expect the Alvheim well 24/6-B-5 at a depth of 720 – 5100 ft.

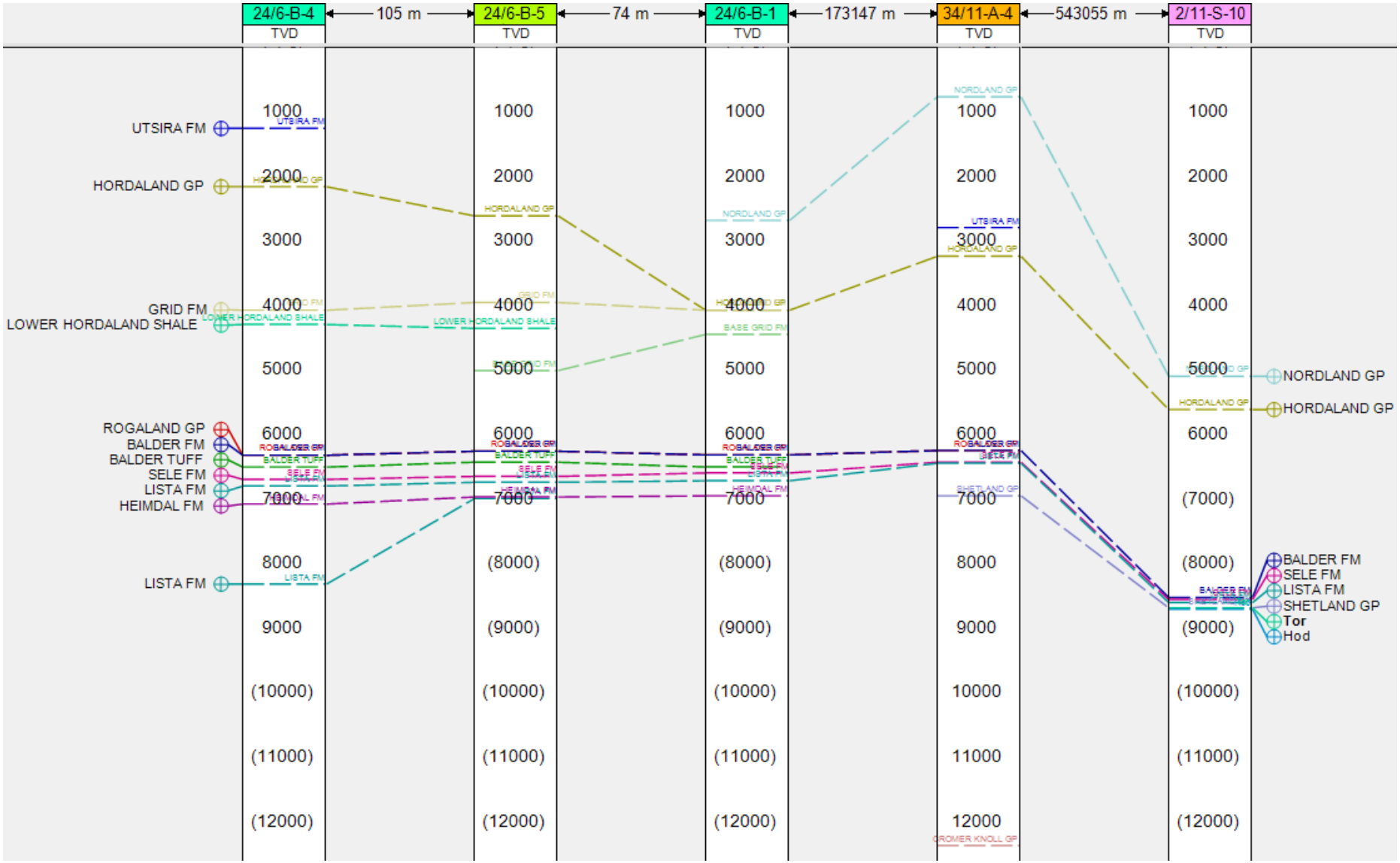

Fig. 14. Stratigraphic Correlation between the wells.

4.2 Multiple Regression

This section presents the multiple regression modelling and application. Fig. 9 shows the details of the modelling workflow. Fig. 15 illustrates a sketch the well 24/6-B-4 (not to the scale), which provides perception about the position/shape of the well. As shown on Fig. 15, the mother pilot well in the Alvheim field is named 24/6-B-4H. This well consists of two branched out wells drilled in the reservoir section one on the top (AY2H), which is considered as the reference well. The second wellbore is right below the reference well in the reservoir section and is called AY1H.

4.2.1 Hypothesis I

According to Hypothesis 1, the reservoir section of the reference well (i.e. AY2H) is modelled by multiple regression technique. The computed curve fitting correlation coefficients are provided in Table 2.

Table 2. Calculated regression coefficients based on hypothesis I.

Well 24/6-B-4 AY2H	Coefficients
Intercept (b0)	- 540.55
X1 (WOB)	0.0041
X2 (Torque)	-0.0011
X3 (RPM)	0.8399
X4 (Fjm)	-3207.86
X5 (FP)	49.33

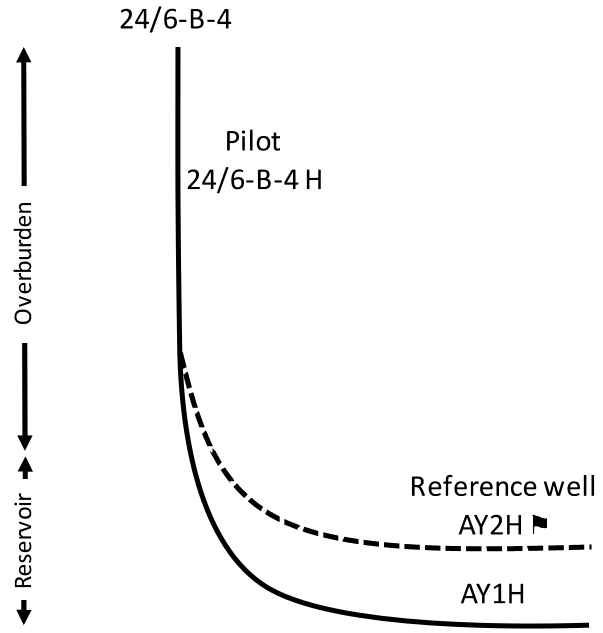

Fig. 15. Sketch of the reference well 24/6-B-4 from the Alvheim field (not-to-scale).

Testing of hypothesis I model on its reference well

Fig. 16 shows the modelled ROP profiles generated by implementing the coefficients from Table 2 on the well where they have been extracted from (i.e. AY2H) and compares with to the actual ROP field data. The result shows excellent match, since the model coefficients are implemented on its original well. The reservoir section model coefficients were then applied on both the branched reservoir (AY1H) and overburden (H) sections of well 24/6-B-4. The modelled ROP and the actual ROP data from the respective wells are presented in Figs. 17 and 18. The results show that the AY2H based model predicts the lower section of the reservoir AY1H data quite good. On the other hand, the most impressive results are those obtained in the overburden section H, where the reservoir based model seems to predict the overburden section data very well.

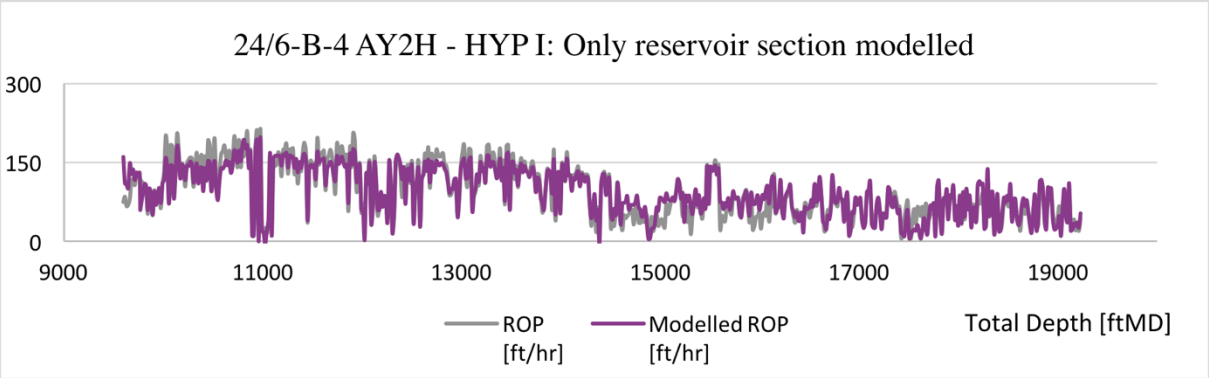

Fig. 16. Multiple regression method applied on well 24/6-B-4 AY2H based on hypothesis I (i.e. method applied only to the reservoir section).

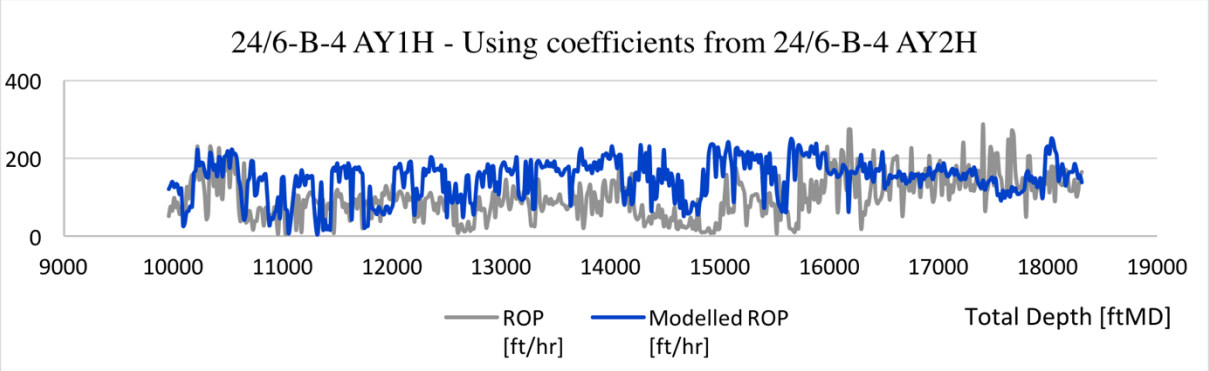

Fig. 17. Multiple regression - 24/6-B-4 AY1H (reservoir section) with coefficients from 24/6-B-4 AY2H.

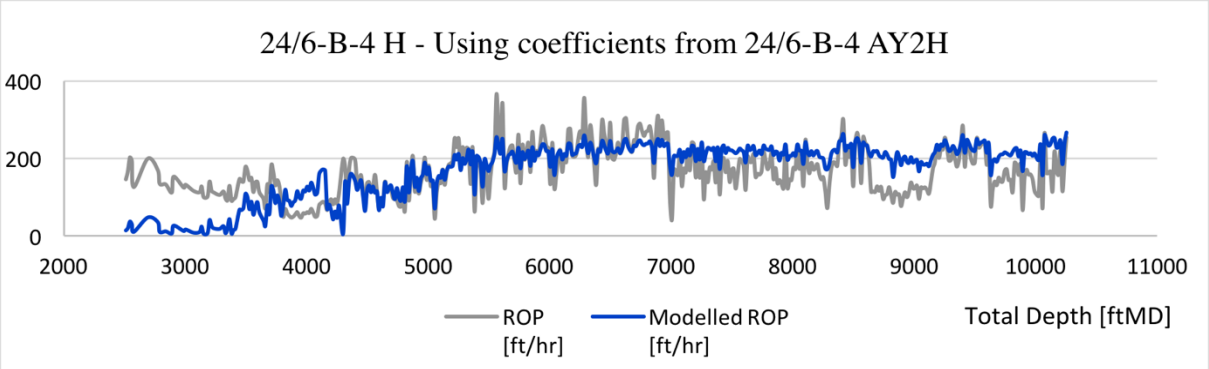

Fig. 18. Multiple regression - 24/6-B-4 H (overburden section) with coefficients from 24/6-B-4 AY2H.

Testing of hypothesis I model on nearby well sections

The coefficients provided in Table 2 are implemented on both reservoirs and overburden sections of the nearby wells. Fig. 19 illustrates the well 24/6-B-1, which is located in the Alvheim field and nearby the reference well 24/6-B-4-AY2H. The well consists of three laterally branched out wells, which are drilled in the reservoir sections.

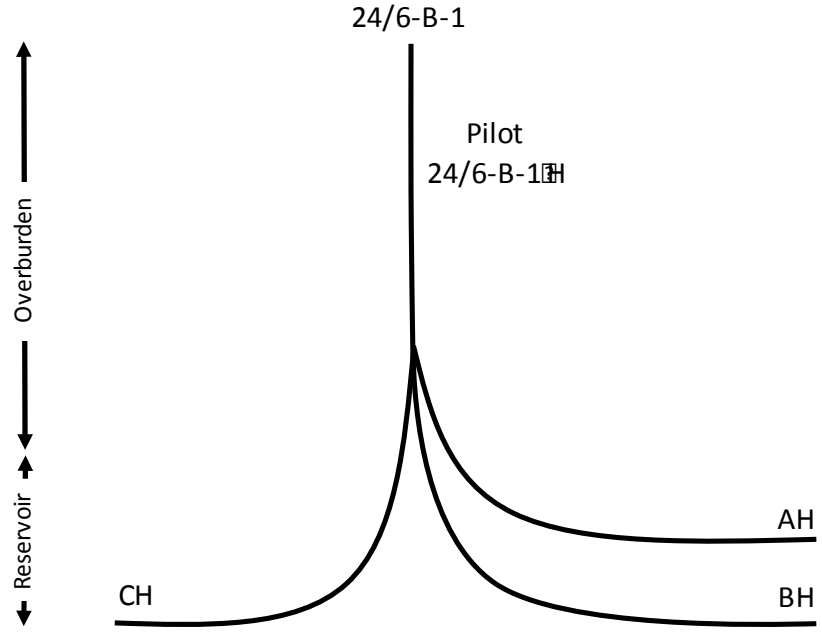

Fig. 19. Sketch of well 24/6-B-1 from the Alvheim field (not to scale).

Fig. 20 shows the reservoir section ROP model prediction and compares it with the measured ROP data of the well 24/6-B-1 AH. Similarly, the other reservoir section wells 24/6-B-1- BH and -CH are displayed on Figs. 21 and 22 respectively. Fig. 23 shows the prediction in the overburden section of the well (i.e well 24/6-B-1 H).

The predicted ROP seems to fit relatively well with the actual ROP, although it deviates in some sections. This well is located on the same block as the reference well, and it is expected to give a good prediction of ROP due to similarities in geological facies. ROP of the reservoir sections AH, BH and CH seems to be poorly modelled in the depth interval [6500, 8300] ftMD.

This could be due to the changes in the geological facies between the well and the reference well shown in Fig. 14 on page 31. The depth of the Hordaland group varies significantly across the wells. However, the overburden section H seems to be well modelled except for the shallower part above 3000 ftMD.

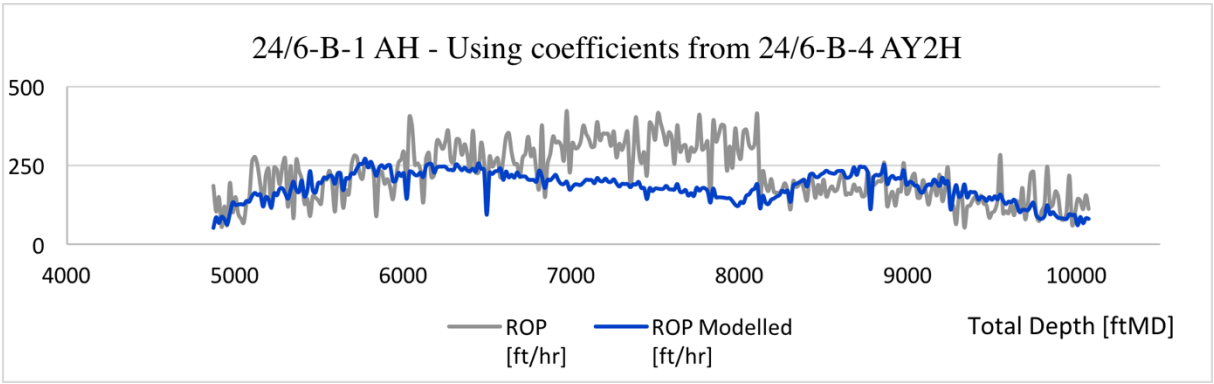

Fig. 20. Multiple regression - 24/6-B-1 AH (reservoir section) with coefficients from 24/6-B-4 AY2H.

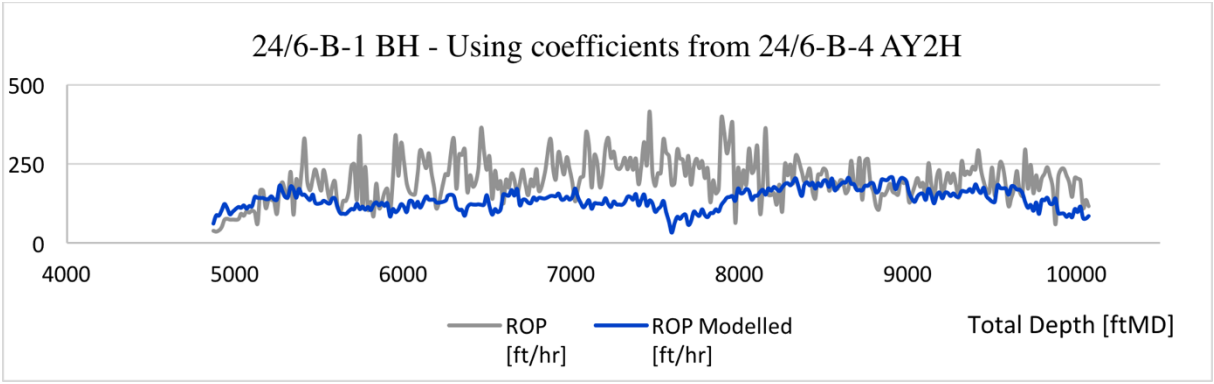

Fig. 21. Multiple regression - 24/6-B-1 BH (reservoir section) with coefficients from 24/6-B-4 AY2H.

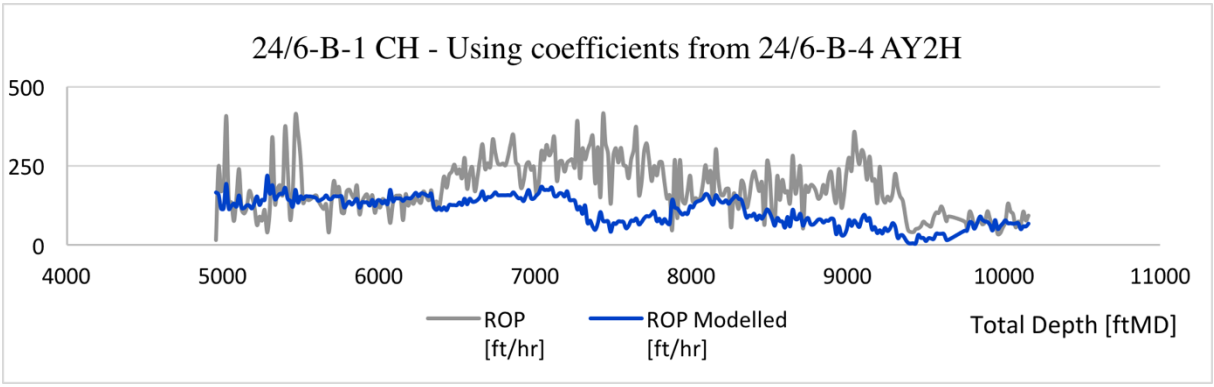

Fig. 22. Multiple regression - 24/6-B-1 CH (reservoir section) with coefficients from 24/6-B-4 AY2H.

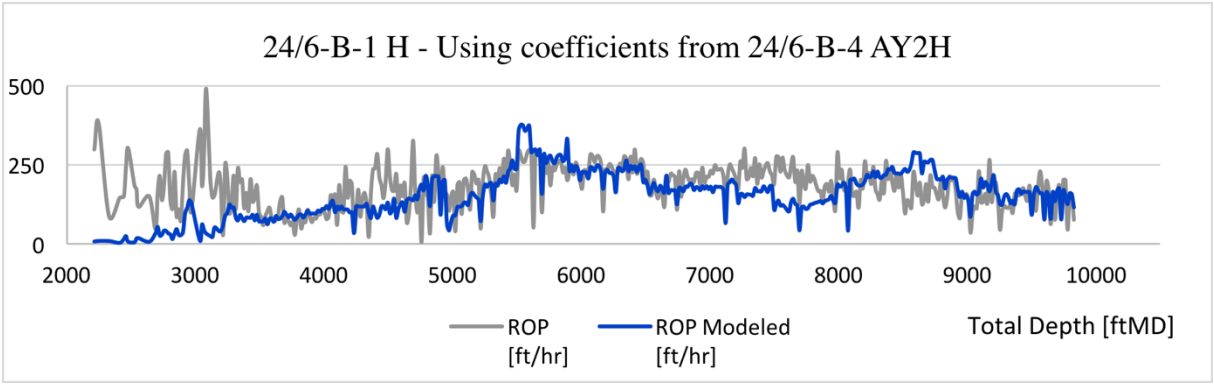

Fig. 23. Multiple regression - 24/6-B-1 H (overburden section) with coefficients from 24/6-B-4 AY2H.

Within Alvheim field, another well, 24/6-B-5 is selected for verification evaluation. The well setup is similar to Fig. 19, which contains three reservoir sections (AY1H, AY2H and AY3H) and an overburden section (H). Fig. 24 illustrates the sketch of the wells. For model prediction, the reference correlation coefficients provided in Table 2 are used here also.

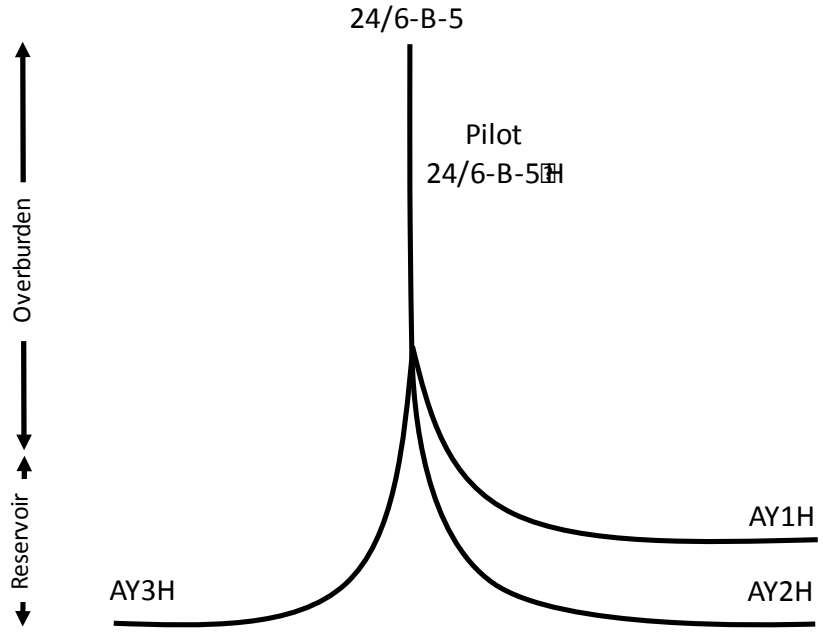

Fig. 24. Sketch of well 24/6-B-5 from the Alvheim field (not to scale).

The comparisons of the predicted ROP and the measured field ROP data of well 24/6-B-5 are displayed in Figs. 25 to 28. Figs. 25 to 27 show the plots of the reservoir sections AY1H, AY2H and AY3H, while Fig. 28 shows the plot for the overburden section H.

The predicted ROP appears to correlate very well with the actual one, although it deviates in some sections. The modelled ROP of the reservoir sections AH, BH and CH seems to correlate quite well with the actual ROP. However, the modelled ROP in the overburden section H deviates from the actual ROP in the depth interval [5500, 10 000] ftMD. This could again be due to the changes in the geological facies between the well and the reference well.

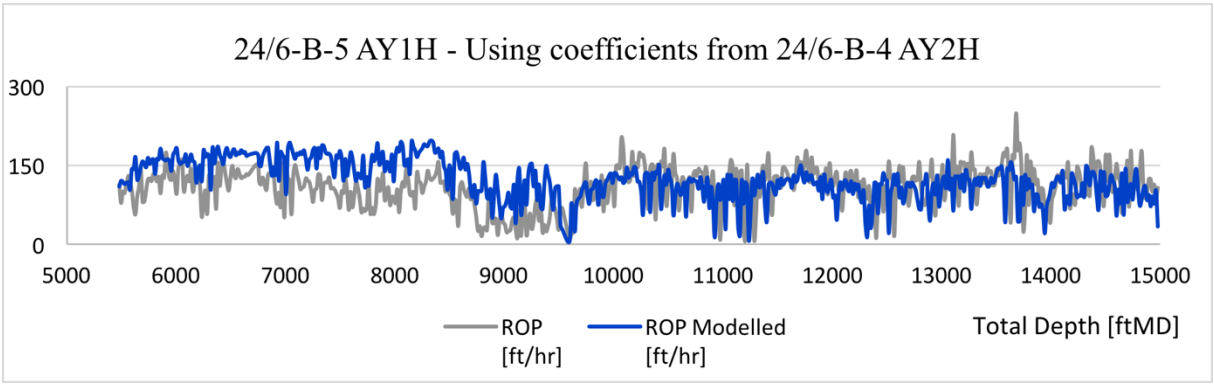

Fig. 25. Multiple regression - 24/6-B-5 AY1H (reservoir section) with coefficients from 24/6-B-4 AY2H.

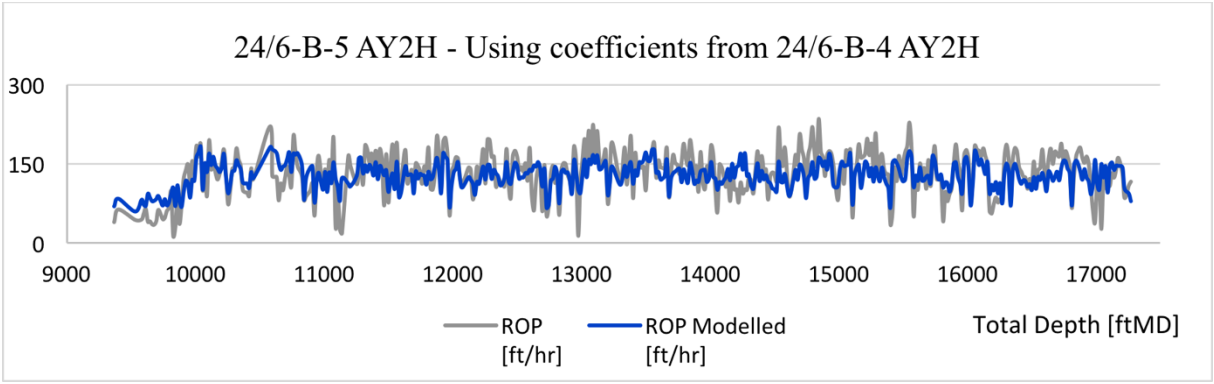

Fig. 26. Multiple regression - 24/6-B-5 AY2H (reservoir section) with coefficients from 24/6-B-4 AY2H.

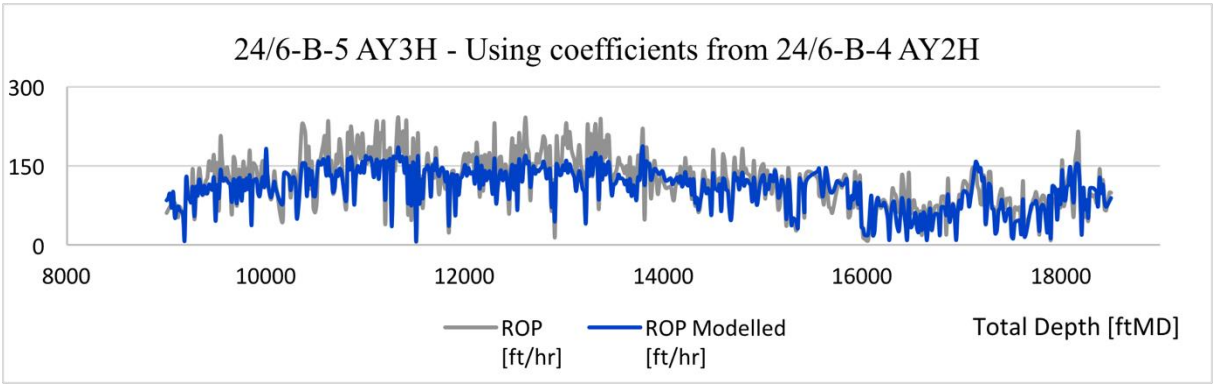

Fig. 27. Multiple regression - 24/6-B-5 AY3H (reservoir section) with coefficients from 24/6-B-4 AY2H.

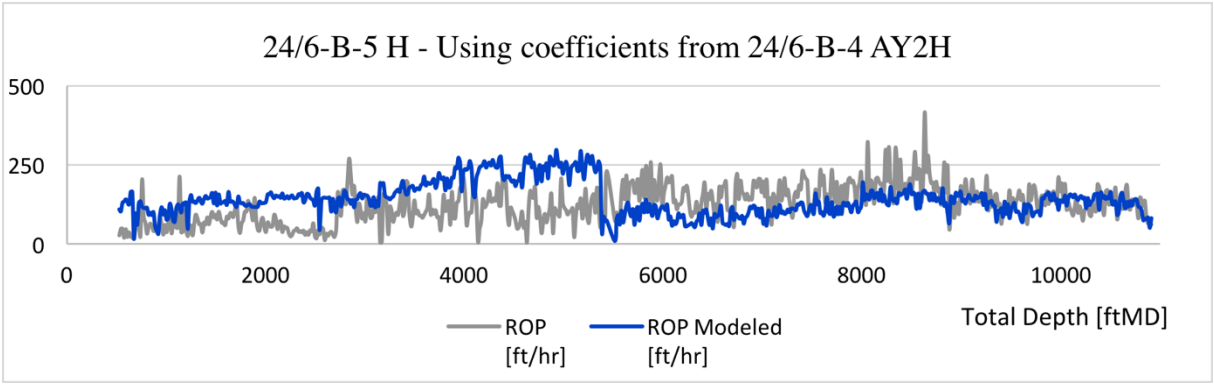

Fig. 28. Multiple regression - 24/6-B-5 H (overburden section) with coefficients from 24/6-B-4 AY2H.

Testing of hypothesis I model on far field wells

The following section presents the modelling results of well 34/11-A-4 in Kvitebjørn field. A sketch of the well is illustrated in Fig. 29.

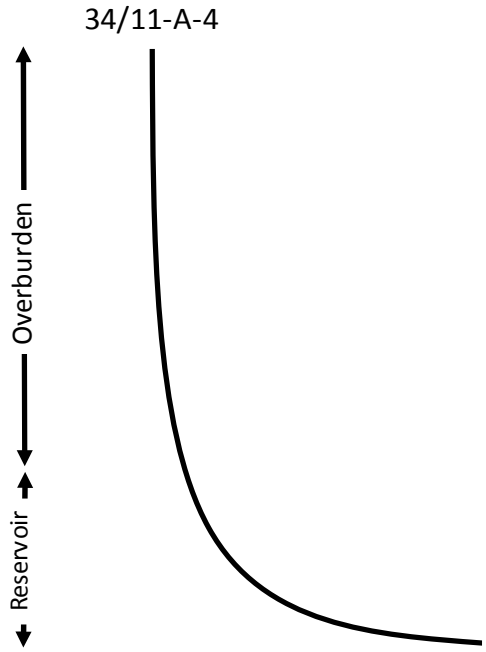

Fig. 29. Sketch of well 34/11-A-4 from the Kvitebjørn field (not to scale).

The modelled ROP results obtained by implementing the reference well coefficients on both reservoir and overburden sections of well 34/11-A-4 are presented in Fig. 30. This Kvitebjørn well is located about 173 km away from the Alvheim reference well as shown in Fig. 8 on page 20. Some changes in the geological facies between the wells can be observed in Fig. 14 on page 31. This explains the reason for the big deviation between the predicted and the actual ROP plots. Another possible reason for the bad results is that the model was established based on the reservoir section of well 24/6-B-4 only. The validity of this reason is confirmed later in this subchapter from hypothesis II, where both of the reservoir and the overburden sections of the reference well are modelled.

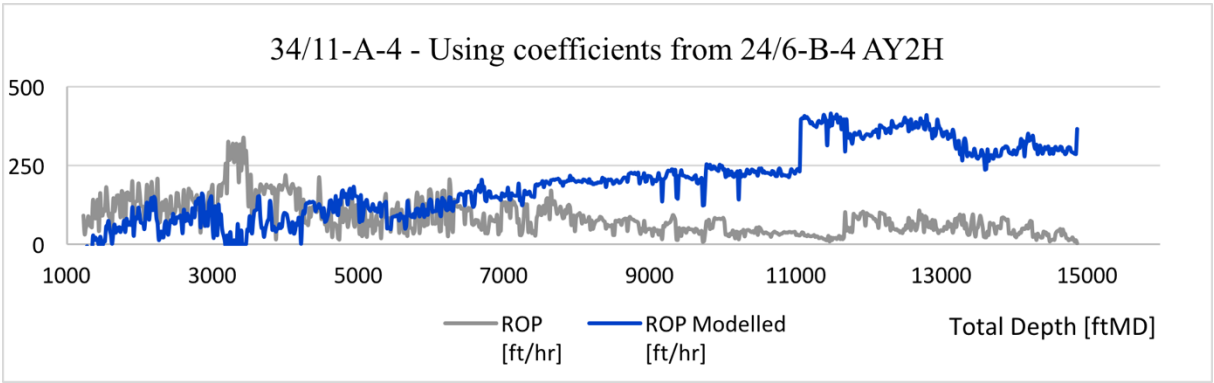

Fig. 30. Multiple regression - 34/11-A-4 with coefficients from 24/6-B-4 AY2H.

Fig. 31 illustrates a sketch of well 34/11-A-5 located in the Kvitebjørn field.

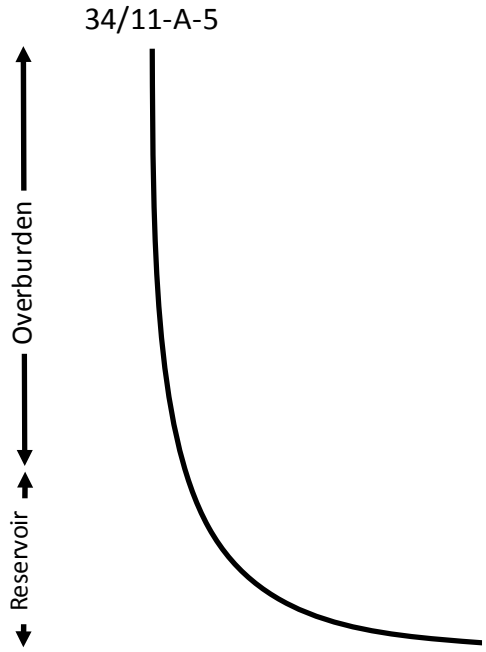

Fig. 31. Sketch of well 34/11-A-5 from the Kvitebjørn field (not to scale).

Fig. 32 shows the predicted ROP of well 34/11-A-5 by applying the coefficients on both the reservoir and the overburden sections. This well is also located in Kvitebjørn field which is located about 173 km away from the Alvheim reference well as shown in Fig. 8 on page 20. The ROP also seems to be poorly modelled at some depth-points. The long distance and remarkable changes in the geological facies between this well and the reference well are the reasons for this inaccuracy of the model

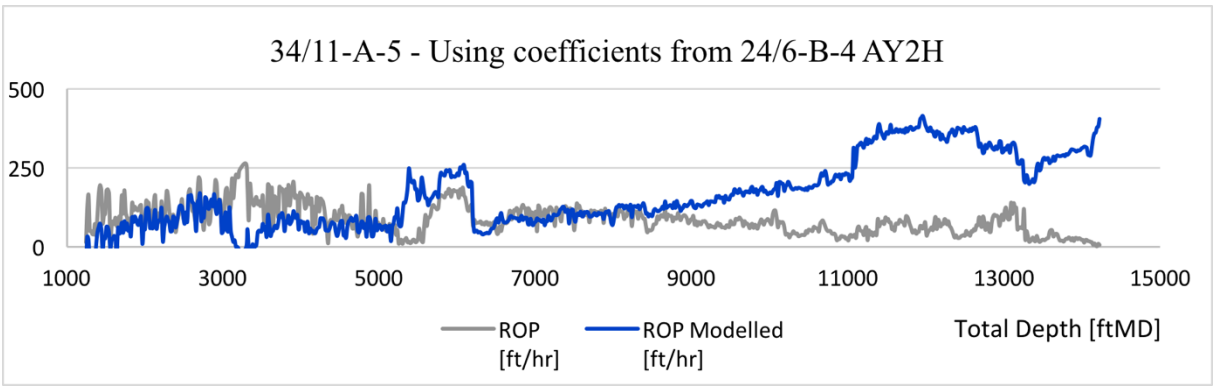

Fig. 32. Multiple regression - 34/11-A-5 with coefficients from 24/6-B-4 AY2H.

Testing of hypothesis I model on very far field wells

As mentioned earlier, the reference well (24/6-B-4 AY2H) is located far away from the Valhall field well (2/11-S-10) on which the reference derived model to be applied. Fig. 33 illustrates the sketch of the well.

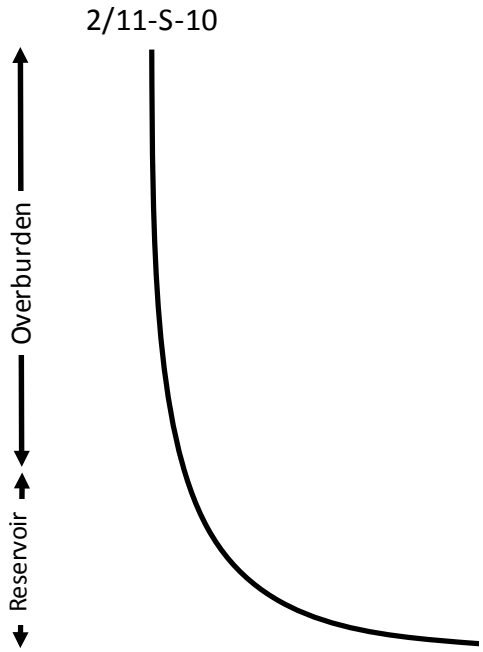

Fig. 33. Sketch of well 2/11-S-10 from the Valhall field (not to scale).

The resulting ROP of applying the coefficients on both reservoirs and overburden sections of well 2/11-S-10 are shown in Fig. 34. This Valhall well is located about 376 km away from the Alvheim reference well as shown in Fig. 8 on page 20. The ROP plot shows fairly good results up to 11 000 ftMD (this corresponds to 8 700 ftTVD). As shown in Fig. 14 on page 31, similarities in geological facies are found in the shallower part of the well which is above 8 700 ftTVD. However, the model appears to predict very poor ROP values after this depth point. This is due to the long distance between the well and the reference.

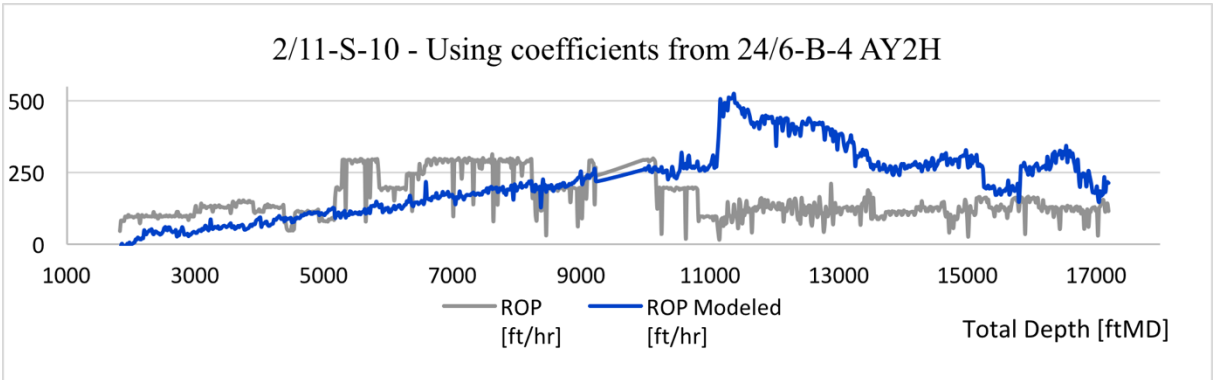

Fig. 34. Multiple regression - 2/11-S-10 with coefficients from 24/6-B-4 AY2H.

4.2.2 Hypothesis II

Hypothesis II modelling approache is based on modelling of the whole wellbore data and application of the model on nearby wells. This has been applied by Morten Adamsen Husvæg (2015) [10].

In Alvheim field, the reference well in this case consists of the overburden and the reservoir section (i.e., 24/6-B-4 H & AY2H). (See Fig. 35). Applying multiple regression technique, the calculated coefficients obtained from the well are provided in Table 3.

Table 3. Calculated regression coefficients based on hypothesis II.

Well 24/6-B-4	Coefficients
Intercept (b0)	- 471.71
X1 (WOB)	0.0038
X2 (Torque)	-0.0010
X3 (RPM)	0.5684
X4 (Fjm)	-1787.17
X5 (FP)	44.80

Testing of hypothesis II model on its reference well

Fig. 35 shows the resulting ROP values of implementing the coefficients on the well where they were produced (i.e. H and AY2H) and compares it with the actual ROP field data. Comparing with the results obtained in hypothesis I, hypothesis II modelling approach shows quite similar in the depth interval [9000, 19000] ftMD.

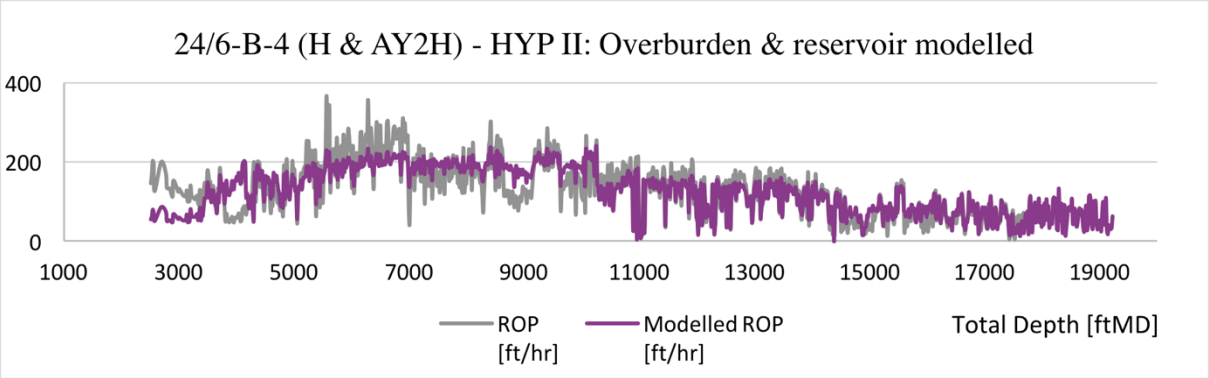

Fig. 35. Multiple regression method applied on well 24/6-B-4 based on hypothesis II (i.e. method applied on both reservoir and overburden sections).

Testing of hypothesis II model on nearby wells

The resulting ROP values of implementing the coefficients provided in Table 3 on the remaining Alvheim wells are plotted in Figs. 36 and 37. Wells 24/6-B-1 and 24/6-B-5 seem to give similar results to those obtained in hypothesis I.

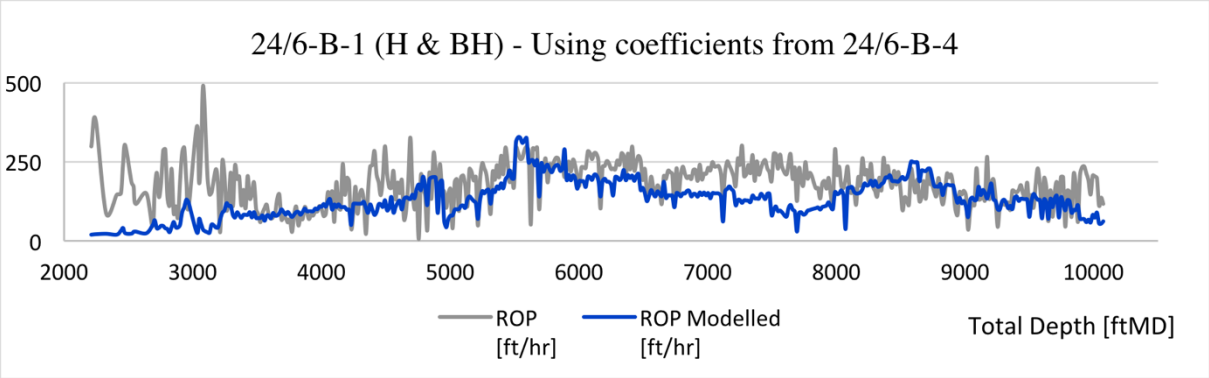

Fig. 36. Multiple regression - 24/6-B-1 with coefficients from 24/6-B-4.

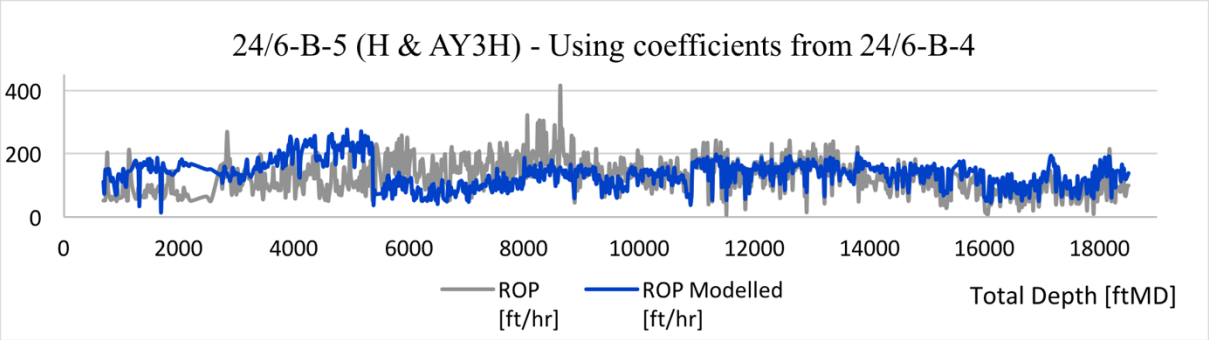

Fig. 37. Multiple regression - 24/6-B-5 with coefficients from 24/6-B-4.

Testing of hypothesis II model on very far and very far field wells

The ROP model derived from the Alvheim field, (i.e., using coefficients fromTable 3) are applied to the far field data (i.e. Kvitebjørn and Valhall) prediction. The comparison between the field data and the model prediction are displayed on Figs. 38 to 40. As shown, well 34/11-A-4 shows some improvement at the deepest part of the well and appears to give better results than those obtained in hypothesis I. However, wells 34/11-A-4, 34/11-A-5 and 2/11-S-10 seem to give similar results to those obtained in hypothesis I. Knowing that the deviation between the actual and the modelled ROP is somehow reduced when using hypothesis II. This is shown in the time analysis performed in chapter 5.1.

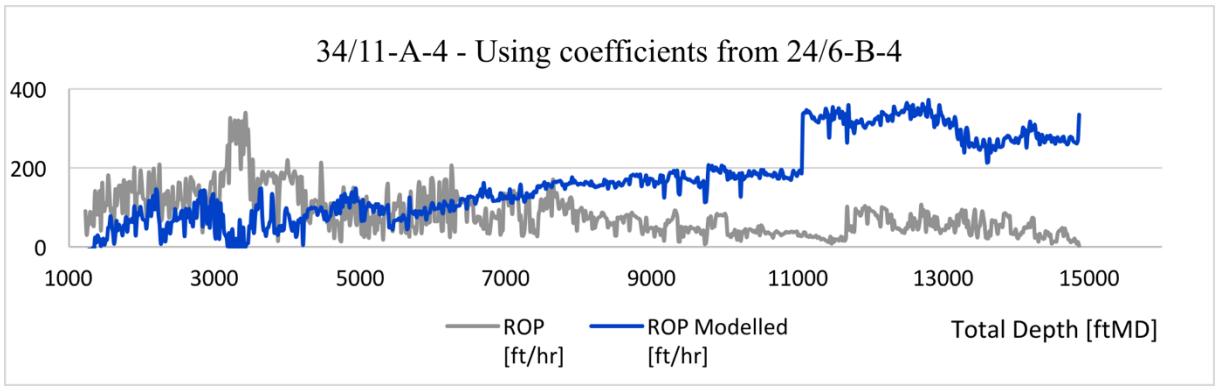

Fig. 38. Multiple regression - 34/11-A-4 with coefficients from 24/6-B-4.

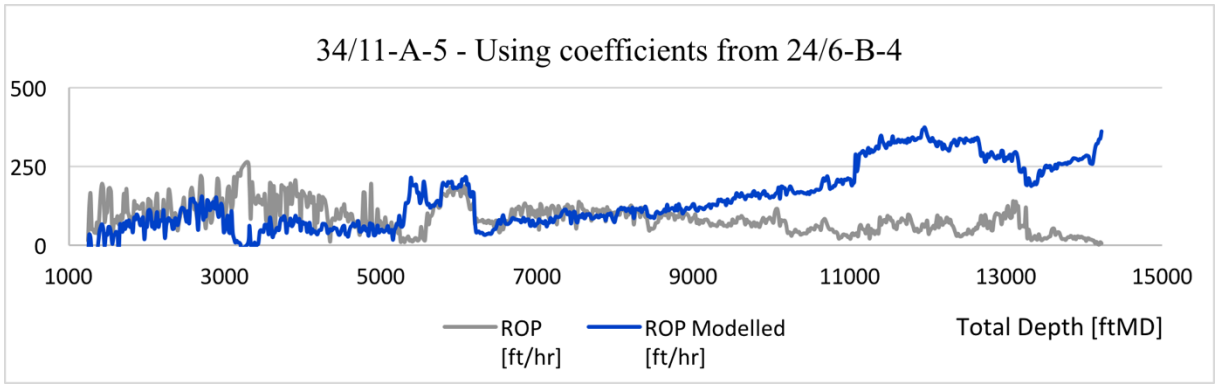

Fig. 39. Multiple regression - 34/11-A-5 with coefficients from 24/6-B-4.

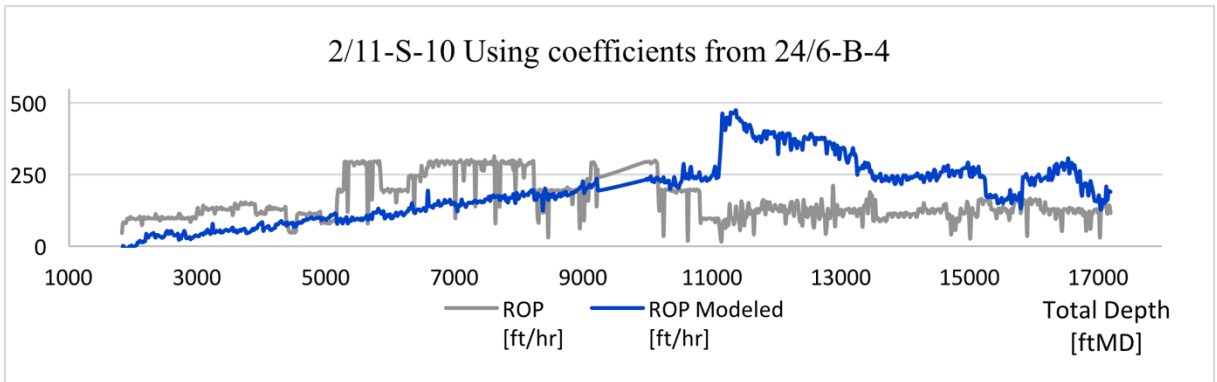

Fig. 40. Multiple regression - 2/11-S-10 with coefficients from 24/6-B-4.

4.3 The Method of Least Squares

This section presents the method of least squares modelling results. Fig. 10 shows the details of the modelling workflow. As shown in the previous section, the multiple regression based hypothesis II modelling has shown better results than hypothesis I. Therefore; this section chose hypothesis II-based ROP modelling by using the least squares coefficients method. The calculated least squares coefficients obtained from the six wells are provided in Tables 4 to 9.

Table 4. Well 24/6-B-4 least squares coefficients.

	Coefficients
Intercept (b0)	0.0000
X1 (WOB)	0.0000
X2 (Torque)	0.0000
X3 (RPM)	0.0000
X4 (Fjm)	0.0000
X5 (FP)	9.7819

Table 5. Well 24/6-B-1 least squares coefficients.

	Coefficients
Intercept (b0)	0.0000
X1 (WOB)	0.0016
X2 (Torque)	0.0000
X3 (RPM)	1.0243
X4 (Fjm)	0.0000
X5 (FP)	0.0000

Table 6. Well 24/6-B-5 least squares coefficients.

	Coefficients
Intercept (b0)	0.0000
X1 (WOB)	0.0016
X2 (Torque)	0.0007
X3 (RPM)	0.5809
X4 (Fjm)	0.0000
X5 (FP)	2.8029

Table 7. Well 34/11-A-4 least squares coefficients.

	Coefficients
Intercept (b0)	79.866
X1 (WOB)	0.0003
X2 (Torque)	0.0000
X3 (RPM)	0.0000
X4 (Fjm)	0.0108
X5 (FP)	0.0000

Table 8. Well 34/11-A-5 least squares coefficients.

	Coefficients
Intercept (b0)	0.0000
X1 (WOB)	0.0000
X2 (Torque)	0.0000
X3 (RPM)	0.2800
X4 (Fjm)	7096.3
X5 (FP)	0.0000

Table 9. Well 2/11-S-10 least squares coefficients.

	Coefficients
Intercept (b0)	49.206
X1 (WOB)	0.0000
X2 (Torque)	0.0008
X3 (RPM)	0.5160
X4 (Fjm)	0.0000
X5 (FP)	0.0035

Note that the model is given in Eq. 3.3 as:

$$Modelled\ ROP = b_0 + b_1 WOB + b_2 Torque + b_3 RPM + b_4 F_{jm} + b_5 FP \tag{4.1}$$

Testing of hypothesis II model on the reference well

The first analysis was performed on Alvheim field wells. Fig. 41 shows the comparison between the reference ROP of 24/6-B-4 (H and AY2H) well data with the least squares based ROP model. The least squares coefficients were derived from the reference well and the coefficients are shown in Table 4. As shown, the model is entirely dominated by the FP (formation pressure) corresponding coefficient. The predicted ROP appears to fit well with the actual one. The method of least squares attempts to reduce the differences between the predicted and the actual values of the ROP.

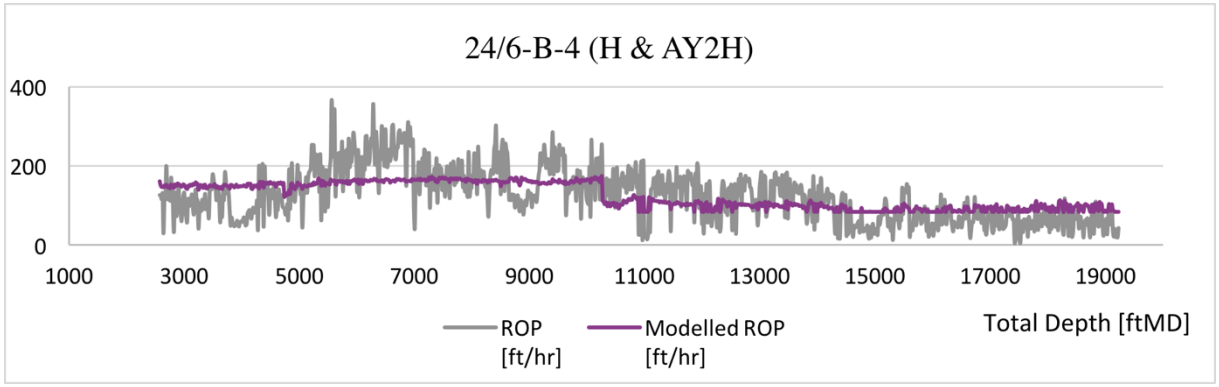

Fig. 41. Method of least squares applied on well 24/6-B-4 (the pilot well H and the first lateral well AY2H).

The same coefficients were implemented on the second lateral section AY1H of the Alvheim well (see Fig. 15**)**. The resulting ROP model prediction and field data are plotted in Fig. 42. The model prediction seems to be nearly constant throughout the whole drilling depth. These coefficients will be applied on the other five wells in the next section. This is to be done to analyze the applicability and limitations of these coefficients both on close-by and remote wells.

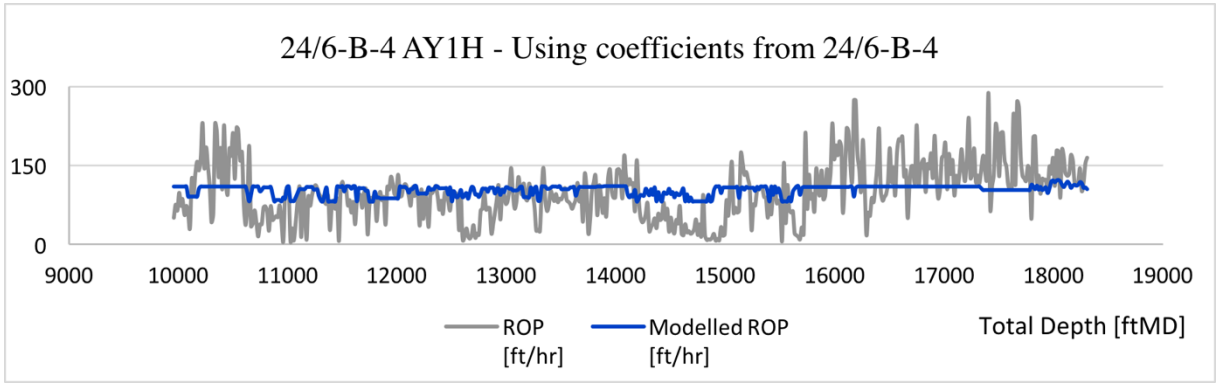

Fig. 42. Method of least squares - 24/6-B-4 AY1H (the second lateral section) with coefficients from 24/6-B-4 (H and AY2H).

Testing of hypothesis II model on nearby wells

Figs. 43 to 47 show the resulting ROP model obtained by implementing the least squares coefficients on the well which they were extracted from. The model is also applied to the remaining Alvheim wells (24/6-B-1 and 24/6-B-5), and the results are plotted in the Figs. 43 and 44. Some deviating results can be observed in both wells. However, these coefficients seem to correlate better with the actual ROP than those obtained by multiple regression method.

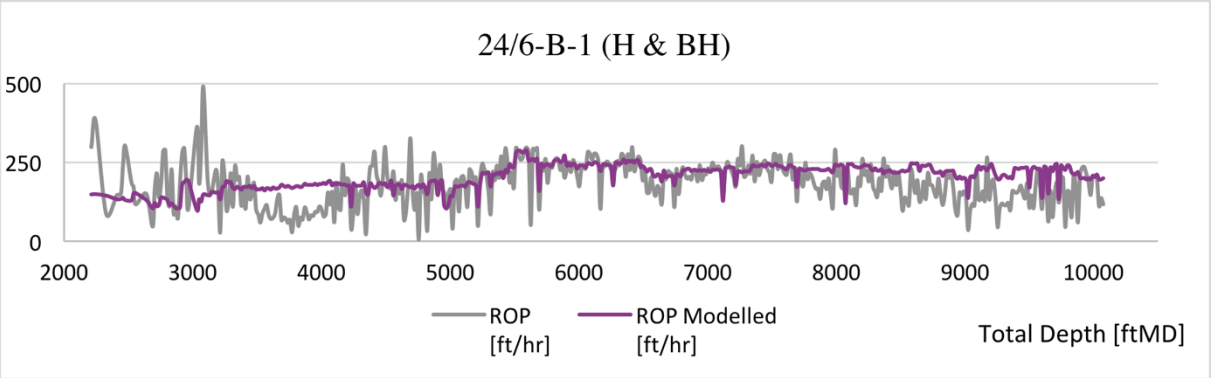

Fig. 43. Method of least squares applied on well 24/6-B-1 (the pilot well H and the lateral well BH).

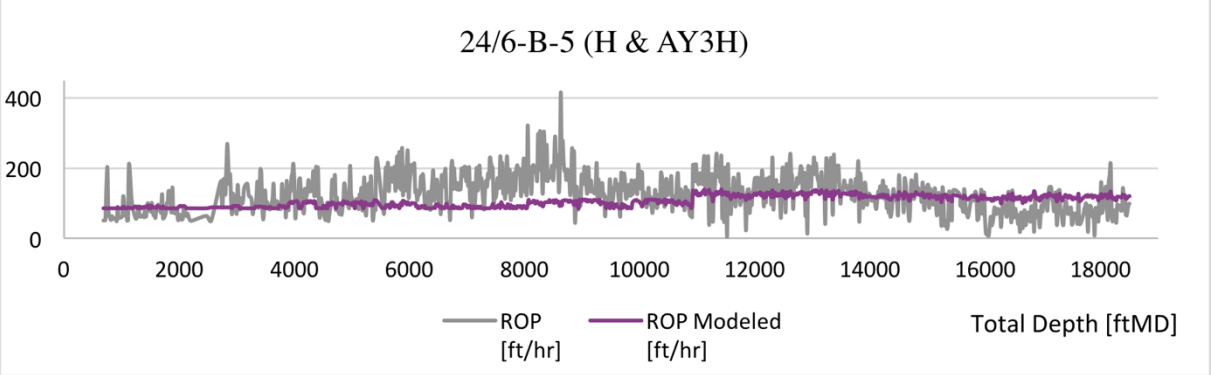

Fig. 44. Method of least squares applied on well 24/6-B-5 (the pilot well H and the lateral well AY3H).

Testing of hypothesis II model on far and very far wells

Figs. 45 to 47 show the modelled ROP plots of the Kvitebjørn and Valhall wells. The results are fairly good but less predictive than the previously obtained results in Alvheim field. This is due to the distance between the Kvitebjørnd field and the Alvheim field where the reference well is located. However, wells 34/11-A-4 and 34/11-A-5 have better results compared to well 2/11-S-10. Fig. 47 shows the results of the Valhall well 2/11-S-10 and appear to be the worst among all wells. This is expected, due to the remoteness of this well from the reference well. Moreover, this well had the worst results in advance when the multiple regression method was applied. However, it shows better results than those acquired in the multiple regression method.

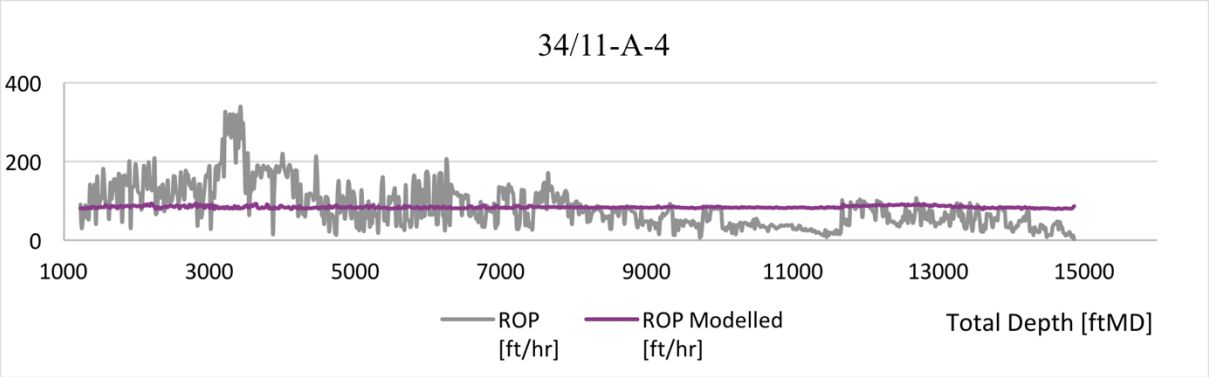

Fig. 45. Method of least squares applied on well 34/11-A-4.

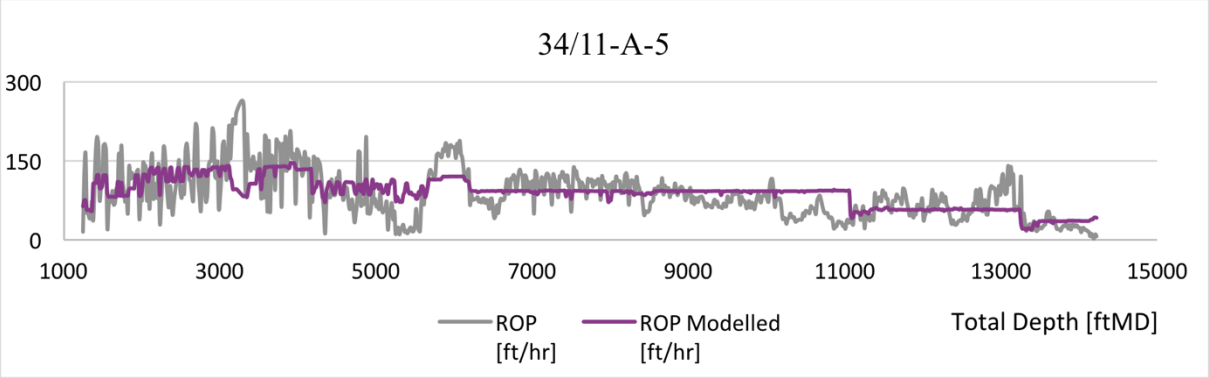

Fig. 46. Method of least squares applied on well 34/11-A-5.

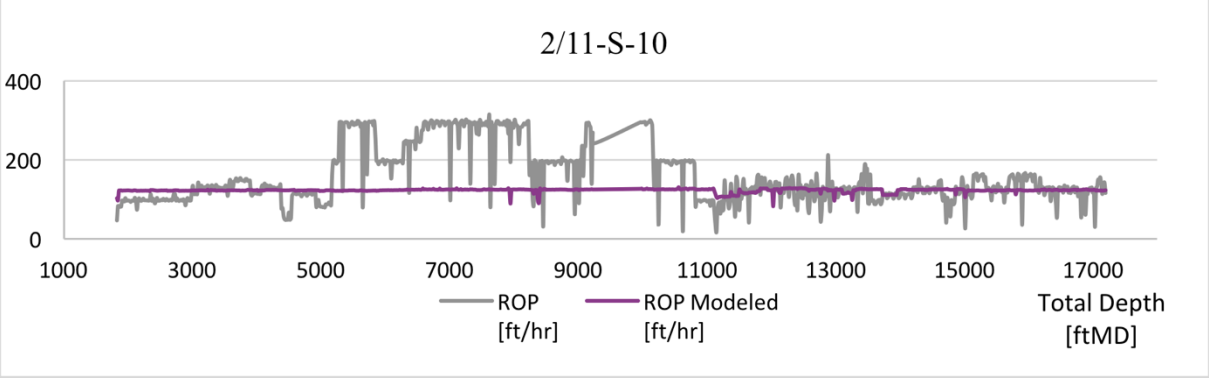

Fig. 47. Method of least squares applied on well 2/11-S-10.

Testing of hypothesis II model on nearby wells

The ROP model profiles obtained by implementing the reference well coefficients (i.e. well 24/6-B-4) on the other five wells are presented in this section. The coefficients are tested on all lateral sections of the wells in case of multiple lateral sections. At first, the analysis of the Alvheim wells is presented. The ROP modelling and comparison results on well 24/6-B-1 are displayed in Figs. 48 to 50. This well shows fairly good results. The predicted ROP deviates from the actual one in the depth interval [6500, 8 300] ftMD. As discussed before, this is due to the depth change of the Hordaland group between this well and the reference (see Fig. 14 on page 31).

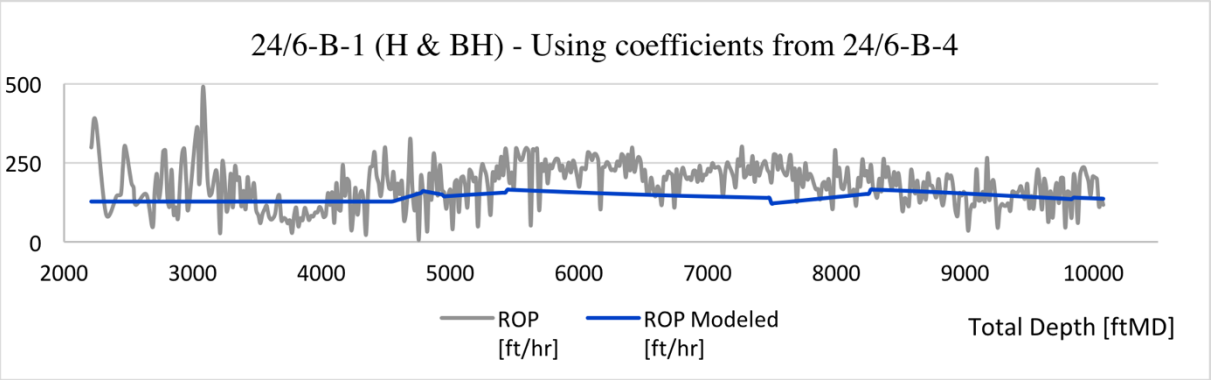

Fig. 48. Method of least squares - 24/6-B-1 (the pilot well H and the lateral well BH) with coefficients from 24/6-B-4 (H and AY2H).

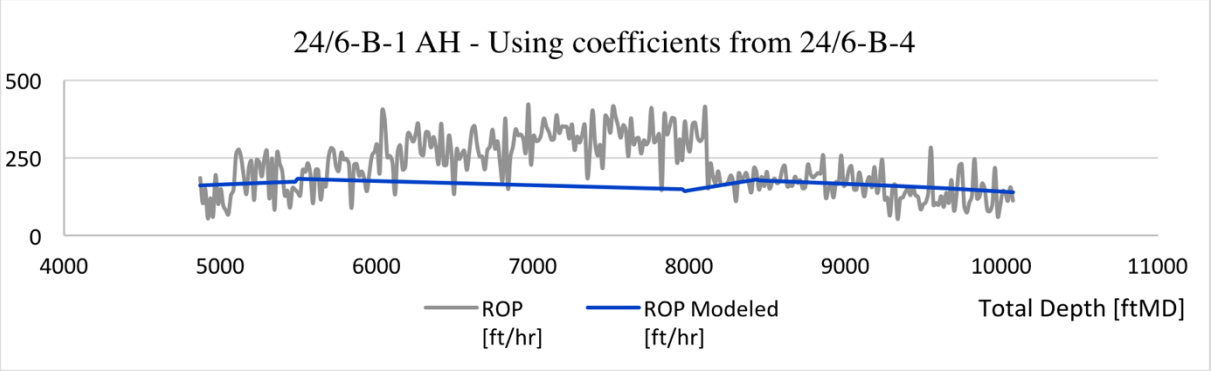

Fig. 49. Method of least squares - 24/6-B-1 (the lateral well AH) with coefficients from 24/6-B-4 (H and AY2H).

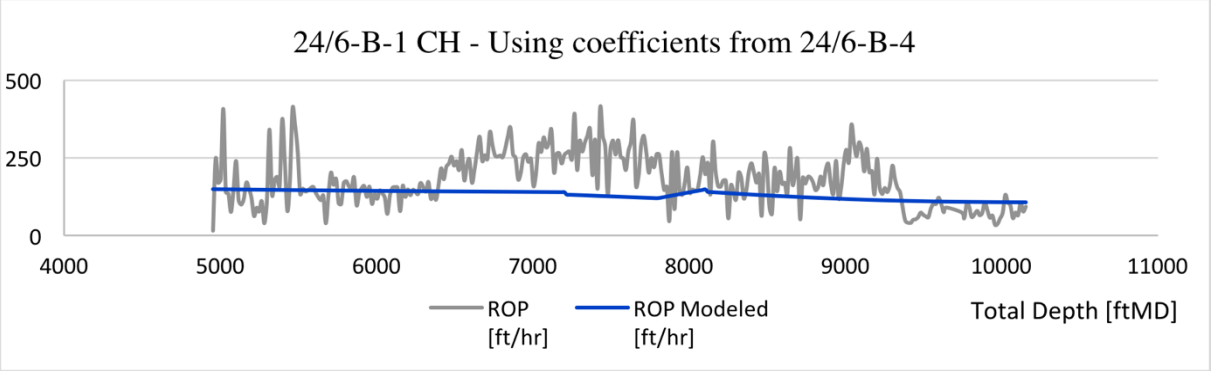

Fig. 50. Method of least squares - 24/6-B-1 (the lateral well CH) with coefficients from 24/6-B-4 (H and AY2H).

Similarly, the ROP analysis in Alvheim well 24/6-B-5 is plotted in Figs. 51 to 53. The results also seem to correlate very well with the actual ROP. Both of the Alvheim wells 24/6-B-4 and 24/6-B-5 have good results due to their proximity to the reference well 24/6-B-4.

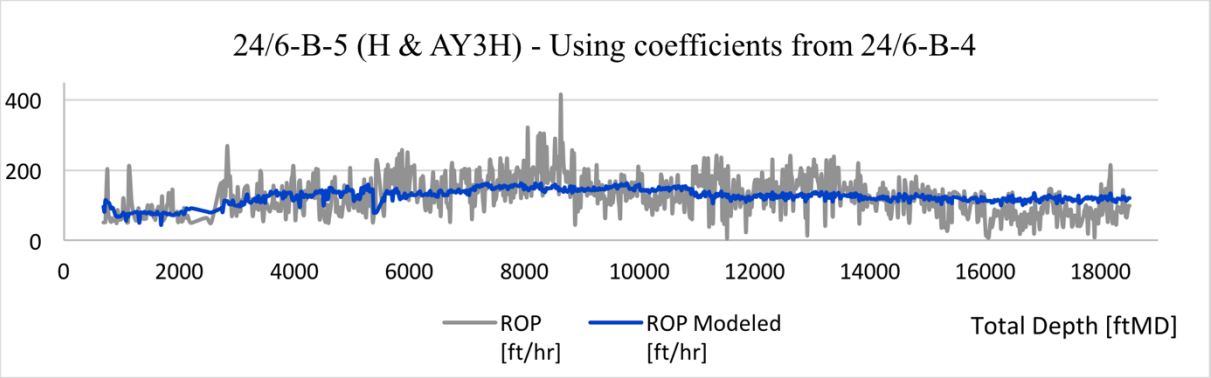

Fig. 51. Method of least squares - 24/6-B-5 (the pilot well H and the lateral well AY3H) with coefficients from 24/6-B-4 (H and AY2H).

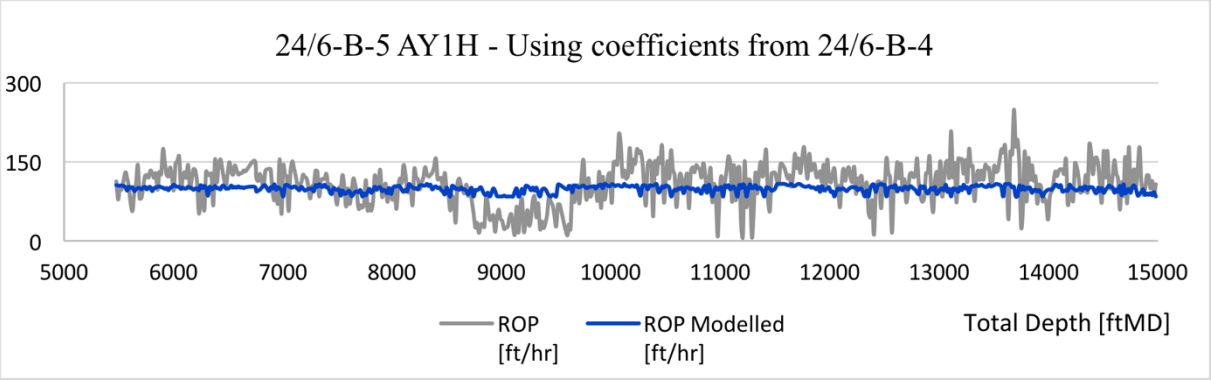

Fig. 52. Method of least squares - 24/6-B-5 (the lateral well AY1H) with coefficients from 24/6-B-4 (H and AY2H).

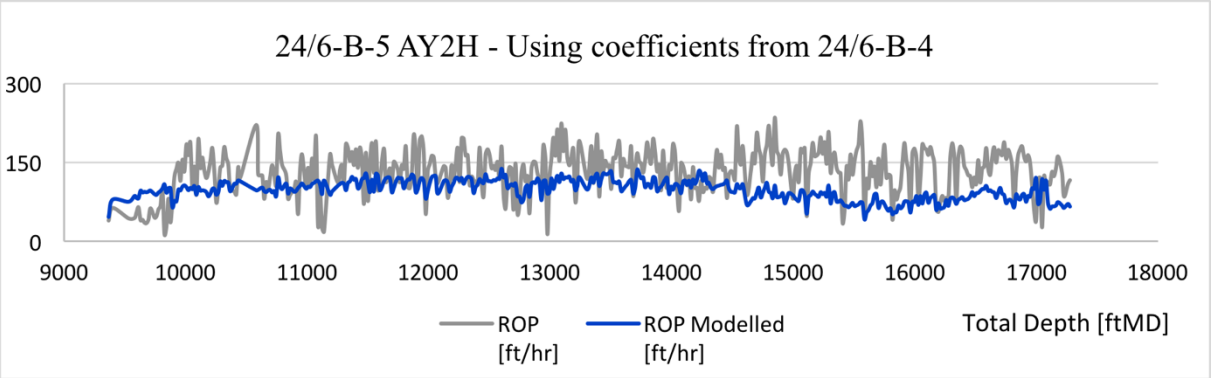

Fig. 53. Method of least squares - 24/6-B-5 (the lateral well AY2H) with coefficients from 24/6-B-4 (H and AY2H).

Testing of hypothesis II model on far and very far wells

The reference well coefficients are also applied for modelling the far field data, which are the Kvitebjørn and the Valhall wells 34/11-A-4, 34/11-A-5 and 2/11-S-10. The analysis results are shown in Figs. 54 to 56. As shown, these wells appear to correlate fairly good with the actual ROP despite its great distance from the reference well.

However, the ROP appears also to be poorly modelled at some depth points in wells 34/11-A-4 and 2/11-S-10. These wells are located away from the Alvheim reference well as shown in Fig. 8 on page 20, indicating the existence of differences in geological facies.

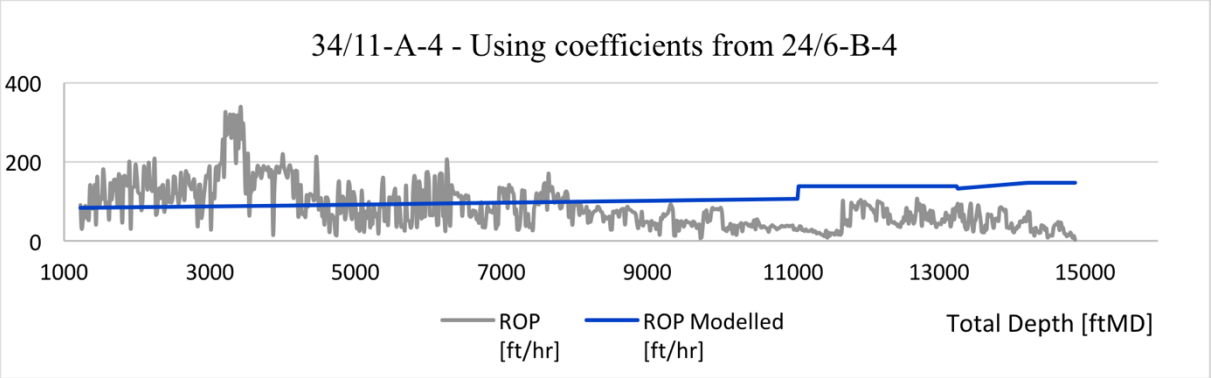

Fig. 54. Method of least squares - 34/11-A-4 with coefficients from 24/6-B-4 (H and AY2H).

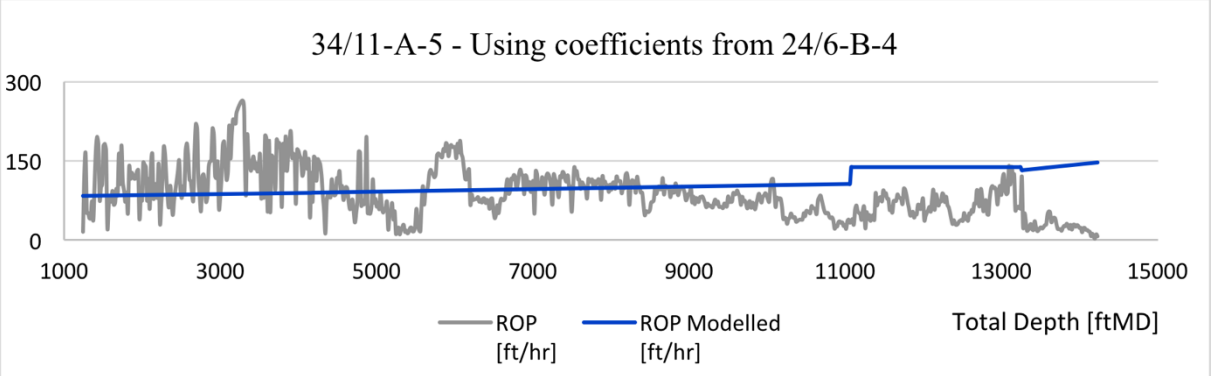

Fig. 55. Method of least squares - 34/11-A-5 with coefficients from 24/6-B-4 (H and AY2H).

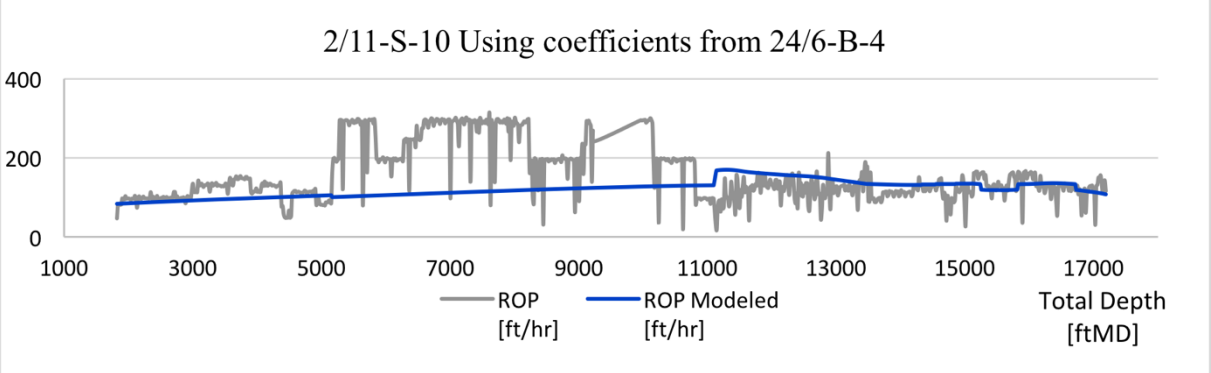

Fig. 56. Method of least squares – 2/11-S-10 with coefficients from 24/6-B-4 (H and AY2H).

4.4 MSE - Mechanical Specific Energy

The workflow of the MSE based ROP model presented in Fig. 11 is applied to field data in a similar way as presented in section 4.2 and 4.3. Unlike the previous modelling approach, MSE, as proposed by Teale [2], has been derived based on the concept of mechanical specific energy. The model is a function of drilling operational parameters such as torque, WOB and RPM. The modelling assumes that the amount of energy that is required to drill a certain volume of rock is correlative within nearby wells. This assumption creates high inaccuracy when applying this method, especially when the method is implemented on remote wells. This is due to the MSE dependence on both the compressive strength and the pressure of rocks, which can vary significantly between wells.

Testing of MSE on the reference well

The MSE profile of the drilling section has been first calculated using both the actual ROP and the modelled ROP. Both MSE results are compared Fig. 57. The result shows very good match.

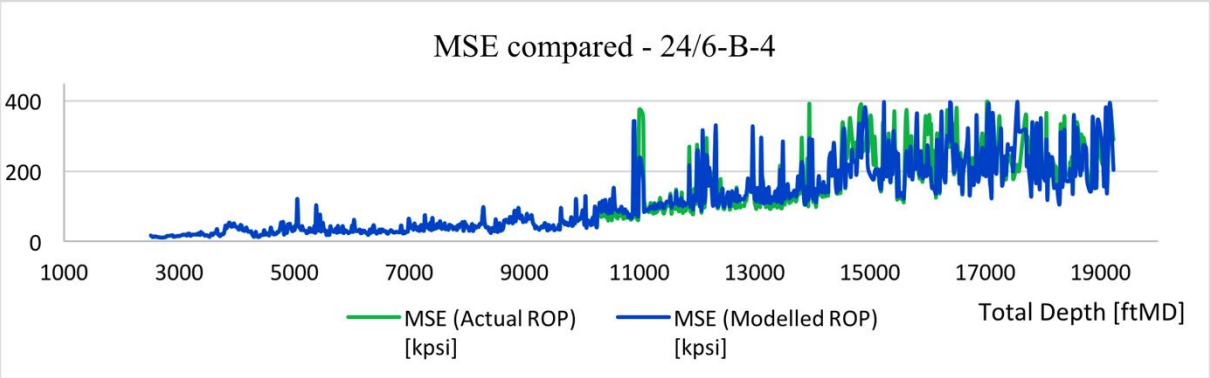

Fig. 57. MSE values calculated from i) the actual ROP and ii) the modelled ROP are compared for the reference well 24/6-B-4 AY2H.

Testing of MSE on nearby wells

The MSE somewhat estimates the uniaxial compressive strength by considering a certain efficiency factor (30-40% [44]). If wells are correlated laterally, there is a chance of the mechanical and elastic properties to be nearly comparable. To investigate the validity of the assumption, whether or not the wells are correlating laterally, one can compare uniaxial compressive strengths. This indirectly assumes that the formation requires a comparable amount of energy (MSE) to crush the rock. This is the commonly used approach when using ROP optimization software (such as the DROPS software). Here also the MSE of the reference well (i.e. well 24/6-B-4) were compared with the nearby and far field wells. The results are presented in the following section.

The Alvheim wells, which are considered as nearby wells from the reference well, are first analyzed.

Fig. 58 shows the comparison of the MSE between wells 24/6-B-1 and 24/6-B-4. As indicated earlier, the MSE profile was computed from the measured drilling parameters of the wells. The result shows a deviation, but generally quite good. To investigate the effect of the predicted MSE on the ROP prediction, nearby wells drilling data were used along with the reference well MSE values. Based on these, and the workflow presented in Fig. 11, ROP was predicted, and the results are compared with the measured ROP of nearby/far wells data. The application of this method is illustrated in Figs. 59 to 61. The model prediction results correlate fairly good with the actual ROP. The predicted ROP deviates from the actual one in the same depth intervals as in previous methods. As mentioned before, this happens due to the depth change of the Hordaland group between this well and the reference (see Fig. 14 on page 31).

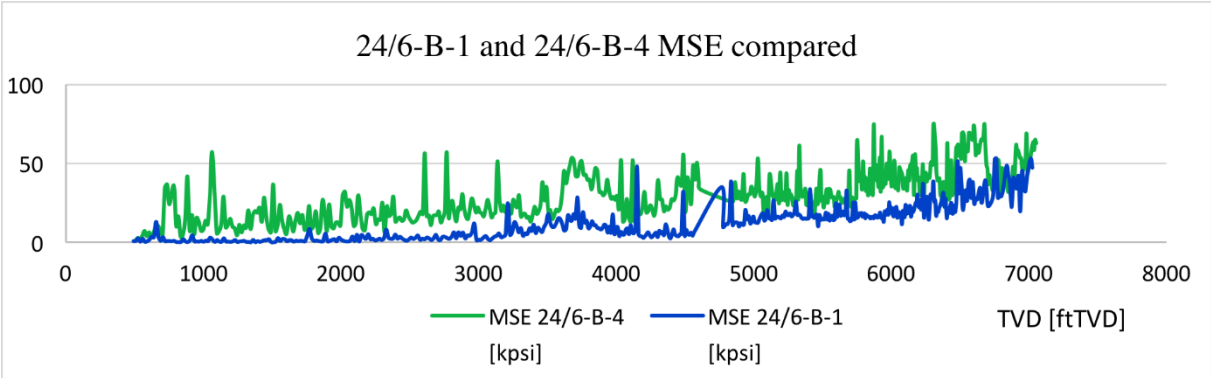

Fig. 58. 24/6-B-1 and 24/6-B-4 MSE compared versus the true vertical depth (TVD).

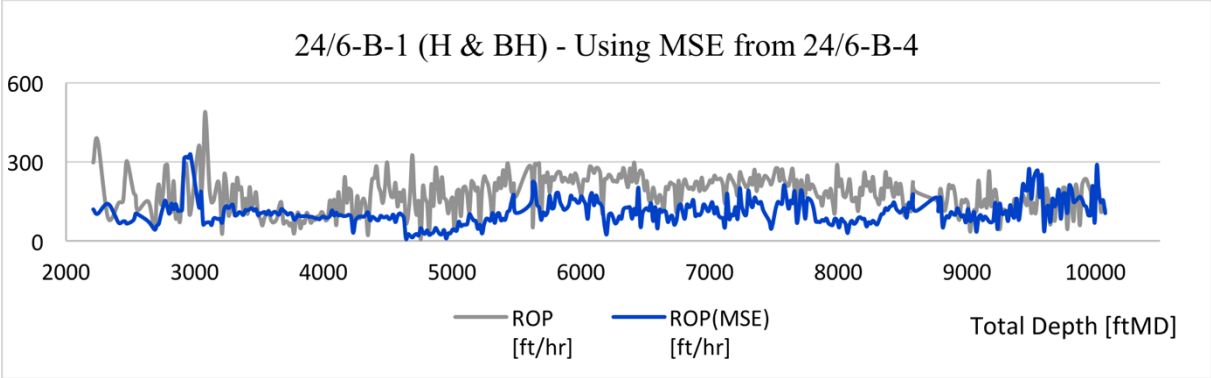

Fig. 59. MSE - 24/6-B-1 (H and BH) with MSE from 24/6-B-4.

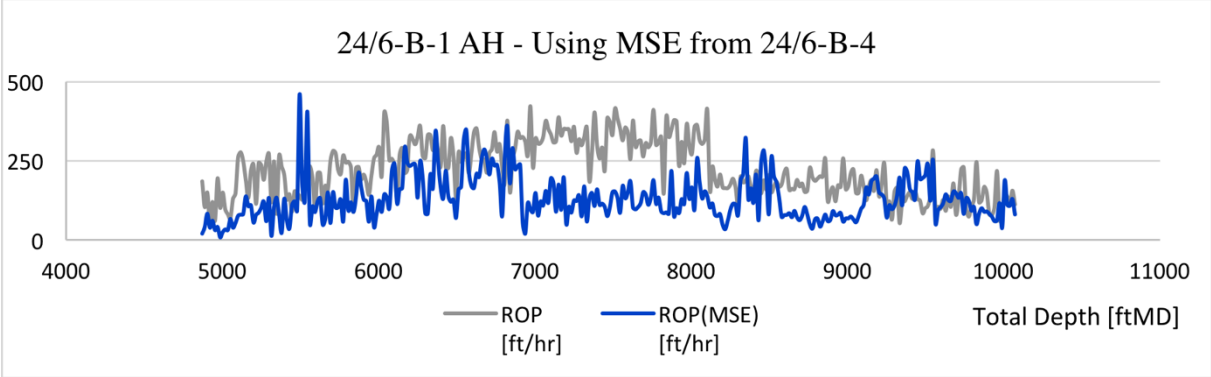

Fig. 60. MSE - 24/6-B-1 AH with MSE from 24/6-B-4.

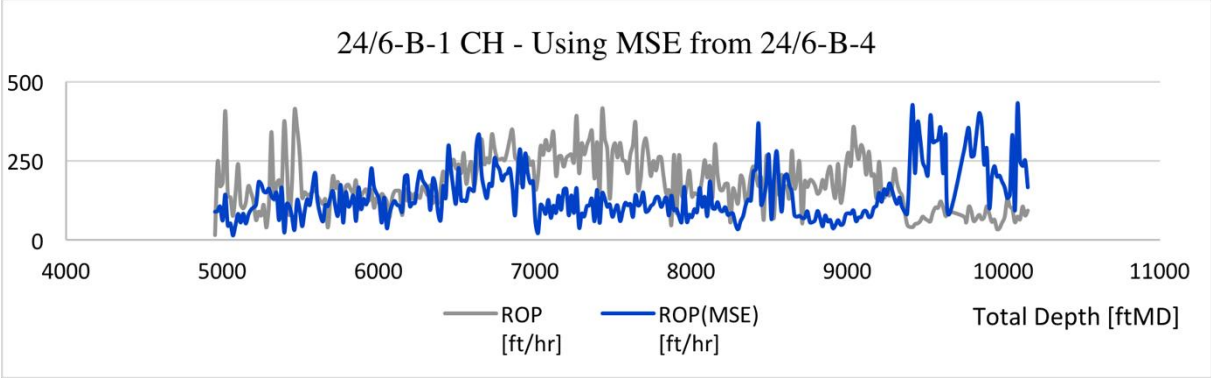

Fig. 61. MSE - 24/6-B-1 CH with MSE from 24/6-B-4.

Well 24/6-B-5 results are shown in Figs. 62 to 65. Fig. 62 compares the MSE values of the reference well with their corresponding values in well 24/6-B-5. The results of this Alvheim well also seem to correlate very well with the actual ROP. Both of the Alvheim wells 24/6-B-4 and 24/6-B-5 have good results due to their proximity to the reference well 24/6-B-4.

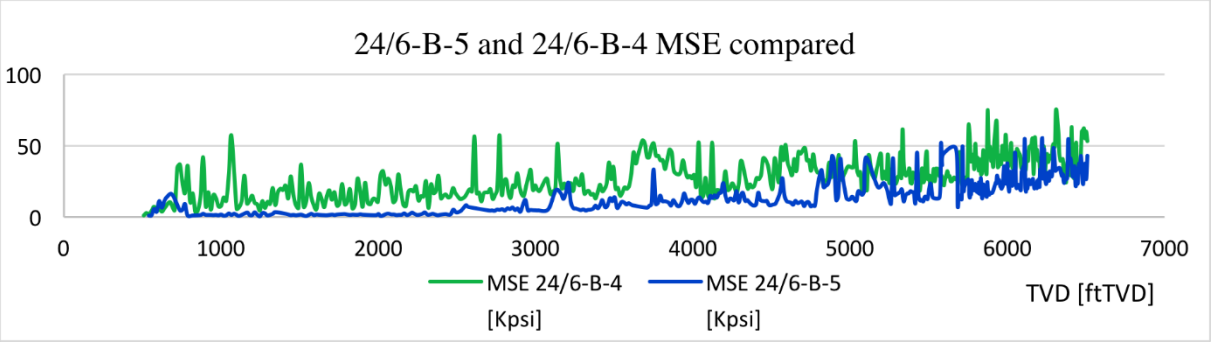

Fig. 62. 24/6-B-5 and 24/6-B-4 MSE compared versus the true vertical depth (TVD).

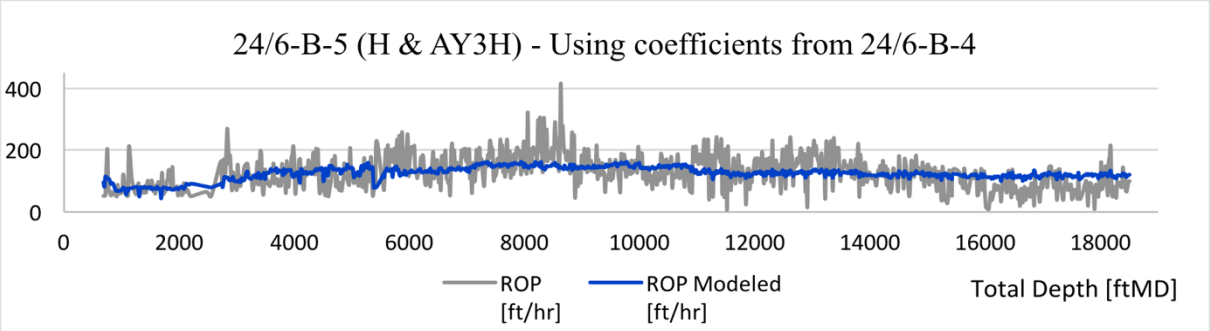

Fig. 63. MSE - 24/6-B-5 (H and AY3H) with MSE from 24/6-B-4.

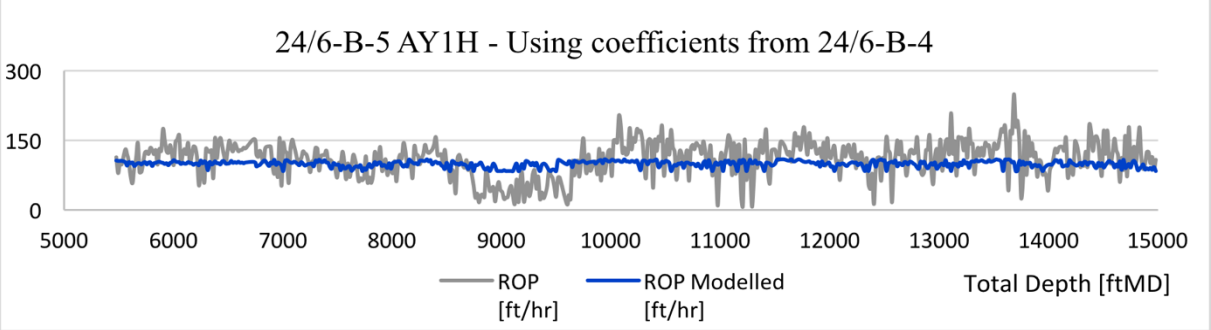

Fig. 64. MSE - 24/6-B-5 AY1H with MSE from 24/6-B-4.

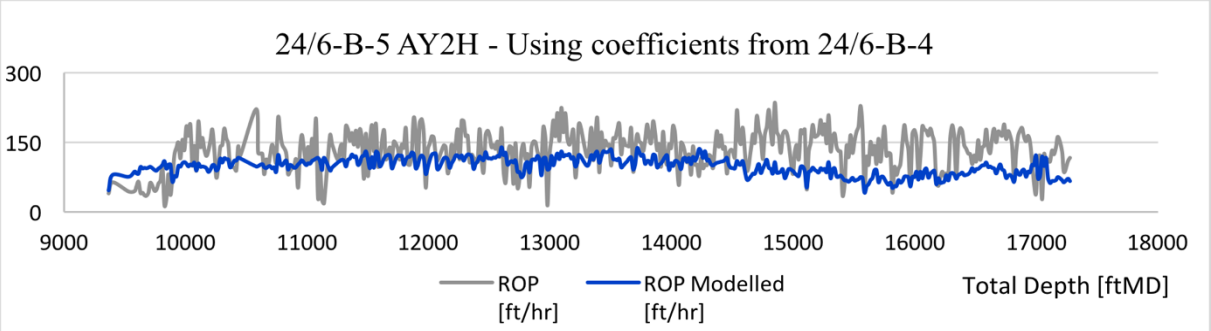

Fig. 65. MSE - 24/6-B-5 AY2H with MSE from 24/6-B-4.

Testing of MSE on far field wells

As shown in Table 1, the wells of Alvheim and Kvitebjørn fields have TVDs that exceed the TVD of the reference well, which is 7 076 ftTVD. Therefore, the MSE method is applied only on well-sections that are above 7 076 ftTVD.

Well 34/11-A-4 results are shown in Figs. 66 and 67. Fig. 66 compares the MSE values of the reference well with their corresponding values in well 34/11-A-4. As discussed, the Kvitebjørn well is located about 173 km away from the Alvheim reference well; this is shown in Fig. 8 on page 20. Some geological differences can be observed between the wells in Fig. 14 on page 31, especially on the top of the overburden. The Utsira formation depth varies between this well and the reference well. In addition to the disappearance of the Nordland group in the reference well. This explains the reason for the big deviation between the predicted and the actual ROP plots in the overburden section.

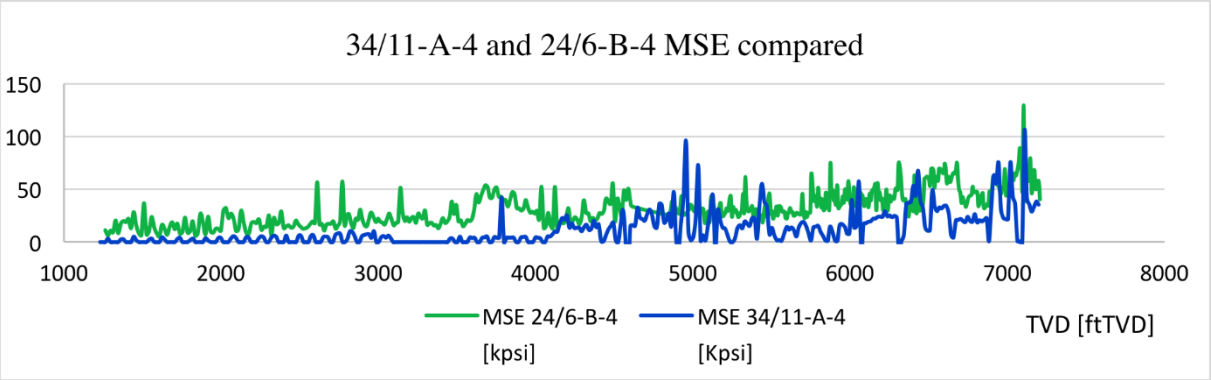

Fig. 66. 34/11-A-4 and 24/6-B-4 MSE compared versus the true vertical depth (TVD).

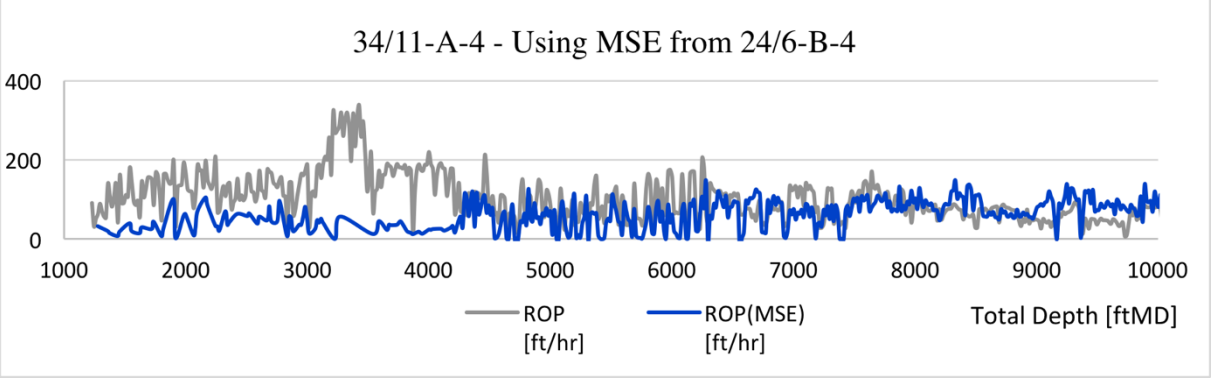

Fig. 67. MSE - 34/11-A-4 with MSE from 24/6-B-4.

Well 34/11-A-5 modelling results are presented in Figs. 68 and 69. Fig. 68 compares the MSE profile of the reference well with their corresponding values in well 34/11-A-5. The results show that the ROP seems to be poorly modelled at most depth points. Again, the long distance and the geological differences between this well and the reference well are the reasons for inaccuracy in results.

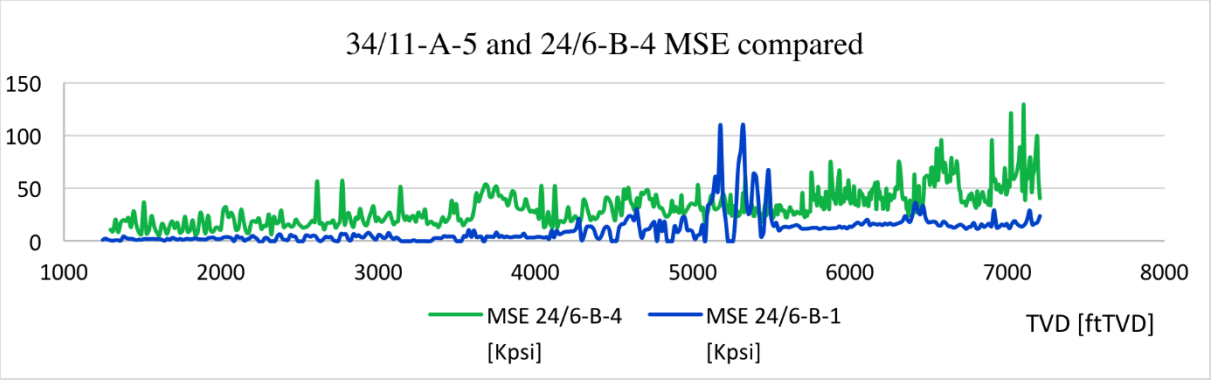

Fig. 68. 34/11-A-5 and 24/6-B-4 MSE compared versus the true vertical depth (TVD).

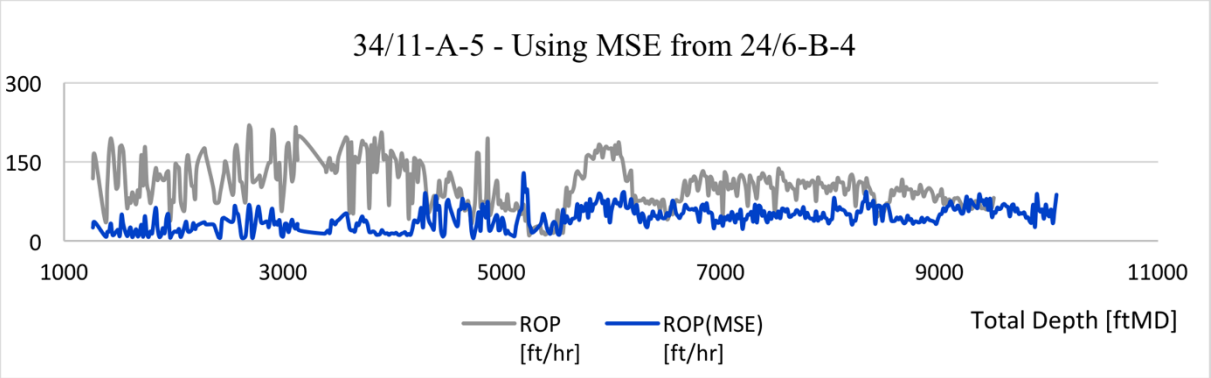

Fig. 69. MSE - 34/11-A-5 with MSE from 24/6-B-4.

Testing of MSE on very far field wells

Well 2/11-S-10 results are presented in Figs. 70 and 71. Fig. 70 compares the MSE values of the reference well with their corresponding values in well 2/11-S-10. This Valhall well is located about 376 km away from the Alvheim reference well as shown in Fig. 8 on page 20. The ROP seems to be very poorly modelled due to the long distance between the two wells. However, the part above 11 000 ftMD (corresponds to 8 700 ftTVD) shows slightly better results. This is due to the existence of similarities in the geological facies above the 8 700 ftTVD as shown in Fig. 14 on page 31.

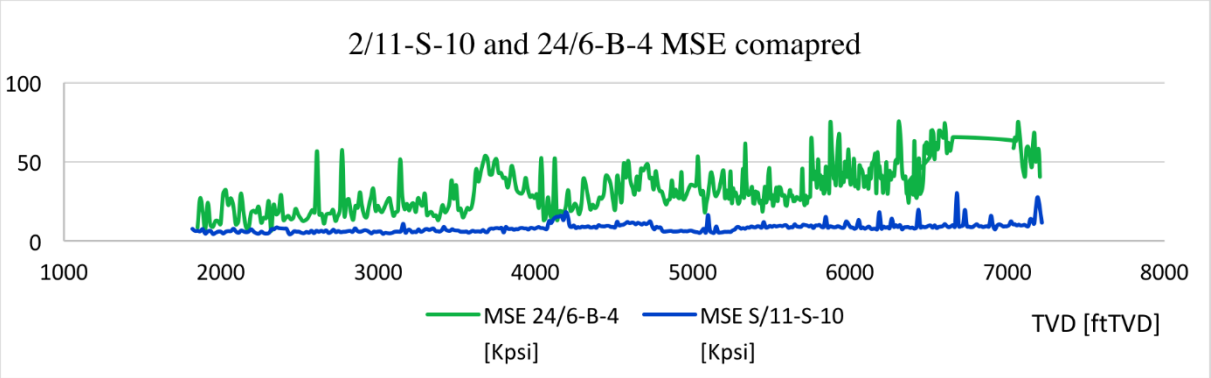

Fig. 70. 2/11-S-10 and 24/6-B-4 MSE compared versus the true vertical depth (TVD).

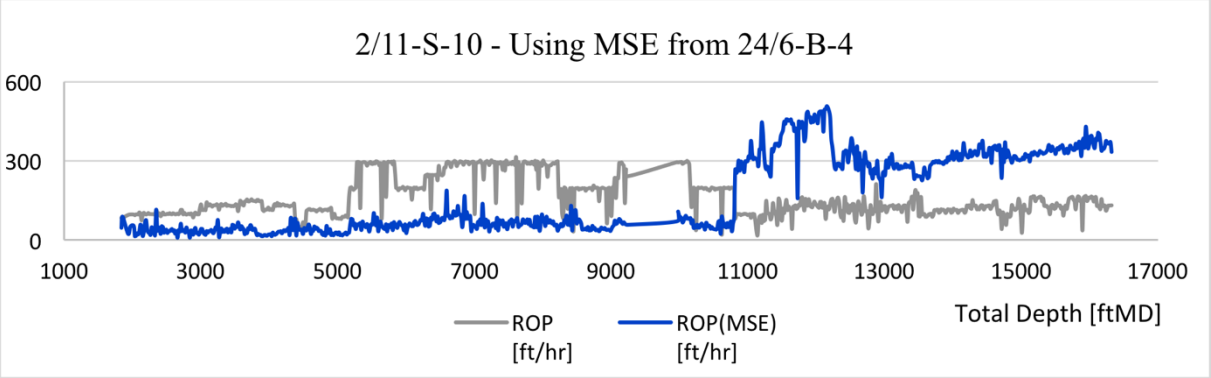

Fig. 71. MSE - 2/11-S-10 with MSE from 24/6-B-4.

4.5 Drillability D-Exponent

The D-exponent based derived-ROP model is shown in Eq. (3.7) and in the workflow illustrated in Fig. 12. The model clearly shows that it is a function of the main operational parameters. This technique assumes that the drillability of a well is correlative within nearby wells provided that the lateral geology features are quite similar. The areal limitation for the applicability will need to investigate through modelling as has been done in the previous sections. The D-exponent depends on both the strength and the pressure of rocks, which can differ significantly between wells. The D-exponent is proportional to rock strength and increases linearly with depth for normally pressured formations. While it decreases with depth for abnormally pressurized formations (shales).

The modelling and results analysis performed on the field wells are presented in this section.

Testing of D-exponent on the reference well

During modelling, the D-exponents profile of the well has been first calculated using the modelled ROP. Then both actual and calculated D-exponents are compared as shown in Fig. 72. As shown the calculated profiles run in parallel with minor deviation gap.

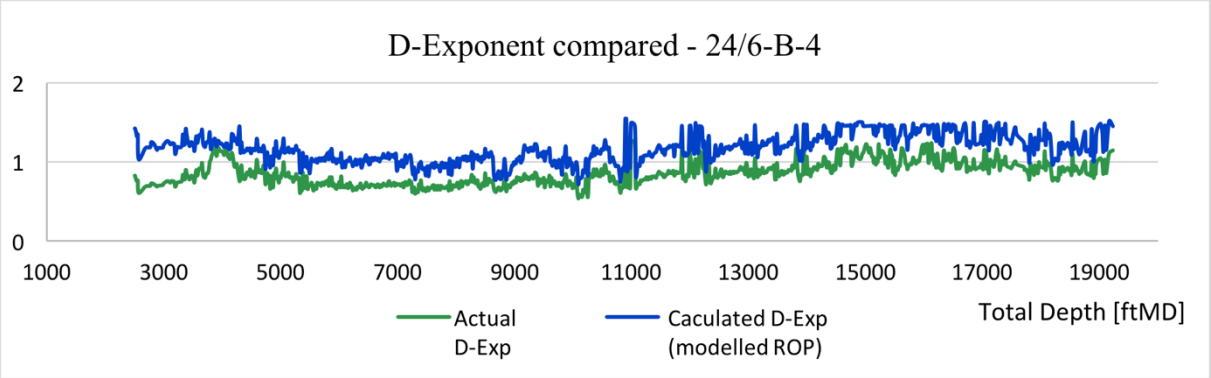

Fig. 72. Actual D-exponent values and D-exponent values calculated using modelled ROP are compared for the reference well 24/6-B-4 AY2H.

Testing of D-exponent on nearby wells

Similarly, the D-exponent method is tested by comparing the reference well (i.e. well 24/6-B-4) with the other five wells.

The method is applied on all lateral sections of the wells in case of multiple lateral sections. The Alvheim wells results were first considered for the analysis. Well 24/6-B-1 results are presented in Figs. 73 to 76. Fig. 73 compares the D-exponents of the reference well (24/6-B-4) with the D-exponents of the nearby well 24/6-B-1. As shown, the results here correlate very well. The predicted ROP deviates from the actual one in the same depth intervals as in previous methods. Again, this is due to the depth change of the Hordaland group between this well and the reference (see Fig. 14 on page 31).

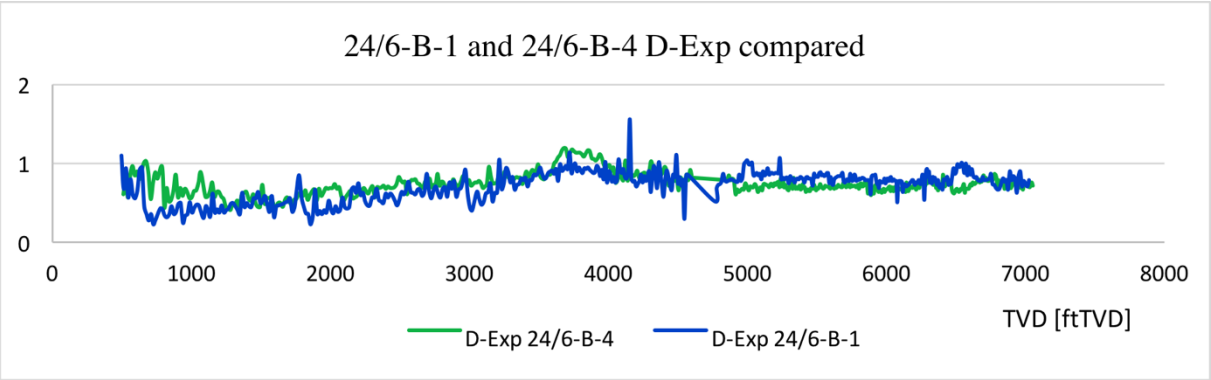

Fig. 73. 24/6-B-1 and 24/6-B-4 D-exponents compared versus the true vertical depth (TVD).

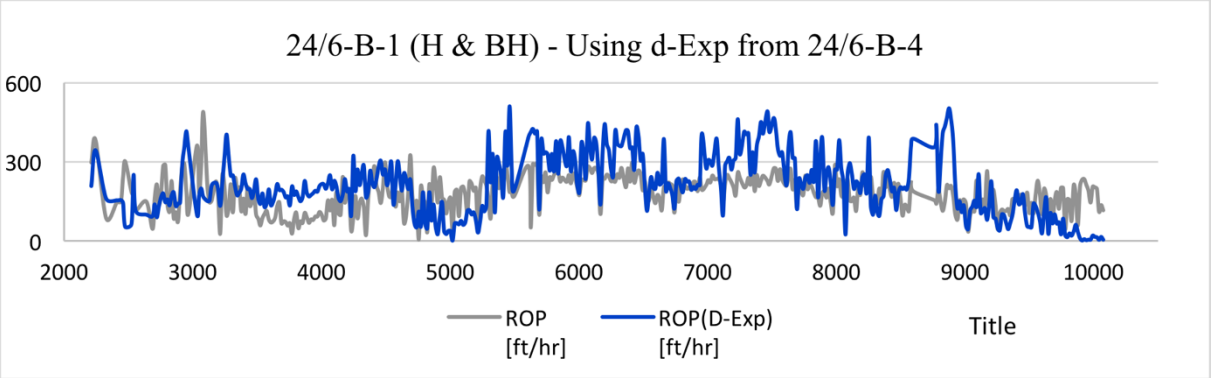

Fig. 74. D-exponent - 24/6-B-1 (H and BH) with D-exponents from 24/6-B-4.

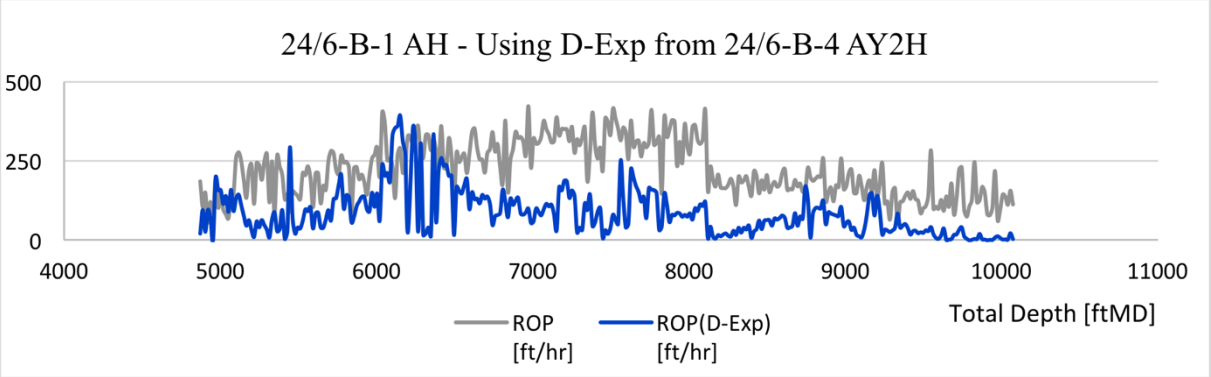

Fig. 75. D-exponent - 24/6-B-1 AH with D-exponents from 24/6-B-4.

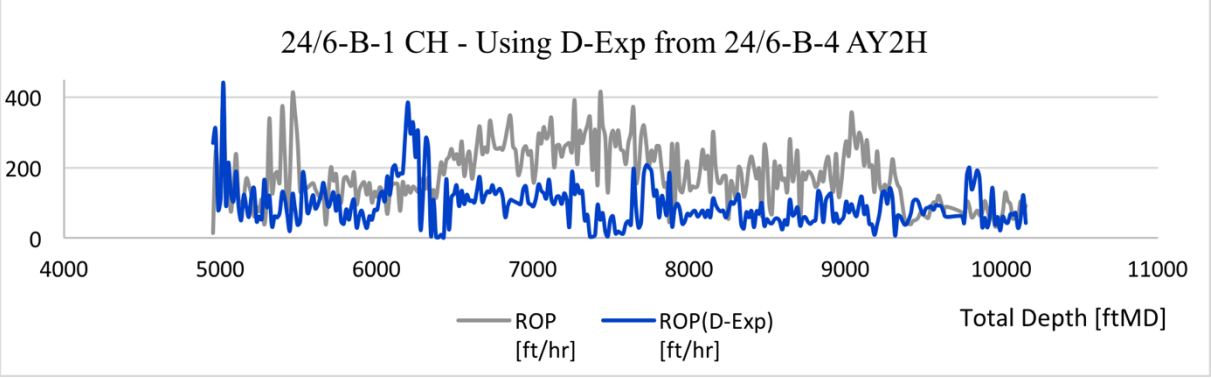

Fig. 76. D-exponent - 24/6-B-1 CH with D-exponents from 24/6-B-4.

Figs. 77 to 80 display the modelling results of well 24/6-B-5. Fig. 77 compares the D-exponents of the reference well with their corresponding values in well 24/6-B-5. The results of this Alvheim well also seem to correlate very well with the actual ROP due to its proximity to the reference well 24/6-B-4.

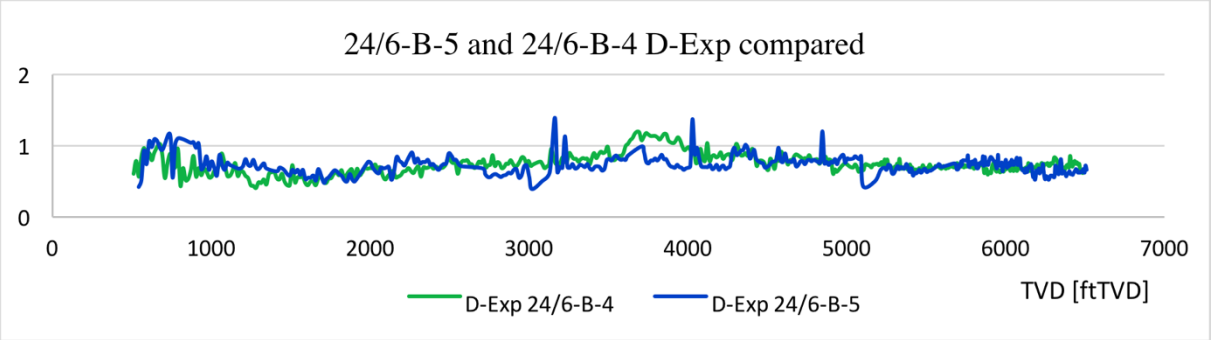

Fig. 77. 24/6-B-5 and 24/6-B-4 D-exponents compared versus the true vertical depth (TVD).

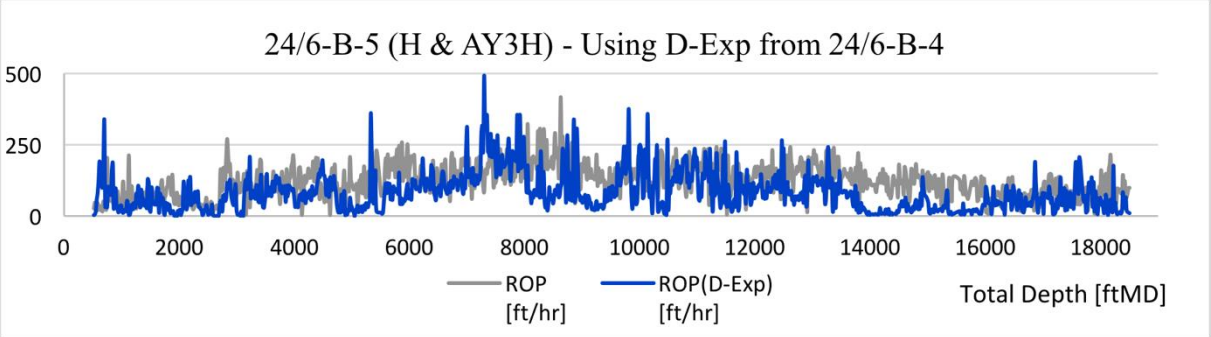

Fig. 78. D-exponent -24/6-B-5 (H and AY3H) with D-exponents from 24/6-B-4.

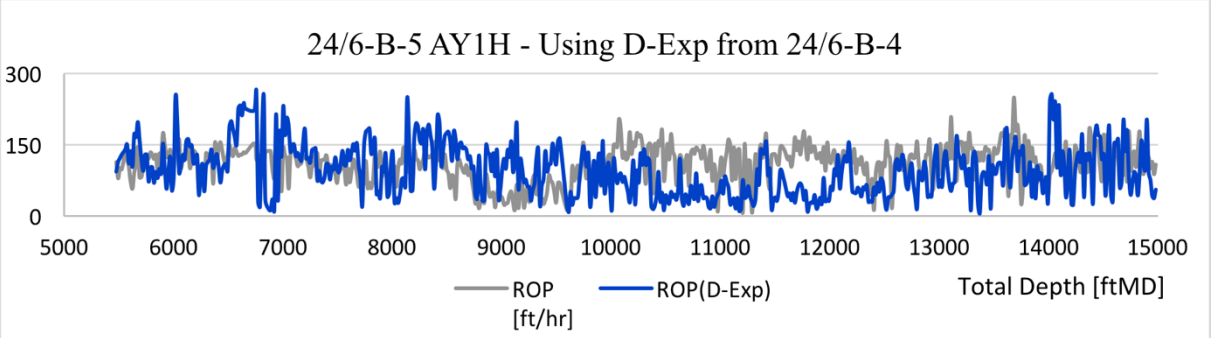

Fig. 79. D-exponent - 24/6-B-5 AY1H with D-exponents from 24/6-B-4.

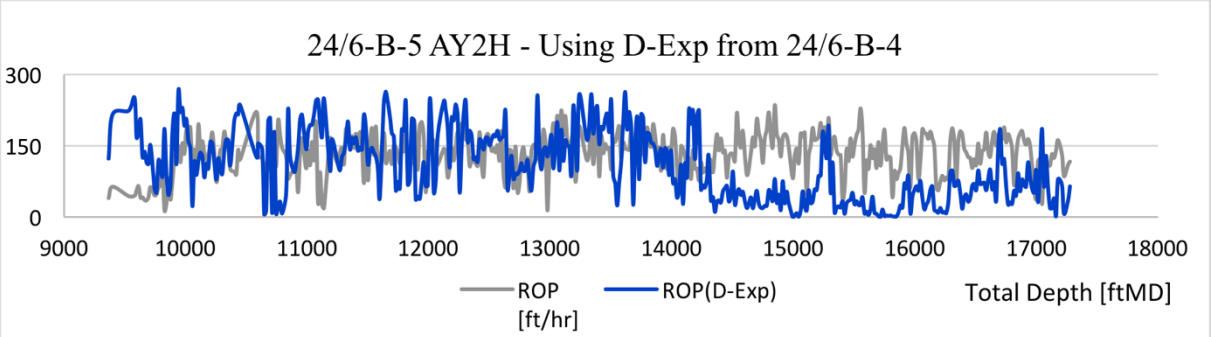

Fig. 80. D-exponent - 24/6-B-5 AY2H with D-exponents from 24/6-B-4.

Testing of D-exponent on far field wells

As mentioned, the wells of Alvheim and Kvitebjørn fields have TVDs that exceed the TVD of the reference well, which is 7 076 ftTVD. Therefore, the D-exponent method is applied only on well-sections that are above 7 076 ftTVD.

Well 34/11-A-4 results are plotted in Figs. 81 and 82. Fig. 81 compares the D-exponents of the reference well with their corresponding values in well 34/11-A-4. The predicted ROP correlates well except for the overburden section. As mentioned, this is due to the depth variations of the Utsira formation between this well and the reference well, in addition to the disappearance of the Nordland group in the reference well (see Fig. 14 on page 31).

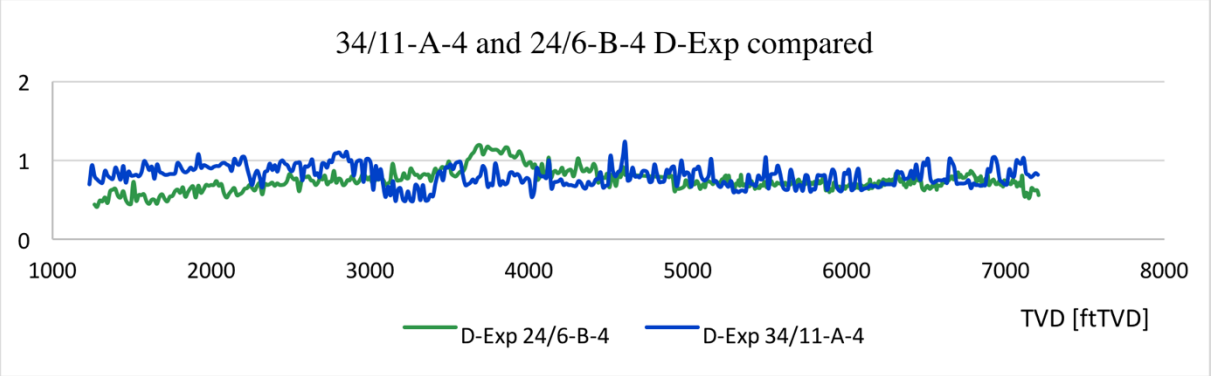

Fig. 81. 34/11-A-4 and 24/6-B-4 D-exponents compared versus the true vertical depth (TVD).

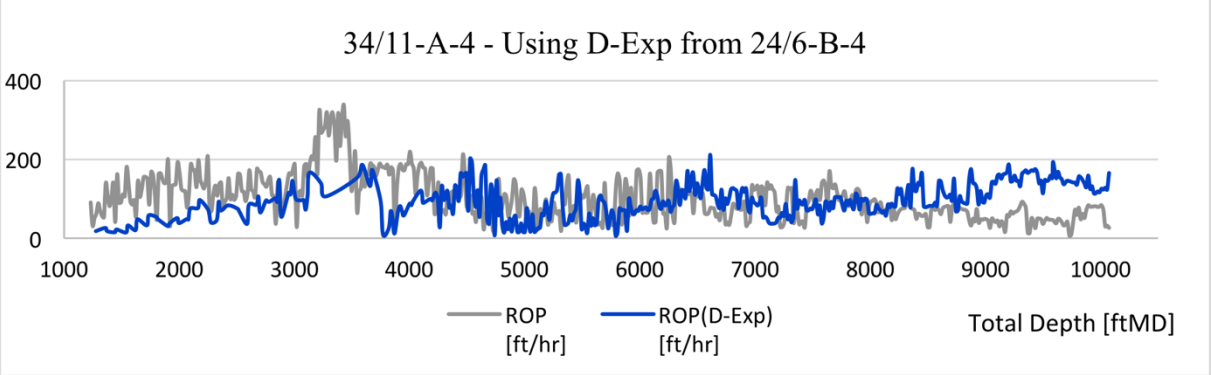

Fig. 82. D-exponent - 34/11-A-4 with D-exponents from 24/6-B-4.

Well 34/11-A-5 results are shown in Figs. 83 and 84. Fig. 83 compares the D-exponents of the reference well with their corresponding values in well 34/11-A-5.

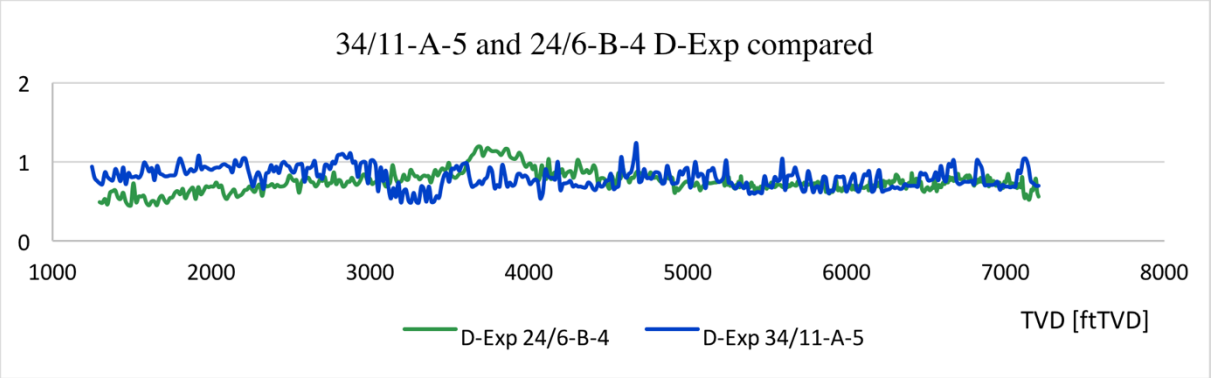

Fig. 83. 34/11-A-5 and 24/6-B-4 D-exponents compared versus the true vertical depth (TVD).

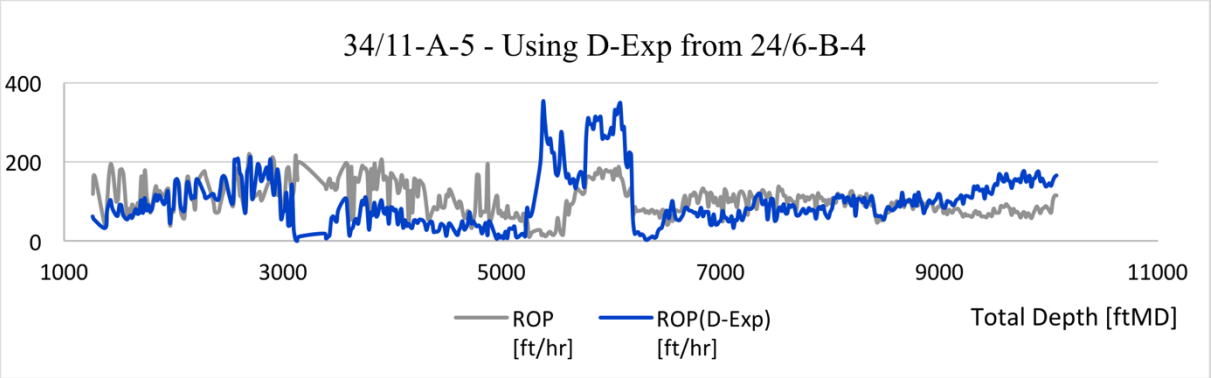

Fig. 84. D-exponent – 34/11-A-5 with D-exponents from 24/6-B-4.

Testing of D-exponent on very far field wells

Well 2/11-S-10 results are presented in Figs. 85 and 86. Fig. 85 compares the MSE values of the reference well with their corresponding values in well 2/11-S-10. The ROP seems to be very poorly modelled due to the remoteness of the well from the reference well (see Fig. 8 on page 20).

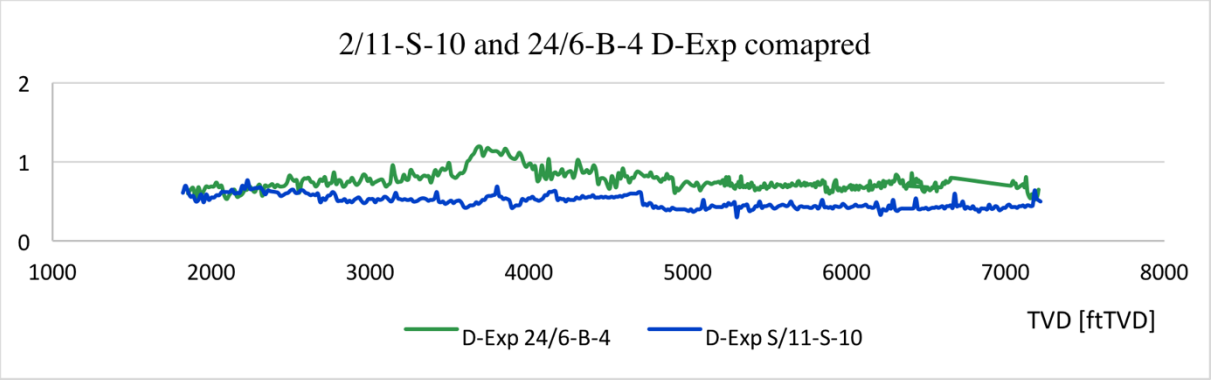

Fig. 85. 2/11-S-10 and 24/6-B-4 D-exponents compared versus the true vertical depth (TVD).

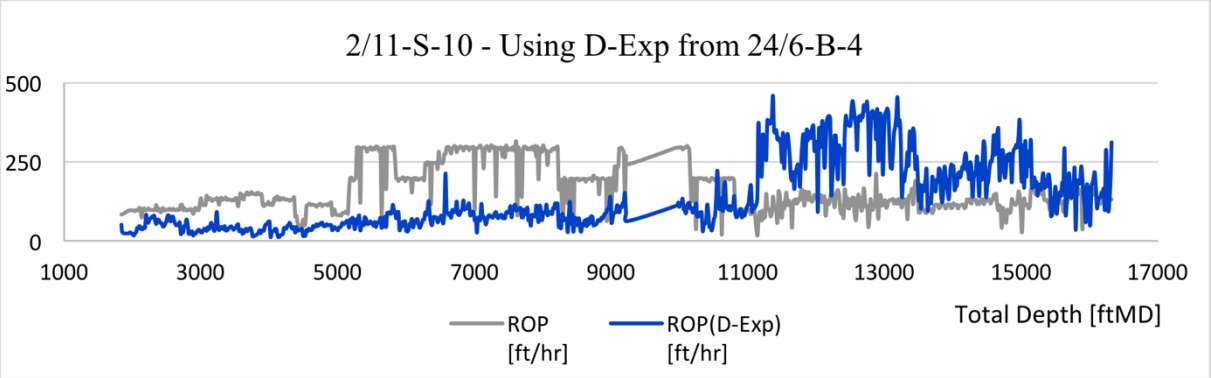

Fig. 86. D-exponent - 2/11-S-10 with D-exponents from 24/6-B-4.

4.6 Warren Model

The Warren ROP model is a function of several parameters as shown in Eq. (2.12). Based on the Warren model, a new workflow has been designed and implemented on the considered field data (see Fig. 13). The model is applied to both reservoirs and overburden sections of the reference well 24/6-B-4. The calculated constants of this well are provided in Table 10.

Table 10. Calculated Warren constants from the reference well 24/6-B-4.

	Constants
a	3.995 x 10-05
b	6.8471
b	3.4834 x 10-09

The resulting ROP values of implementing the constants on the well where they were generated (i.e. 24/6-B-4 H and AY2H) are presented in Fig. 87. The predicted ROP appears to fit well with the field data.

Testing of Warren model on the reference well

The same constants are also implemented on the second lateral section AY1H of the Alvheim well. Fig. 88 shows the model prediction along with the field data. The results show that the model almost nearly captures the measured data. Comparing the position of the reference well with the section lateral reservoir section, they are positioned at different depths and don't seem to have common geological features. To further investigate the applicability and limitation, theses constants will be applied to the other five wells.

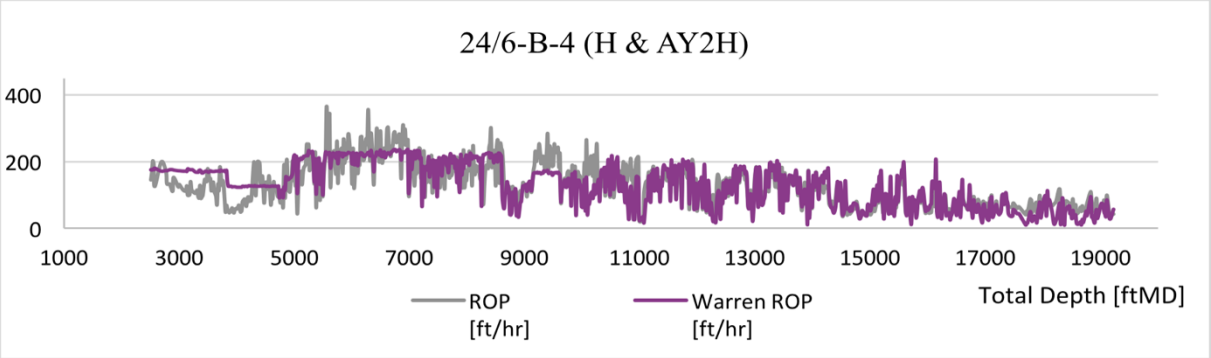

Fig. 87. Warren model applied on well 24/6-B-4 (H and AY1H).

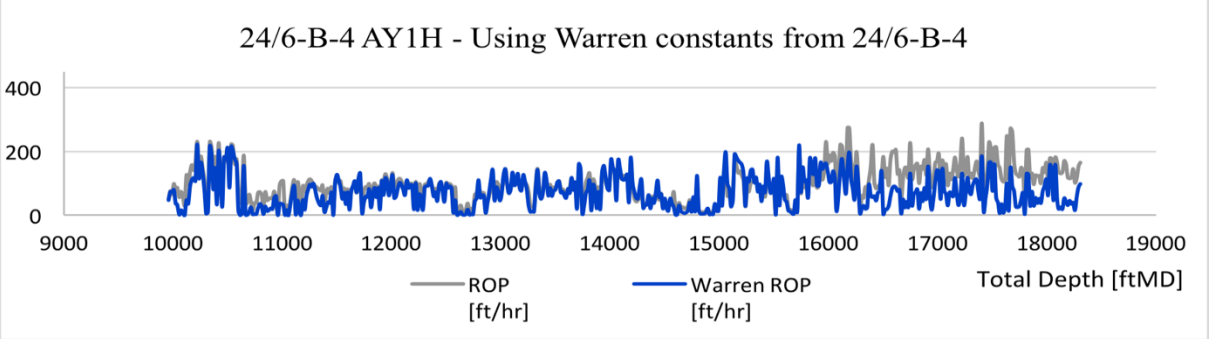

Fig. 88. Warren model - 24/6-B-4 AY1H with Warren constants from 24/6-B-4.

Testing of Warren model on nearby wells

The following Figs. in this section show the results of implementing the Warren constants produced from well 24/6-B-4 on the other five wells. The method is applied on all lateral sections of the wells in case of multiple lateral sections.

Well 24/6-B-1 results are presented in Figs. 89 to 91. The predicted ROP seems to fit relatively well with the actual ROP. However, the predicted ROP deviates from the actual one in the same depth intervals as in previous methods. This is due to the depth change of the Hordaland group between this well and the reference well. (see Fig. 14 on page 31).

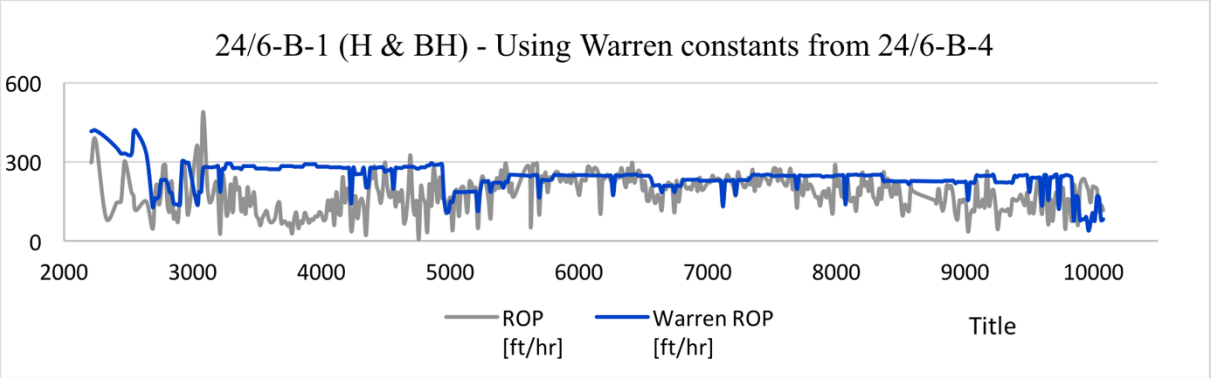

Fig. 89. Warren model - 24/6-B-1 (H and BH) with Warren constants from 24/6-B-4.

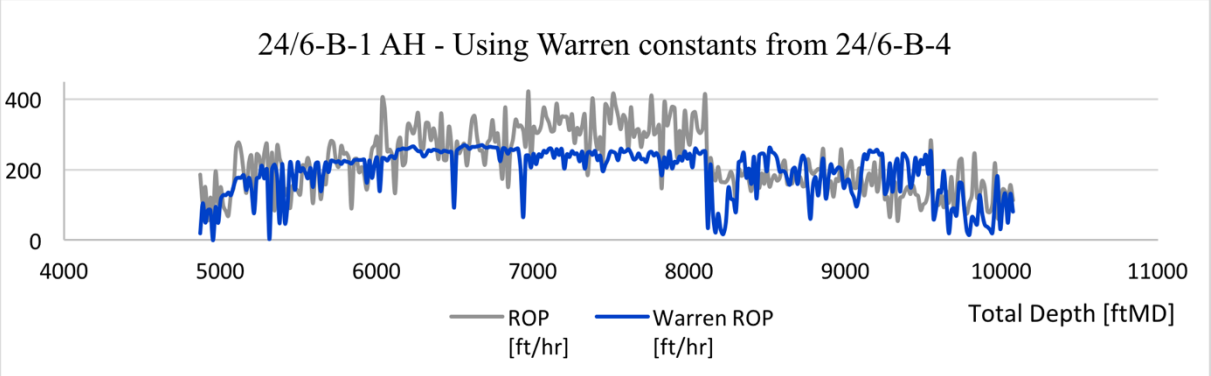

Fig. 90. Warren model - 24/6-B-1 AH with Warren constants from 24/6-B-4.

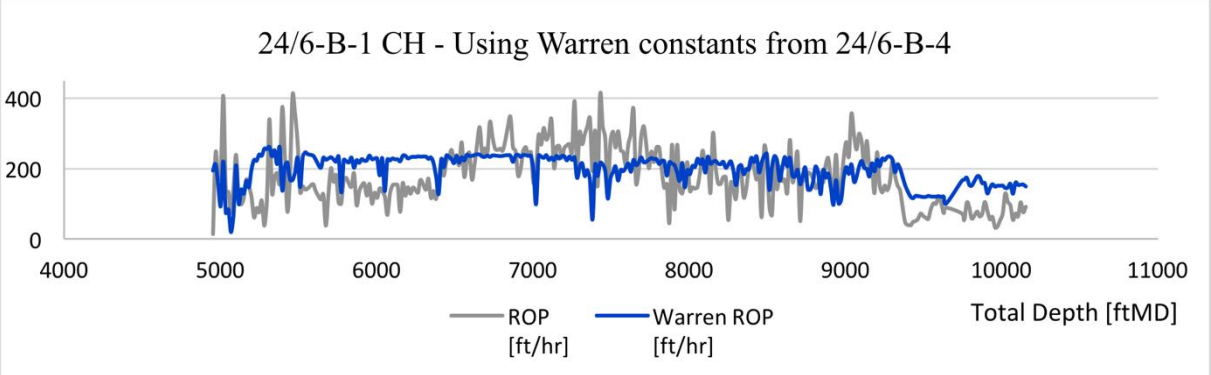

Fig. 91. Warren model - 24/6-B-1 CH with Warren constants from 24/6-B-4.

Well 24/6-B-5 results are presented in Figs. 92 to 94. The predicted ROP seems to fit relatively well with the actual ROP. Both of the Alvheim wells 24/6-B-4 and 24/6-B-5 have good results due to their proximity to the reference well 24/6-B-4.

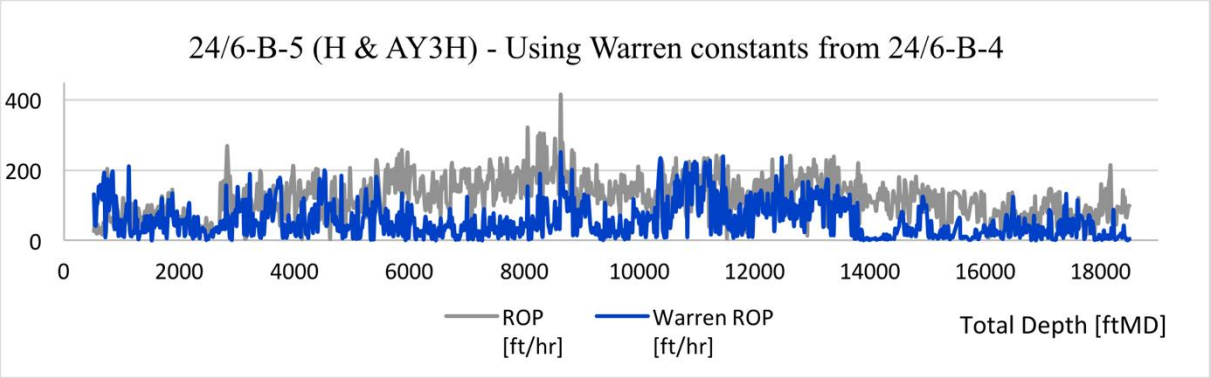

Fig. 92. Warren model - 24/6-B-5 (H and AY3H) with Warren constants from 24/6-B-4.

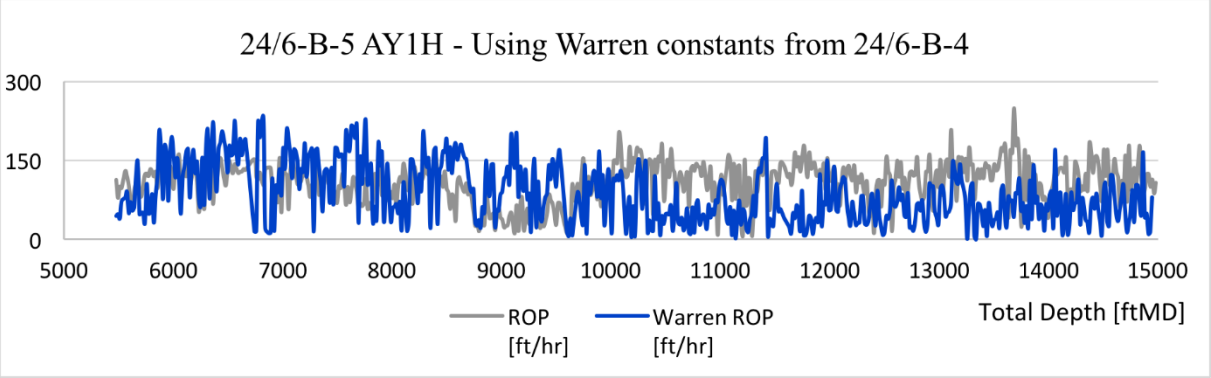

Fig. 93. Warren model - 24/6-B-5 AY1H with Warren constants from 24/6-B-4.

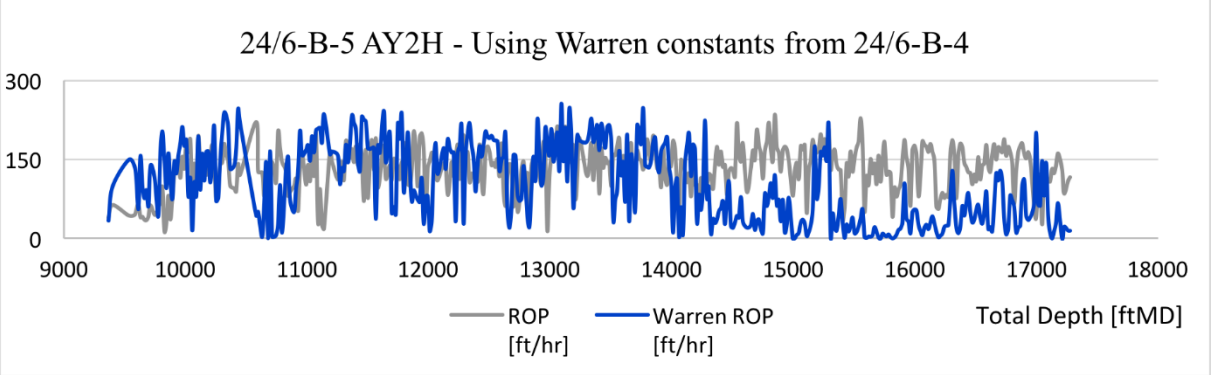

Fig. 94. Warren model - 24/6-B-5 AY2H with Warren constants from 24/6-B-4.

Testing of Warren model on far field wells

The resulting ROP of implementing the constants generated from well 24/6-B-4 on well 34/11-A-4 are presented in Fig. 95. This Kvitebjørn well is located about 173 km away from the Alvheim reference well as shown in Fig. 8 on page 20. The observed and discussed geological differences between the wells are the reason behind the big deviation between the predicted and the actual ROP (see Fig. 14 on page 31).

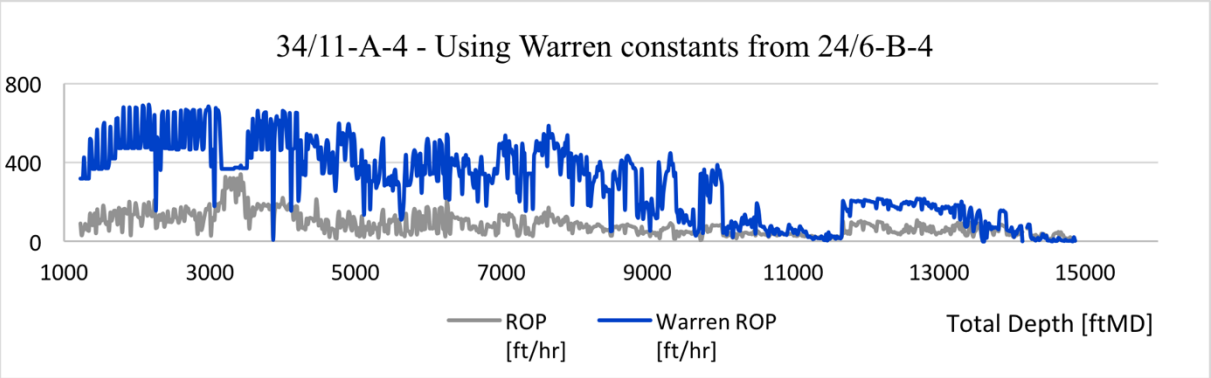

Fig. 95. Warren model - 34/11-A-4 with Warren constants from 24/6-B-4.

New Warren constants were calculated for this well to see how the results improve. The constants are shown in Table 11. The resulting ROP of implementing these constants on the well where they were produced is plotted in Fig. 96. There is a noticeable improvement in results. However, there are still some deviations between the predicted and the actual ROP.

Table 11. New calculated Warren constants from well 34/11-A-4.

	Constants
a	7.1772 x 10-08
b	24.3549
b	-7.2483 x 10-05

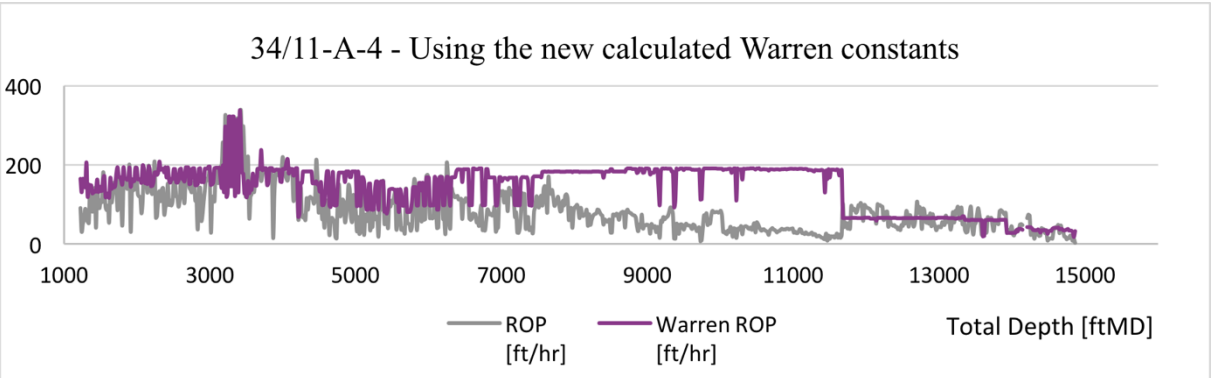

Fig. 96. Warren model applied on 34/11-A-4 with the new calculated Warren constants.

The resulting ROP of implementing the Warren constants generated from well 24/6-B-4 on well 34/11-A-5 are presented in Fig. 97. The ROP seems to be very poorly modelled. The ROP is then modelled using the newly calculated warren constants from the nearby well 34/11-A-4. The results are presented in Fig. 98 and seem to be much better than previous results. This indicates that the constants are valid only within the same region (i.e. locally).

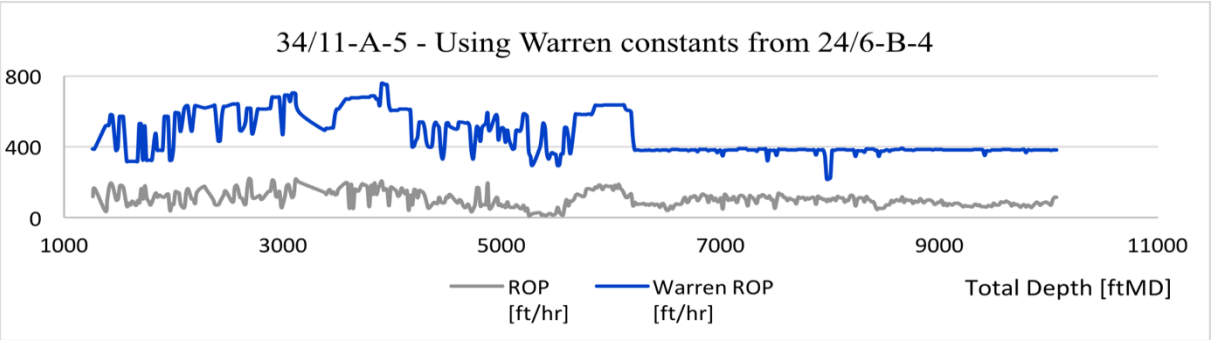

Fig. 97. Warren model - 34/11-A-5 with Warren constants from 24/6-B-4.

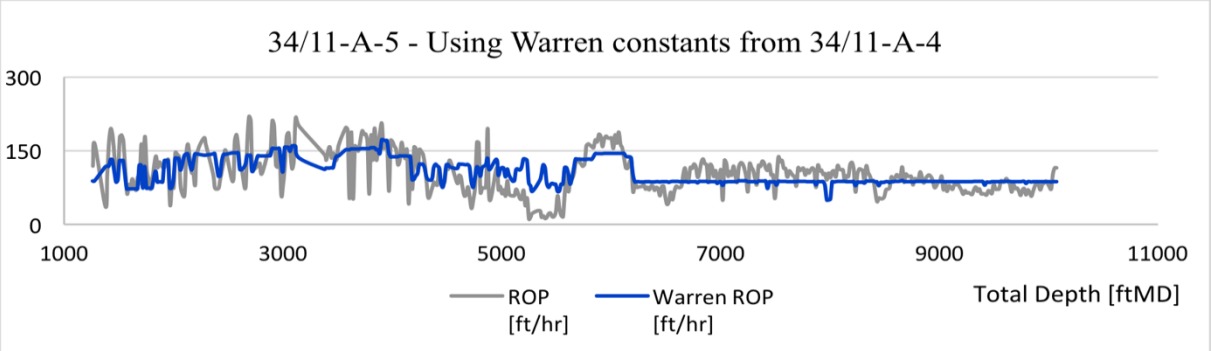

Fig. 98. Warren model - 34/11-A-5 with the new calculated Warren constants from 34/11-A-4.

Testing of Warren model on very far field wells

The Valhall well 2/11-S-10 ROP plot is shown in Fig. 99. The results appear to correlate fairly good with the actual ROP despite its great distance from the reference well. However, the ROP appears also to be poorly modelled at depths above 5 200 ftMD. Again, this is due to the remoteness of the wells from the Alvheim reference well as shown in Fig. 8 on page 20, which indicates the existence of differences in geological facies.

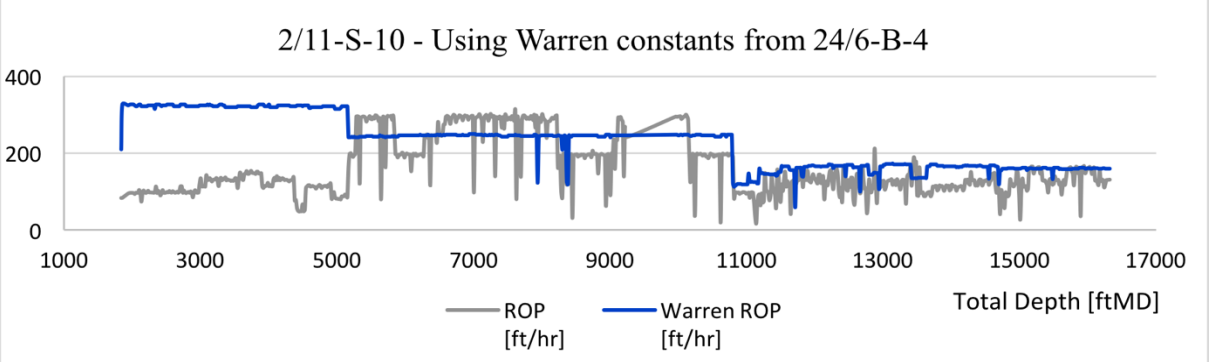

Fig. 99. Warren model - 2/11-S-10 with Warren constants from 24/6-B-4.

Chapter 5

Modelling Analysis

Different analysis methods are presented in this chapter seeking better evaluation of the ROP modelling. The purpose of this analysis is to determine how well the modelling of ROP matches the actual ROP. It also aims to analyze the performance of the ROP, whether or not it is well modelled. Two techniques are developed and discussed in this chapter to analyze the ROP modelling.

5.1 Time Analysis

Analysis of time differentiation aims to examine the difference between fulfilling the drilling process by using the time calculated out of the predicted ROP and the real time of the actual ROP. By having the variation between the two times, a better insight of the required time to fulfil the drilling process is determined. This method helps us evaluate the accuracy of the different used methods by assessing the time spent to complete the drilling operation. This is done by calculating the averaged value of the ROP. This method improves the attitude of the methods that might not have a good ROP prediction, but still have a good overall drilling time estimation [10].

In order to predict the drilling time used, the value of depth together with the ROP value can be applied in Eq. (5.1) where ROP is calculated by feet per hour. By applying the values in Eq. (5.1), pragmatic results are available in order to compare and differentiate the actual time and the estimated drilling time of each method.

$$t_r = \frac{depth_{drilled}}{ROP} \tag{5.1}$$

Here t_r is the drilling time in hours.

By finding a time deviation that every method has of actual drilling time, we can determine the consistency of each method.

The actual drilling time of each well is first calculated using Eq. (5.1). This is done by dividing the total depth of each well by the average ROP. The same thing is done for each well in each method in order to estimate the drilling time out of the predicted ROP values. The time deviation that each method has from the actual drilling time is calculated using Eq. (5.2).

$$\% \, Deviation = \frac{Estimated \; ROP_{avg} - Actual \; ROP_{avg}}{Actual \; ROP_{avg}} \; 100\% \qquad (5.2)$$

The results of time comparison analysis are presented in terms of positive and negative percentage values in Table 12. Positive values mean that the predicted drilling time for a certain method is longer than the actual drilling time, and vice versa for negative values.

Table 12. Time comparison for the different methods.

Field	Well	Method					
		Multiple Regression		Least squares	D-exp	MSE	Warren Model
		HYP I	HYP II	HYP II			
Alvheim	24/6-B-4 ⚑	+0.00	+0.00	-2.95	–	–	+9.69
	24/6-B-1	+44.49	+34.75	-3.76	-24.65	+63.44	-8.08
	24/6-B-5	-5.28	-5.13	-1.13	+44.84	+51.45	+111.20
Kvitebjørn	34/11-A-4	-56.55	-49.76	+22.52	-0.24	+63.60	-46.49
	34/11-A-4 with the new Warren constants	–	–	–	–	–	-7.11
	34/11-A-5	+3.31	+7.15	+2.47	+8.71	+99.59	-76.70
	34/11-A-5 with the new Warren constants	–	–	–	–	–	-20.90
Valhall	2/11-S-10	-25.56	-16.85	+30.41	-3.18	-6.27	-37.16

It has been preciously observed that all wells gave approximately the same ROP plots in both hypothesis I and II. However, hypothesis II is more accurate and shows less deviation from the actual ROP in most of the wells. The method of least squares attempts to reduce the difference between the predicted and the actual values of the ROP. This is clearly observed by both of the ROP plots and the time analysis.

The D-exponent method shows much better results than those obtained by the MSE method, although both depend on the strength and properties of the rocks. The MSE values may vary by thousands of psi while the D-exponent may vary only by a few decimal fractions. This makes the implementation of MSE method more challenging and less accurate than the other methods.

Well 24/6-B-5 shows some high values of time deviation, precisely in Warren model, although it has good results when considering its ROP plots. Well 2/11-S-10 has a similar situation, where it shows low values of time deviation despite its poor results when its ROP plots. This is due to the fact that the analysis may improve the attitude of the methods that might not have a good ROP prediction, but still have a good overall drilling time estimation and vice versa.

Well 24/6-B-1 shows higher deviation values in the multiple regression analysis than those obtained by the other Alvheim well 24/6-B-5. This is due to the geological differences discussed before between the well 24/6-B-1 and the reference well.

5.2 Parametric Sensitivity Analysis

A parametric sensitivity analysis is applied to determine the most influential drilling operational parameters on the developed ROP model. This is intended to predict which parameters can have a noticeable effect on the penetration rate in order to be aware of these parameters when drilling a new nearby well. The idea is to advice operators when planning to drill branched wells in the same formation with the objective of drilling with higher speed to reduce the non-productive time and thereby reduce the costs.

All the operational drilling parameters used in the ROP model (i.e. WOB, torque, RPM and F_{jm}) are increased and reduced by 10% separately for the reference well 24/6-B-4. The results of increasing and reducing the parameters are plotted against the actual modelled ROP in order to see if any improvement is obtained. This can show us the parameters with the greatest impact on the ROP.

After finding these influential parameters, they are adjusted by 10% in the other five wells to see how the ROP values vary. ROP averages are then calculated in order to calculate the saved time and costs of the adjustments.

The analysis is performed on the model which was developed using the multiple regression analysis and the second hypothesis presented in chapter 4.2.2 (i.e. using coefficients in Table 3**)**. The results of increasing and reducing the operational drilling parameters (WOB, torque, RPM and F_{jm})) for the reference well are presented in Figs. 100 to 103 respectively.

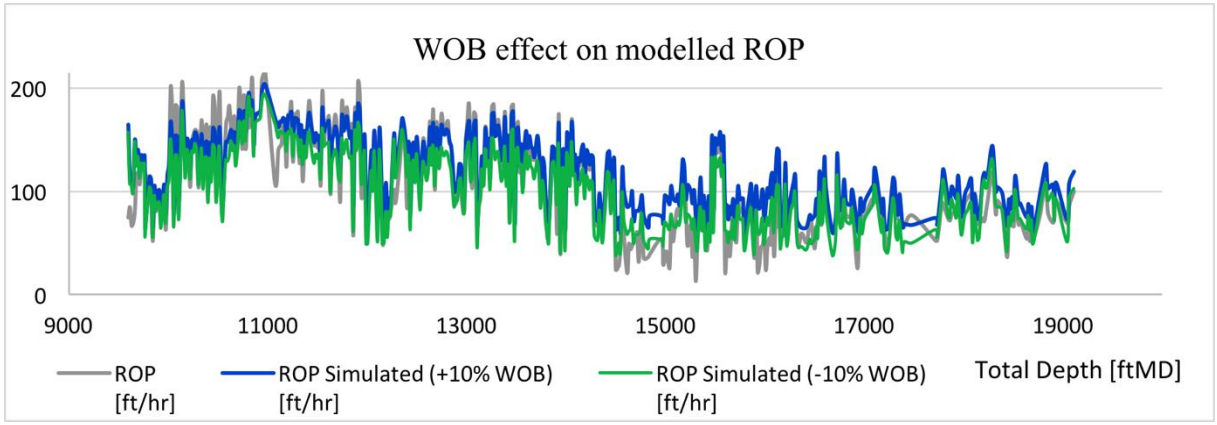

Fig. 100. Sensitivity analysis - Actual ROP values are compared with the ROP values modelled with increasing/decreasing WOB values by 10%.

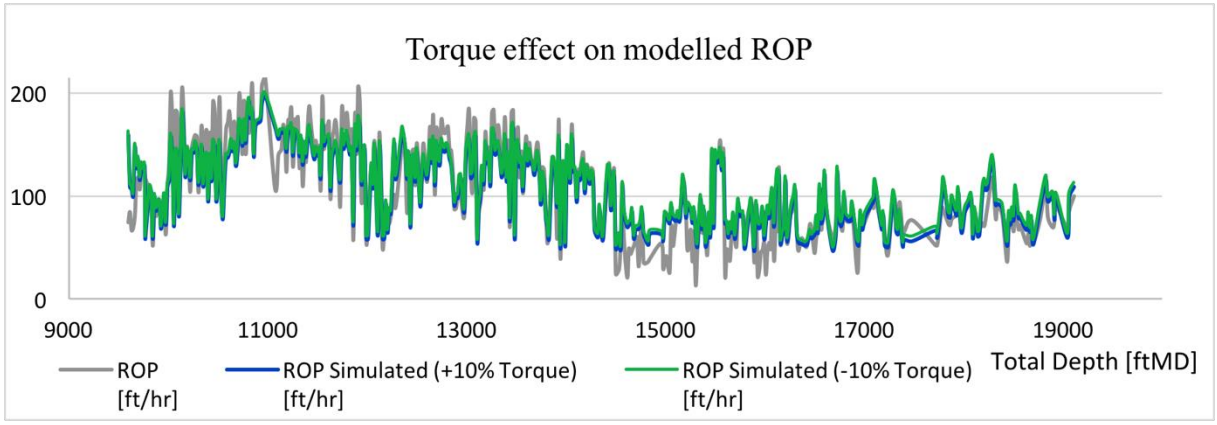

Fig. 101. Sensitivity analysis - Actual ROP values are compared with the ROP values modelled with increasing/decreasing torque values by 10%.

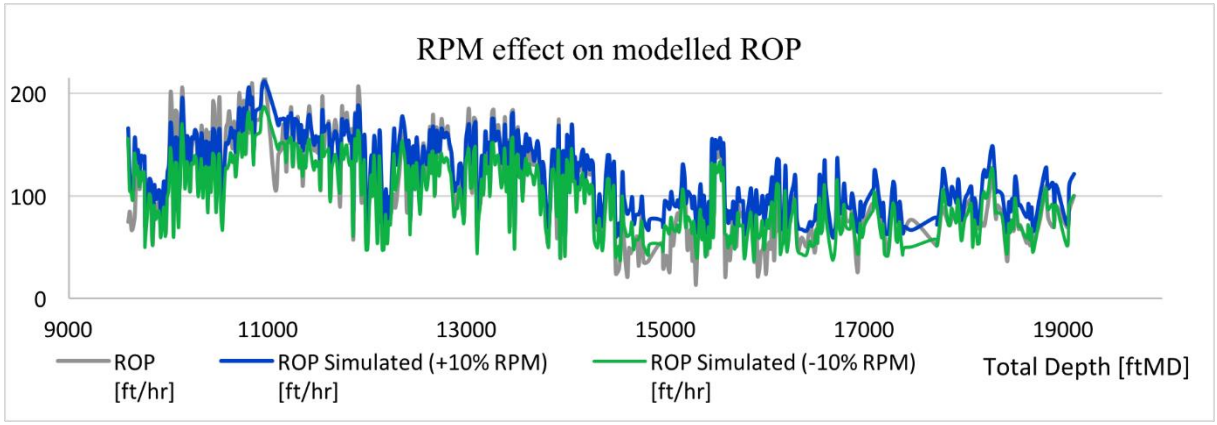

Fig. 102. Sensitivity analysis - Actual ROP values are compared with the ROP values modelled with increasing/decreasing RPM values by 10%.

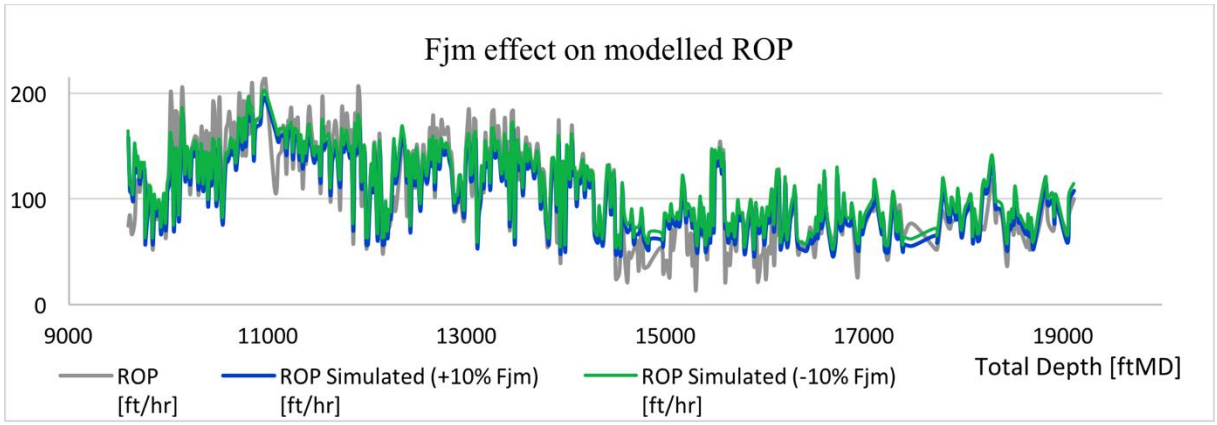

Fig. 103. Sensitivity analysis - Actual ROP values are compared with the ROP values modelled with increasing/decreasing F_{jm} values by 10%.

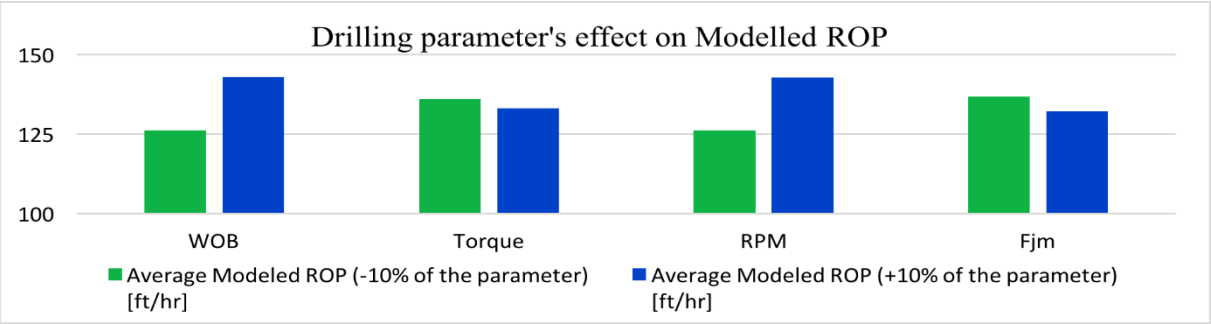

Fig. 104. Sensitivity analysis - Predicted average ROP for increasing/decreasing the different drilling parameters by 10%.

The average ROP of the results are shown in Fig. 104 in order to make it easier to determine the parameters that affect the model most. The WOB and the RPM are obviously the parameters with the greatest impact on the ROP model in the reference well. This is expected since the corresponding coefficients for these two parameters have the highest positive values as shown in Table 3 on page 41. Note that the FP (formation pressure) corresponding coefficient is not used in this analysis because it is not an operational parameter.

The WOB and the RPM are then increased by 10% for the other wells. The results of this increasing are presented in Figs. 105 to 109. The ROP averages of these results are shown in Fig. 110. This analysis aims to advice drillers when planning to drill branched wells in the same formation to optimize the drilling operation.

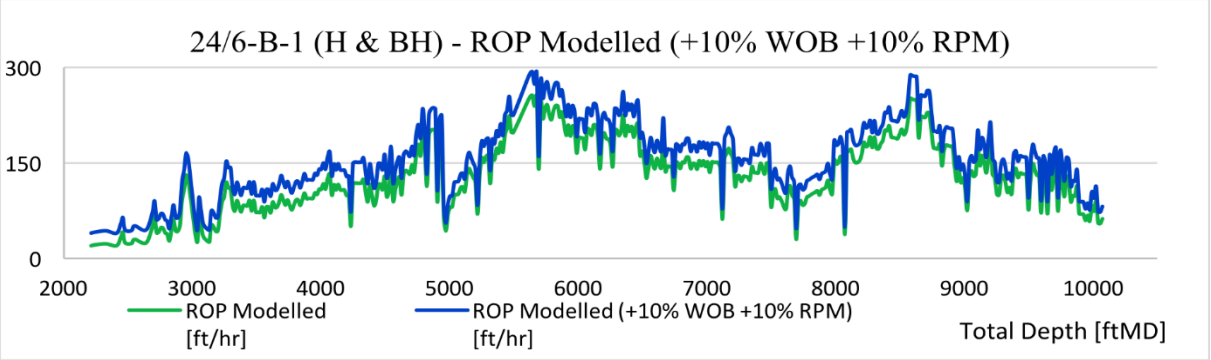

Fig. 105. Sensitivity analysis – The modelled ROP with an increase of the WOB and the RPM by 10% and the actual modelled ROP are compared for well 24/6-B-1 H.

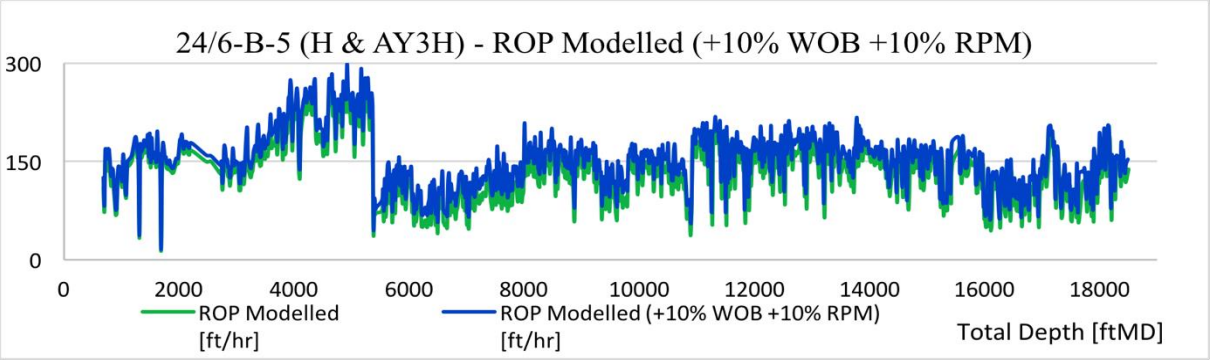

Fig. 106. Sensitivity analysis – The modelled ROP with an increase of the WOB and the RPM by 10% and the actual modelled ROP are compared for well 24/6-B-5.

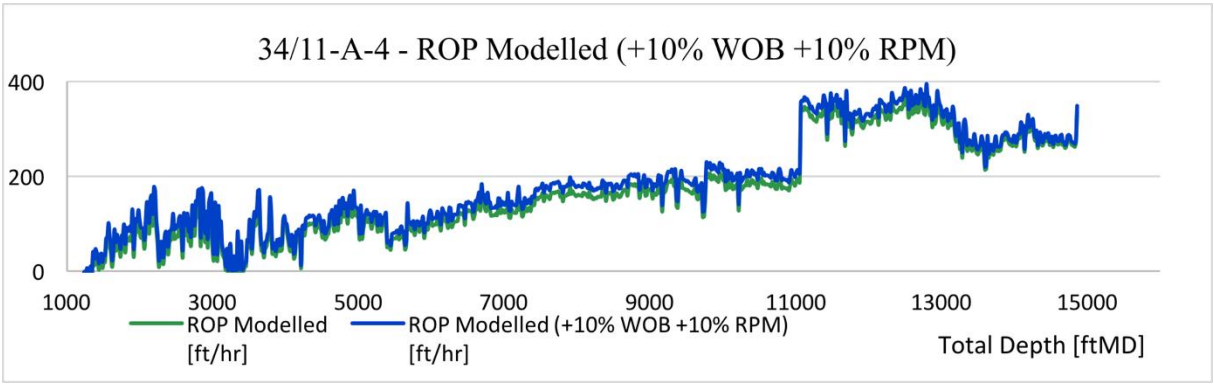

Fig. 107. Sensitivity analysis – The modelled ROP with an increase of the WOB and the RPM by 10% and the actual modelled ROP are compared for well 34/11-A-4.

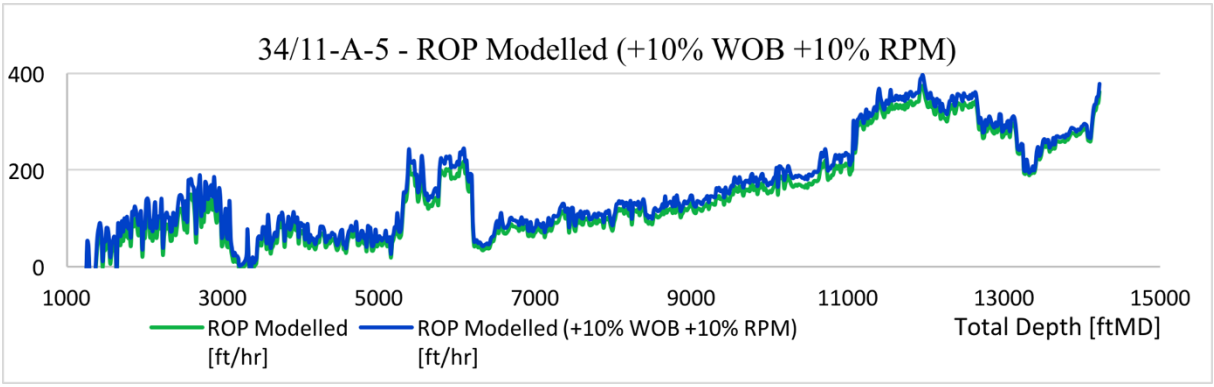

Fig. 108. Sensitivity analysis – The modelled ROP with an increase of the WOB and the RPM by 10% and the actual modelled ROP are compared for well 34/11-A-5.

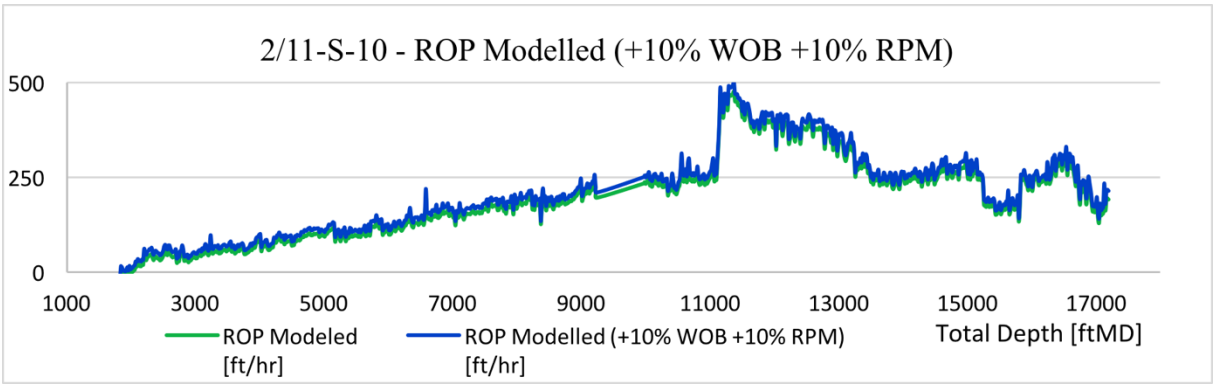

Fig. 109. Sensitivity analysis – The modelled ROP with an increase of the WOB and the RPM by 10% and the actual modelled ROP are compared for well 2/11-S-10.

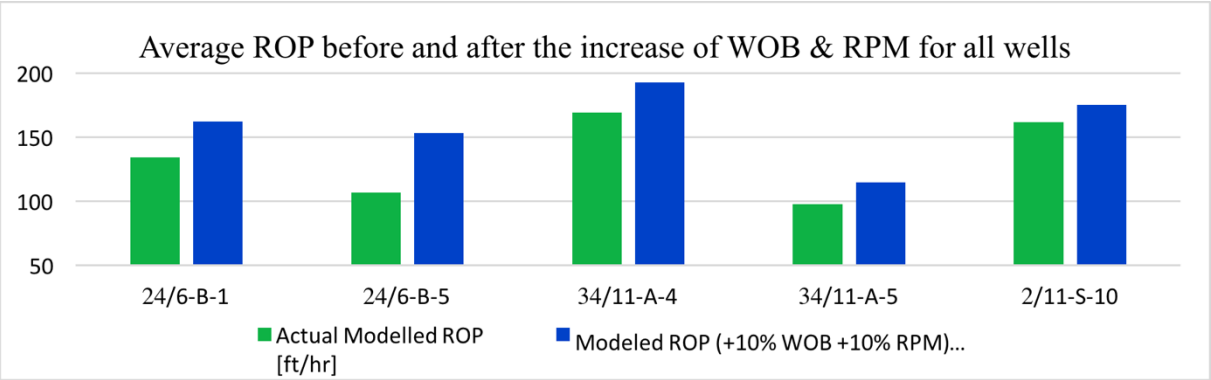

Fig. 110. Average ROP for all plots in Figs.** 105 **to** 109**.

The saved time of increasing the WOB and RPM by 10% for the five wells is calculated using Eq. (5.1). The saved time varies between 8 - 16 hours. This corresponds to 81 - 165 thousand USD. The assumed average rig rate for semisubmersibles is 250 thousand dollars per day; this assumption is based on data from last year [74]. Figs. 111 and 112 introduce the time and the expenditures saved in the form of histograms for each well.

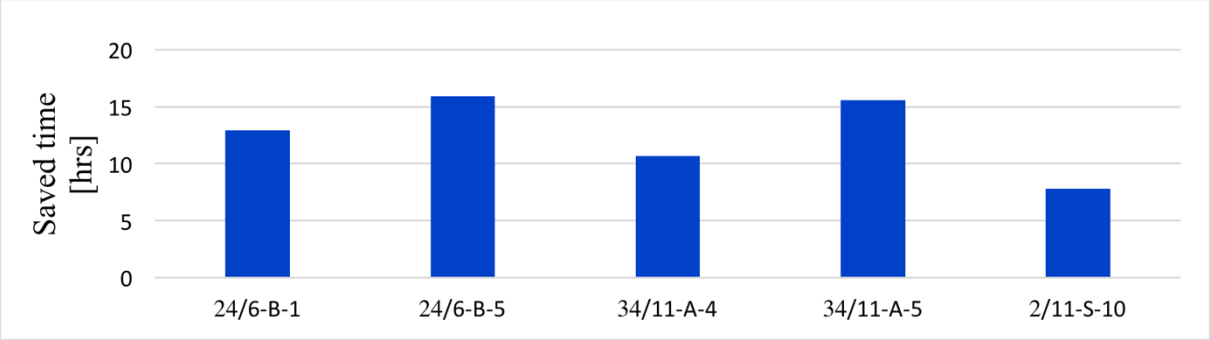

Fig. 111. Amount of time saved after the WOB and the RPM increase by 10%.

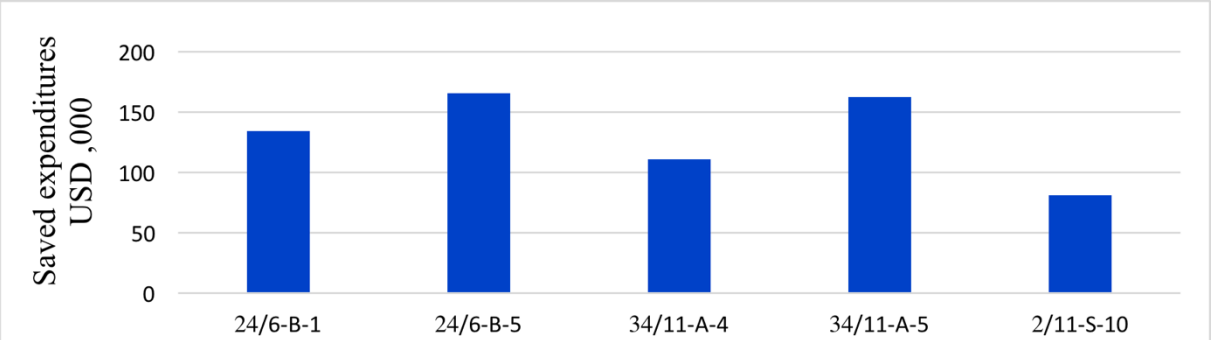

Fig. 112. Amount of money saved after the WOB and the RPM increase by 10%.

Chapter 6

Summary and Discussion

For better ROP modelling and prediction, it is important to evaluate different modelling approaches and test the models for laboratory and field data. This section presents the summary and analysis of the results presented in Chapters 4 and 5 regarding the model prediction and limitations of application. In addition, the developed ROP optimization procedure will be presented step by step.

6.1 Model Prediction and Limitations

Some relationships in the trends were obtained by the different methods, especially in the Alvheim wells where the reference well is located. It was expected of the different methods to give similar good results in the Alvheim wells. This is due to the small changes in geology between the Alvheim wells.

According to previous studies and experiments, we can conclude that there is good agreement with the work done by Morten Adamsen Husvæg [10].

Multiple Regression Analysis
The major pattern in the observations is that the developed model (using multiple regression analysis) is only applicable for nearby wells. The model is developed based on two hypotheses that models i) the reservoir section and ii) the whole borehole of the reference well. However, hypothesis II is more accurate and shows less deviation from the actual ROP in most of the wells.

Method of Least Squares
This method was applied on the hypothesis II-based ROP model since it has shown better results in the multiple regression analysis. This method improved the developed model by multiple regression analysis and reduced the differences between the predicted and the actual values of the ROP. It has also shown good results when the reference well coefficients were implemented on the other five wells. However, this seems to have some weaknesses when considering the values of these coefficients, where all the coefficients equal to zero except the FP (formation pressure) corresponding coefficient (see Table 4). This is not physical true because the main parameters making the drilling operation are not included in the model.

Warren Based Modelling

Similar to Warren model, the calculated constants from one well may only be applicable for close-by wells. This is clearly observed by both of the ROP plots and the time analysis. The Kvitebjørn wells have shown very poor results when using the reference-well-based Warren constants. These results were significantly improved when we recalculated the Warren constant based on one of the Kvitebjørn wells. This indicates that the constants are valid only within the same region and may be applicable to neighbouring wells. However, by using the new calculated Warren constant, this model seems to produce the best ROP predictions among the used methods, particularly in the distant wells.

D-exponent Method

Moreover, the D-exponent method has shown the very good results in both time analysis and predicted ROP plots shown chapter 4. However, Warren model is considered to be best methods model in this thesis when it comes to the application on both nearby and remote wells.

MSE Based Method

The D-MSE method has shown very poor results compared to those obtained by the D-exponent method. As mentioned before, this is due to the fact that the MSE values may vary by thousands of psi while the D-exponent may vary only by a few decimal fractions.

Time Analysis and Sensitivity Study

The parametric sensitivity analysis has also shown that the WOB and the RPM are the most influential parameters on the developed ROP model. By increasing each with 10%, the drilling time was reduced by 8 - 16 hours. This corresponds to 81 - 165 thousand dollars if the rig rate is 250 thousand dollars per day [74].

6.2 Modelling Limitation Summary

ROP prediction is evaluated for the different used methods in this section. A summary of the main limitations of the different methods assessed against the area of application is shown in Table 13. Colour coding is used to evaluate better the overall ROP prediction of the different methods (green is good, yellow is moderate, and red is poor).

Table 13. The modelling limitation summary for the different methods. Colour coding is used to evaluate the ROP prediction of each method (where green is good, orange is moderate, and red is poor).

Method	Area of application		
	On the originating well	**Nearby**	**Faraway**
Multiple Regression (section 4.2)	• Excellent prediction of ROP of both HYP I and II. • 100% correct overall drilling-time estimation.	• Very good prediction of ROP of both HYP I and II. • Pretty good overall drilling-time estimation	• Poor ROP prediction of both hypotheses. • Very good overall drilling-time estimation.
Least Squares (section 4.3)	• Reasonable prediction of ROP. • Very good overall drilling-time estimation, due to reduced differences between the predicted and the actual ROP. • Poor reliability.	• Reasonable ROP prediction of HYP II. • Very good overall drilling-time estimation. • Poor reliability	• Reasonable ROP prediction of HYP II. • Very good overall drilling-time estimation. • Poor reliability.
Warren Model (section 4.6)	• Excellent prediction of ROP. • Slightly good overall drilling-time estimation.	• Good ROP prediction. • Pretty good overall drilling-time estimation	• Pretty good ROP prediction when applying recalculating the constants.
D-Exponent (section 4.5)	• Some deviation between actual and calculated D-EXP values. • Good ROP prediction	• Good ROP prediction. • Very good overall drilling-time estimation.	• Slightly good ROP prediction. • Very good overall drilling-time estimation.
MSE (section 4.4)	• Some deviation between actual and calculated MSE values. • Good ROP prediction	• Good ROP estimation. • Bad overall drilling-time estimation.	• Poor ROP estimation. • Good overall drilling-time estimation.

The results variations of the different methods show why the ROP modelling may be challenging. The results have shown how applicable the different methods are, and have defined their area of application. These have also helped in developing an optimization process to reduce time and expenditures of the drilling process. This process is summarized in the next section.

6.3 ROP Optimization Process

In this thesis, new methods of ROP optimization have been developed and tested in chapters 4 and 5. The process of optimization is summarized as follows.

If a well to-be-drilled near a pre-drilled well, or if a well to be sidetracked:

1. Stratigraphic and well-to-well correlations are performed.
2. Multiple regression analysis and the modified Warren model are applied to generate the model coefficients (see sections 3.2 and 3.6). Data outliers are removed when applying these techniques.
3. Step 2 is applied to the desired section, depending on the purpose of the model. For example, if the purpose of the model is to predict ROP for a branched lateral well, the model coefficients can be developed based on data from the previous lateral well.
4. The model can be verified on pre-drilled nearby wells.
5. The average ROP and time are computed for the pre-drilled well and used as a reference. These are then compared with the predicted average of the well to-be-drilled.
6. The drilling parameters with the greatest impact on the model are defined. These parameters correspond to the highest positive coefficients developed in step 2. A sensitivity analysis in then performed by increasing these parameters. The average ROP and time are then computed and compared with the reference results specified in step 3.
7. More sensitivity analysis can be performed by combing higher and smaller coefficients. Finally, the best and most realistic combination can be selected and applied to the new well to-be-drilled.

6.4 Modelling Uncertainties

- The modelling approaches are based on one single well, this may reduce the reliability and the predictability of the models.
- Data quality and data outliers.
- MWD-tools failures and measurements uncertainties.
- The geological differences between the wells and the modelling assumptions made (e.g. the assumptions made on the MSE and the D-Exp workflows in sections 4.4 and 4.5).

Chapter 7

Conclusions

In the industry, there are software, practices and methods used to optimize drilling operation. Among others, ROP is one of the optimization consideration. The primary objective of this thesis work was to model ROP based on existing well data, and test its application to a nearby well to-be-drilled. However, this type of modelling and application needs to be tested to investigate the extent of the limitation.

To answer the research question addressed, a methodology has been designed to model and test their limits of application. For this, two hypothesis and five modelling approaches have been tested on six wells in the NCS. The wells are located in the Alvheim, Kvitebjørn, and Valhall fields. Of these, in Alvheim field, 24/6-B-4 well was considered as a reference and used for modelling. The reference model was then tested on several nearby, far and very far field well data.

Based on considered field data, wells, and the modelling strategies, the results are summarized as follows:

In terms of modelling
In general, the predictive power of the different models varies. Except for the least square method, the modelling methods show quite good match with the field data.

In terms of limitation
The models seem to work well when applying within the same block on nearby wells. Analysis of the well-to-well correlation chart indicates the similar lateral geological features between the wells. When applying on far fields, some of the modelling technics work well. However, the degree of the prediction is not as good as on the nearby wells.

ROP optimization
The reservoir-section-based model has shown excellent results when it was applied on the other branched lateral sections of the well. Based on this observation, ROP optimization procedure has been developed. The method is designed to be applied when planning to drill a new well within the same reservoir section. Based on the positive and high-value coefficient, one can increase the associated operational parameter during drilling a new well to increase the ROP. In this thesis, the method is illustrated with a simple example showing that the drilling time saved ranges between 8 - 16 hours by increasing the WOB and the RPM by 10%.

References

[1] M. Bevilacqua, F. E. Ciarapica, and B. Marchetti, "Acquisition, processing and evaluation of down hole data for monitoring efficiency of drilling processes," *Journal of Petroleum Science Research*, 2013.

[2] R. Teale, "The concept of specific energy in rock drilling," in *International Journal of Rock Mechanics and Mining Sciences & Geomechanics Abstracts*, 1965, vol. 2, no. 1, pp. 57-73: Elsevier.

[3] Petrowiki.org. *File: Devol2 1102final Page 223 Image 0002.png*. Available: http://petrowiki.org/File:Devol2_1102final_Page_223_Image_0002.png. [Accessed: 2017, Feb 06].

[4] D. T. Maulana and B. Marbun, "ROP Modeling for Volcanic Geothermal Drilling Optimization."

[5] E. Galle and H. Woods, "Variable weight and rotary speed for lowest drilling cost," in *AAODC Annual Meeting, New Orleans*, 1960.

[6] J. C. Estes and B. Randall, "Practical Application of Optimized Drilling Operations," in *IADC Drilling Technology Conf., New Orleans*, 1977.

[7] W. Maurer, "The" perfect-cleaning" theory of rotary drilling," *Journal of Petroleum Technology*, vol. 14, no. 11, pp. 1,270-1,274, 1962.

[8] R. Cunningham, "An empirical approach for relating drilling parameters," *Journal of Petroleum Technology*, vol. 30, no. 07, pp. 987-991, 1978.

[9] T. M. Warren, "Drilling model for soft-formation bits," *Journal of Petroleum Technology*, vol. 33, no. 06, pp. 963-970, 1981.

[10] M. A. Husvæg, "ROP modelling and analysis," University of Stavanger, Norway, 2015.

[11] K. Bjørlykke, "Sedimentologi og petroleumsgeologi," p. 177, 2001.

[12] M. Rider and M. Kennedy, "The geological interpretation of well logs: Rider-French," ed: Scotland, 2011.

[13] B. S. Aadnoy, *Modern well design*, 2nd edition ed. CRC Press, 2010.

[14] M. E. Hossain and A. A. Al-Majed, *Fundamentals of sustainable drilling engineering*. John Wiley & Sons, 2015, pp. 334-344.

[15] H. Rabia, *Well engineering & construction*. Entrac Consulting Limited, 2002, pp. 337-351.

[16] A. T. Bourgoyne, K. K. Millheim, M. E. Chenevert, and F. S. Young, "Applied drilling engineering," pp. 194-196, 1986.

[17] M. Varhaug. (2016) The defining series - Bits. *Oilfield Review*. Available: http://www.slb.com/resources/oilfield_review/or_en_intro_article.aspx

[18] M. E. Hossain and A. A. Al-Majed, *Fundamentals of sustainable drilling engineering*. John Wiley & Sons, 2015, p. 368.

[19] H. Rabia, *Well engineering & construction*. Entrac Consulting Limited, 2002, pp. 352-362.

[20] D. V. Swenson, D. L. Wesenberg, and A. K. Jones, "Analytical and experimental investigations of rock cutting using polycrystalline diamond compact drag cutters," in *SPE Annual Technical Conference and Exhibition*, 1981: Society of Petroleum Engineers.

[21] J. F. Brett, T. M. Warren, and S. M. Behr, "Bit whirl: A new theory of PDC bit failure," in *SPE Annual Technical Conference and Exhibition*, 1989: Society of Petroleum Engineers.

[22] A. T. Bourgoyne, K. K. Millheim, M. E. Chenevert, and F. S. Young, "Applied drilling engineering," pp. 190-192, 1986.

[23] P. Macini, M. Magagni, G. Da Dalt, and P. Valente, "Bit performance evaluation revisited by means of bit Index and formation drillability catalogue," in *SPE/IADC Middle East Drilling and Technology Conference*, 2007: Society of Petroleum Engineers.

[24] M. Rastegar, G. Hareland, R. Nygaard, and A. Bashari, "Optimization of multiple bit runs based on ROP models and cost equation: a new methodology applied for one of the Persian Gulf carbonate fields," in *IADC/SPE Asia Pacific Drilling Technology Conference and Exhibition*, 2008: Society of Petroleum Engineers.

[25] A. T. Bourgoyne, K. K. Millheim, M. E. Chenevert, and F. S. Young, "Applied drilling engineering," 1986.

[26] E. Morton and W. Clements, "The Role of Bit Type and Drilling Fluid Type in Drilling Performance," in *International Meeting on Petroleum Engineering*, 1986: Society of Petroleum Engineers.

[27] T. Warren and W. Armagost, "Laboratory drilling performance of PDC bits," *SPE drilling engineering*, vol. 3, no. 02, pp. 125-135, 1988.

[28] A. Bourgoyne Jr and F. Young Jr, "A multiple regression approach to optimal drilling and abnormal pressure detection," *Society of Petroleum Engineers Journal*, vol. 14, no. 04, pp. 371-384, 1974.

[29] T. Warren and A. Sinor, "Drag bit performance modeling," in *SPE Annual Technical Conference and Exhibition*, 1986: Society of Petroleum Engineers.

[30] G. Hareland and P. Rampersad, "Drag-bit model including wear," in *SPE Latin America/Caribbean Petroleum Engineering Conference*, 1994: Society of Petroleum Engineers.

[31] Z. T. Bieniawski, "Estimating the strength of rock materials," *Journal of the Southern African Institute of Mining and Metallurgy*, vol. 74, no. 8, pp. 312-320, 1974.

[32] E. Momeni, D. J. Armaghani, M. Hajihassani, and M. F. M. Amin, "Prediction of uniaxial compressive strength of rock samples using hybrid particle swarm optimization-based artificial neural networks," *Measurement*, vol. 60, pp. 50-63, 2015.

[33] T. Bratton *et al.*, "Rock strength parameters from annular pressure while drilling and dipole sonic dispersion analysis," in *SPWLA 45th Annual Logging Symposium*, 2004: Society of Petrophysicists and Well-Log Analysts.

[34] B. Aadnoy and R. Looyeh, *Petroleum rock mechanics: drilling operations and well design*. Gulf Professional Publishing, 2011.

[35] J. Bellarby, *Well completion design*. Elsevier, 2009, pp. 131-134.

[36] A. Amani and K. Shahbazi, "Prediction of rock strength using drilling data and sonic logs," *International Journal of Computer Applications*, vol. 81, no. 2, 2013.

[37] S. Kahraman, O. Gunaydin, and M. Fener, "The effect of porosity on the relation between uniaxial compressive strength and point load index," *International Journal of Rock Mechanics and Mining Sciences*, vol. 42, no. 4, pp. 584-589, 2005.

[38] M. Fasheloum, "Investigation of drilling parameters indicators," University of Nottingham, 1997.

[39] R. F. Mitchell and S. Miska, *Fundamentals of drilling engineering*. Society of Petroleum Engineers, 2011.

[40] T. Warren, "Penetration rate performance of roller cone bits," *SPE Drilling Engineering*, vol. 2, no. 01, pp. 9-18, 1987.

[41] A. Kuznetcov, "ROP optimization and modelling in directional drilling process," University of Stavanger, Norway, 2016.

[42] T. Eren, "Real-time-optimization of drilling parameters during drilling operations," Middle East Technical University, 2010.

[43] W. L. Koederitz and J. Weis, "A Real-time Implementation of MSE, presented at the AADE 2005 National Technical Conference and Exhibition, held at the Wyndam Greenspoint in Houston, Texas, Apr. 5-7, 2005," AADE-05-NTCE-66.

[44] F. E. Dupriest and W. L. Koederitz, "Maximizing drill rates with real-time surveillance of mechanical specific energy," in *SPE/IADC Drilling Conference*, 2005: Society of Petroleum Engineers.

[45] B. Elahifar, G. Thonhauser, R. K. Fruhwirth, and A. Esmaeili, "ROP Modeling using NeuralNetwork and Drill String Vibration Data," in *SPE Kuwait International Petroleum Conference and Exhibition*, 2012: Society of Petroleum Engineers.

[46] B. Rashidi, G. Hareland, and R. Nygaard, "Real-time drill bit wear prediction by combining rock energy and drilling strength concepts," in *Abu Dhabi International Petroleum Exhibition and Conference*, 2008: Society of Petroleum Engineers.

[47] H. U. Caicedo, W. M. Calhoun, and R. T. Ewy, "Unique ROP predictor using bit-specific coefficient of sliding friction and mechanical efficiency as a function of confined compressive strength impacts drilling performance," in *SPE/IADC Drilling Conference*, 2005: Society of Petroleum Engineers.

[48] R. Pessier and M. Fear, "Quantifying common drilling problems with mechanical specific energy and a bit-specific coefficient of sliding friction," in *SPE Annual Technical Conference and Exhibition*, 1992: Society of Petroleum Engineers.

[49] R. Nygaard and G. Hareland, "Application of rock strength in drilling evaluation," in *Latin American & Caribbean Petroleum Engineering Conference*, 2007: Society of Petroleum Engineers.

[50] M. Bataee, M. Kamyab, and R. Ashena, "Investigation of Various ROP Models and Optimization of Drilling Parameters for PDC and Roller-cone Bits in Shadegan Oil Field," in *International Oil and Gas Conference and Exhibition in China*, 2010: Society of Petroleum Engineers.

[51] H. W. R. Wardlaw, "Optimization of rotary drilling parameters," University of Texas at Austin, 1971.

[52] G. Hareland and L. Hoberock, "Use of drilling parameters to predict in-situ stress bounds," in *SPE/IADC Drilling Conference*, 1993: Society of Petroleum Engineers.

[53] H. Darley, "Designing fast drilling fluids," *Journal of Petroleum Technology*, vol. 17, no. 04, pp. 465-470, 1965.

[54] P. Rampersad, G. Hareland, and P. Boonyapaluk, "Drilling optimization using drilling data and available technology," in *SPE Latin America/Caribbean Petroleum Engineering Conference*, 1994: Society of Petroleum Engineers.

[55] H. Motahhari, G. Hareland, R. Nygaard, and B. Bond, "Method of optimizing motor and bit performance for maximum ROP," *Journal of Canadian Petroleum Technology*, vol. 48, no. 06, pp. 44-49, 2009.

[56] M. E. Hossain and A. A. Al-Majed, *Fundamentals of sustainable drilling engineering*. John Wiley & Sons, 2015, pp. 383-385.

[57] A. T. Bourgoyne, K. K. Millheim, M. E. Chenevert, and F. S. Young, "Applied drilling engineering," pp. 226-227, 1986.

[58] M. E. Hossain and A. A. Al-Majed, *Fundamentals of sustainable drilling engineering*. John Wiley & Sons, 2015, pp. 278-281.

[59] H. Rabia, *Well engineering & construction*. Entrac Consulting Limited, 2002, pp. 26-29.

[60] M. Bingham, "Oil and Gas Jour," *Technical Manual*, 1965.

[61] J. Jorden and O. Shirley, "Application of drilling performance data to overpressure detection," *Journal of Petroleum Technology*, vol. 18, no. 11, pp. 1,387-1,394, 1966.

[62] P. Ablard *et al.*, "The expanding role of Mud logging," *Oilfield Review*, vol. 24, no. 1, pp. 31-32, 2012.
[63] B. Rehm and R. McClendon, "Measurement of formation pressure from drilling data," in *Fall Meeting of the Society of Petroleum Engineers of AIME*, 1971: Society of Petroleum Engineers.
[64] S. Finnestad, "Field Data," Norwegian Petroleum Directorate, email: Svein.Finnestad@npd.no.
[65] Npd.no. *FactPages - Norwegian Petroleum Directorate*. Available: http://factpages.npd.no/factpages/Default.aspx. [Accessed: 2017, Apr 20].
[66] Npd.no. *FactMaps - Norwegian Petroleum Directorate*. Available: http://gis.npd.no/factmaps/html_21/. [Accessed: 2017, Apr 20].
[67] D. E. Berger, "Introduction to multiple regression," *USA: Claremont Graduate University*, 2003.
[68] J. C. Davis and R. J. Sampson, "Statistics and data analysis in geology," p. 461, 1986.
[69] D. C. Montgomery and G. C. Runger, *Applied statistics and probability for engineers*, Fifth ed. John Wiley & Sons, 2010, p. 449.
[70] *Engineering Statistics Handbook, 4.4.3.1 Least Squares*. Available: http://www.itl.nist.gov, http://www.itl.nist.gov/div898/handbook/pmd/section4/pmd431.htm. [Accessed: 2017, Mar 19].
[71] E. W. Weisstein. *Least Squares Fitting*. Available: MathWorld--A Wolfram Web Resource. http://mathworld.wolfram.com/LeastSquaresFitting.html. [Accessed: 2017, Mar 19].
[72] *"stratigraphic correlation" A Dictionary of Earth Sciences*. Available: http://www.encyclopedia.com/science/dictionaries-thesauruses-pictures-and-press-releases/stratigraphic-correlation. [Accessed: 2017, Apr 22].
[73] *Stratigraphy: linking rocks, fossils, and time*. Available: http://www.thisoldearth.net/Geology_Online-1_Subchapters.cfm?Chapter=6&Row=4. [Accessed: 2017, Apr 22].
[74] *IHS Markit. IHS Petrodata Offshore Rig Day Rate Trends*. Available: https://www.ihs.com/products/oil-gas-drilling-rigs-offshore-day-rates.html. [Accessed: 2017, Apr 26].
[75] J. R. Eckel, "Microbit studies of the effect of fluid properties and hydraulics on drilling rate," *Journal of Petroleum Technology*, vol. 19, no. 04, pp. 541-546, 1967.
[76] B. Rashidi, G. Hareland, and A. Wu, "New approach in real-time bit wear prediction," in *Abu Dhabi International Petroleum Exhibition and Conference*, 2010: Society of Petroleum Engineers.

Appendices

Appendix I

Literature Reviewed

Bourgoyne and Young Model

As mentioned before, Bourgoyne and young [28] developed a model that simplifies the rotary drilling process into one single model. Bourgoyne and young introduced in this model the penetration rate as a function of several drilling variables that are considered to have an effect on the ROP which are: formation strength, depth and compaction, bit hydraulics, rotary speed, pore pressure, bit weight, teeth wear and bit diameter.

The following penetration rate (dD/dt) model was selected to predict the effect of the above-mentioned drilling parameters (x_j):

$$\frac{dD}{dt} = exp\left(a_1 + \sum_{j=2}^{8} a_j x_j\right) \quad \text{(A.1)}$$

The constants (a1 - a8) are selected to model the ROP and the drilling behaviour in a given formation type. Eq. (A.1) is linear, and the constants can therefore be determined using multiple regression analysis [28].
The model can also be expressed as [4]:

$$ROP = f_1 * f_2 * f_3 * f_4 * f_5 * f_6 * f_7 * f_8 \quad \text{(A.2)}$$

Where the functions (f_1-f_8) express the various normalized effects on ROP and the constants (a1 - a8) are experimental model constants [46].

The first term (f_1) expresses the effect of rock drillability (proportional with the formation strength) and is given by:

$$f_1 = e^{2.303a_1} \quad \text{(A.3)}$$

The second term (f_2) models the compaction effect and is given by:

$$f_2 = e^{2.303a_2(10{,}000-D)} \quad \text{(A.4)}$$

Where (D) is the depth in feet. The third term models (f_3) the under-compaction due to differential pressure and is given as:

$$f_3 = e^{2.303a_3 D^{0.69}(g_p-9.0)} \quad \text{(A.5)}$$

Where (g_p) is the pore pressure gradient in pounds per gallon equivalent. The fourth term (f_4) is the effect of differential pressure,

$$f_4 = e^{2.303 a_3 D(g_p - \rho_c)} \quad \text{(A.6)}$$

Where (ρ_c) is the mud weight in pound per gallon. The fifth term (f_5) model the effect on ROP caused by changing WOB,

$$f_5 = \left[\frac{\left(\frac{WOB}{d_b}\right) - \left(\frac{WOB}{d_b}\right)_t}{4.0 - \left(\frac{WOB}{d_b}\right)_t} \right]^{a_5} \quad \text{(A.7)}$$

The threshold bit weight $(WOB/d_b)_t$ is estimated using drill-off tests. And the bit weight exponent values are reported to vary between 0.6 and 2.0 [28].

The sixth term (f_6) models the effect of rotary speed (RPM) on the ROP and is given by:

$$f_6 = \left(\frac{N}{60}\right)^{a_6} \quad \text{(A.8)}$$

The seventh term (f_7) models the effect of bit wear on the ROP. It depends on bit type and formation type and is given by:

$$f_7 = e^{-a_7 h} \quad \text{(A.9)}$$

Where (h) is the fractional tooth height worn away given as:

$$h = \frac{DG}{8} * \frac{(Depth_{current} - Depth_{in})}{(Depth_{out} - Depth_{in})} \quad \text{(A.10)}$$

Where (DG) is the IADC dull bit grade reported when the bit is pulled out and has a value that varies between 0 and 8 [46]. The last term (f_8) is the effect of bit hydraulics on the ROP given as:

$$f_8 = \left(\frac{F_j}{1000}\right)^{a_8} \quad \text{(A.11)}$$

Where (F_j) is the hydraulic jet impact force beneath the bit [lbf]. Eckel [75] discovered that ROP was proportional to square root of Reynolds number group $(\rho q/\mu d_n)$. Where (ρ), (q), (μ) and (d_n) are the mud density [lb/gal], the flowrate [gal/min], the apparent viscosity [cp] and the bit nozzle diameter [in] respectively.

$$F_j = \frac{\rho q}{0.35 \mu d_n} \quad \text{(A.12)}$$

Real-Time Bit Wear Model

The eight functions in Bourgoyne and Young model can be inverted in order to obtain the formation drillability function (f_1) shown in the following equation:

$$f_1 = \frac{ROP}{f_1 * f_2 * f_3 * f_4 * f_5 * f_6 * f_7 * f_8} \quad \text{(A.13)}$$

The new suggested model fins the relationship between MSE value and rock drillability and is proposed in the power form as:

$$MSE = K_1 \left(\frac{1}{f_1}\right)^{K_2} \quad \text{(A.14)}$$

Where (K_1 and K_2) constants are obtained from the offset wells data. The (K_1) constant is used for real time application to estimate of the wear function when bit is in the hole. This constant has been normalized in order to adjust the trends of (K_1) and bit wear grade against depth. The normalized inversion of (K_1) is given by:

$$Norm\left(\frac{1}{K_1}\right) = 1 - A * h^B \quad \text{(A.15)}$$

Where (h) is the fractional bit tooth dullness given in Eq. (A.10). The most accurate value of the (B) constant was obtained using typical regressive software and is given as: ($B = 5.6392\ h + 0.4212$). The correlation coefficient for this fit is very good, and the proposed model showed positive results with data [76].

Hareland and Rampersad Model

The general ROP model form for a full efficient bit cleaning is given by [55]:

$$ROP = W_f \left(\frac{G.RPM^{\gamma}.WOB^{\alpha}}{d_b.UCS}\right) \quad \text{(A.16)}$$

Where (γ) and (α) are the ROP model RPM and WOB exponents respectively. (W_f) is the wear function, this function calibrates ROP values for a worn bit. (G) is the ROP model constant determined by the blade and bit geometry.

Maurer Model

The Maurer ROP model was developed assuming incomplete bit tooth and perfect bottomhole cleaning condition. This model is given by [56]:

$$ROP = \frac{K}{S^2}\left[\frac{WOB}{d_b} - \left(\frac{WOB}{d_b}\right)_t\right]^2 N \quad \text{(A.17)}$$

Where K is the constant of proportionality, $(WOb/d_b)_t$ is the threshold bit weight. Bingham

Bingham Model

The Bingham model is a simple experimental model which is a modification of the Maurer model. The threshold bit weight $(WOb/d_b)_t$ is assumed to be negligible in this equation and the bit weight exponent (a_5) is to be determined experimentally. This model has less reliability as it neglects depth of drilling

[57]. Bingham suggested the following laboratory derived equation which is applicable for low WOB and rotational speed (N) [45, 57]:

$$ROP = K\left(\frac{WOB}{d_b}\right)^{a_5} N \tag{A.18}$$

Where (K) is the constant of proportionality that includes the effect of rock strength and (a_5) is the bit weight exponent.

Appendix II

Modelling Implementation

Multiple Regression

The regression data analysis is first performed. The intercept value is represented by the initial value of coefficients (b_0). The other coefficients (b_{1-5}) are then multiplied according to their order with the regression variables (X_{1-5}) as shown in Fig. 113.

Eq. (3.3) is used to model the ROP in this part. Fig. 113 shows how Eq. (3.3) is used in Microsoft Excel software to calculate the modelled ROP listed in column H for each depth point. Cell columns B, C, D, E and F, contain the regression variables (WOB, Torque, RPM, F_{jm} and FP) respectively. The coefficients are listed in cells K18 to K23 and donated by a $ sign to keep their values constant during the whole process.

$$Modelled\ ROP = K\$18 + K\$19 * B2 + K\$20 * C2 + K\$21 * D2 + K\$22 * E2 + K\$23 * F2 \tag{A.19}$$

LOG =K$18+K$19*B2+K$20*C2+K$21*D2+K$22*E2+K$23*F2

	A	B	C	D	E	F	G	H	I	J	K
1	Tot Depth [ft]	WOB [lbf]	TORQUE [ft-lbf]	Bit [rpm]	Fjm [lbf]	FP Eaton [lb/gal]	ROP [ft/hr]	Modelled ROP [ft/hr]			
2	9596	8866	19368	61	0.0100	13.5	74.8	K$23*F2		SUMMARY OUTPUT	
3	9613	7167	18646	62	0.0098	12.6	84.8	111.1			
4	9629	5403	17598	62	0.0101	12.7	67.0	108.3		*Regression Statistics*	
17	9843	9704	15098	88	0.0101	10.8	52.1	59.7			*Coefficients*
18	9859	11269	16234	118	0.0107	11.1	91.7	100.2		Intercept	-540.5473377
19	9875	11137	16381	118	0.0107	10.8	80.7	87.2		X Variable 1	0.00406349
20	9892	10123	15865	118	0.0107	10.2	49.7	50.8		X Variable 2	-0.001055771
21	9908	13739	16212	120	0.0108	10.8	97.1	95.5		X Variable 3	0.839940302
22	9925	12438	15961	120	0.0107	10.3	71.4	69.9		X Variable 4	-3207.857749
23	9941	13497	14891	150	0.0106	10.0	83.9	84.4		X Variable 5	49.32506944

Fig. 113. Eq. (3.3) applied (Microsoft Excel).

Warren Model

Rock strength (UCS) is first calculated as a function of MSE in Microsoft Excel software. The 1st term $\left(\frac{S^2 {d_b}^3}{NWOB^2} ROP\right)$, the 2nd term $\left(\frac{1}{N d_b} ROP\right)$ and the 3rd term $\left(\frac{d_b \gamma_f \mu}{F_{jm}} ROP\right)$ of Eq. (3.8) are then calculated in Microsoft Excel software. The procedure is shown in Figs. 114, 115 and 116 respectively.

PI | =G2*I2^2*A2^3/(D2*B2^2)

	A	B	C	D	E	F	G	H	I	J
1	Bit D [in]	WOB [lbf]	TORQUE [ft-lbf]	Bit [rpm]	Fjm [lbf]	FP Eaton [lb/gal]	ROP [ft/hr]	Calculated MSE [kpsi]	UCS [psi]	1st TERM
2	9.5	8866	19368	61	0.0100	13.5	74.8	84.1	29445	=G2*I2^2*A2^3/(D2*B2^2)
3	9.5	7167	18646	62	0.0098	12.6	84.8	72.6	25419	14745

Fig. 114. The 1st term of Eq. (3.8) calculated (Microsoft Excel).

PI | =G2/(D2*A2)

	A	B	C	D	E	F	G	H	I	J	K
1	Bit D [in]	WOB [lbf]	TORQUE [ft-lbf]	Bit [rpm]	Fjm [lbf]	FP Eaton [lb/gal]	ROP [ft/hr]	Calculated MSE [kpsi]	UCS [psi]	1st TERM	2nd TERM
2	9.5	8866	19368	61	0.0100	13.5	74.8	84.1	29445	11598	=G2/(D2*A2)
3	9.5	7167	18646	62	0.0098	12.6	84.8	72.6	25419	14745	0.14393

Fig. 115. The 2nd term of Eq. (3.8) calculated (Microsoft Excel).

PI | =D2*A2*K$5*B2/C2

	A	B	C	D	E	F	G	H	I	J	K
1	Bit D [in]	MW IN [lbm/gal]	Fjm [lbf]	ROP [ft/hr]	Calculated MSE [kpsi]	UCS [psi]	1st TERM	2nd TERM	3rd TERM		
2	9.5	1.0	0.0100	74.8	84.1	29445	11598	0.1291	=D2*A2*K$5*B2/C2		μ [cp]
3	9.5	8.3	0.0098	84.8	72.6	25419	14745	0.1439	10276712		15

Fig. 116. The 3rd term of Eq. (3.8) calculated (Microsoft Excel).

Cell column J in Fig. 114 calculates the 1st term for $n *$ depth-points. The 1st term column can be written as an (n x 1) x-vector. Cell column K in Fig. 115 calculates the 2nd term for n $*$ depth-points. The 2nd term column can be written as an (n x 1) y-vector. Cell column I in Fig. 116 calculates the 3rd term for n $*$ depth-points. The same is done for the 3rd term column, it is written as an (n x 1) z-vector.

Eq. (3.10) is then solved for Warren constants a, b and c in MATLAB software. Warren ROP can then be calculated using Eq. (3.11) as shown in Fig. 117. The used a, b and c constants in Fig. 117 equal to 3.995e-05, 6.8471 and 3.4834e-09 respectively.

PI | =A2/(3.9955e-05*C2 + 6.8471*D2 + 3.4834e-09*E2)

	A	B	C	D	E	F
1	ROP [ft/hr]	UCS [psi]	1st TERM	2nd TERM	3rd TERM	Warren ROP [ft/hr]
2	74.8	29445	11598	0.1291	1069703	=A2/(3.9955e-05*C2 + 6.8471*D2 + 3.4834e-09*E2)
3	84.8	25419	14745	0.1439	10276712	52.6

Fig. 117. ROP calculated using Warren model and the constants (a. b and c).